Synthesis, Characterization and Properties of Semi-aromatic Polyamide Thermosets

Li, Ming

DOI
10.4233/uuid:8e3dd0ce-5269-4b53-8cdf-00cd3cb87eed

Publication date
2017

Document Version
Final published version

Citation (APA)
Li, M. (2017). *Synthesis, Characterization and Properties of Semi-aromatic Polyamide Thermosets*. [Dissertation (TU Delft), Delft University of Technology]. https://doi.org/10.4233/uuid:8e3dd0ce-5269-4b53-8cdf-00cd3cb87eed

Synthesis, Characterization and Properties of Semi-aromatic Polyamide Thermosets

Proefschrift

ter verkrijging van de graad van doctor
aan de Technische Universiteit Delft,
op gezag van de Rector Magnificus Prof. ir. K. C. A. M. Luyben,
voorzitter van het College voor Promoties,
in het openbaar te verdedigen op
maandag 22 mei 2017 om 12:30 uur

door

Ming LI

Master of Science in Materials Science
Shanghai Jiao Tong University, Shanghai, China
geboren te Hebei, China

Dit proefschrift is goedgekeurd door de promotor:
Prof. dr. T. J. Dingemans

Samenstelling promotiecommissie:

Rector Magnificus	voorzitter
Prof. dr. T.J. Dingemans	Technische Universiteit Delft, promotor

Independent members:

Prof. dr. C.E. Koning	Technische Universiteit Eindhoven
Dr. R. Rulkens	DSM
Prof. dr. W.A. Groen	Technische Universiteit Delft
Prof. dr. S.J. Picken	Technische Universiteit Delft
Prof. dr. E.J.R. Sudhölter	Technische Universiteit Delft
Prof. dr. ir. S. van der Zwaag	Technische Universiteit Delft

The research carried out in this thesis is funded by the Dutch Polymer Institute (DPI), postbus 902, 5600 AX Eindhoven, Project #743.

ISBN: 978-94-6186-805-3

mingli.198802@gmail.com

Published by: Gildeprint

CONTENTS

CHAPTER 1 INTRODUCTION 1

1.1 POLYAMIDES 2
1.2 SEMI-AROMATIC POLYAMIDES 2
1.2.1 MONOMER COMPOSITION OF SEMI-AROMATIC POLYAMIDES 2
1.2.2 SEMI-CRYSTALLINE POLYPHTHALAMIDES 4
1.2.3 AMORPHOUS POLYPHTHALAMIDES 7
1.3 POLY(DECAMETHYLENE TEREPHTHALAMIDE) (PA 10T) 9
1.4 POLYAMIDE THERMOSETS 11
1.4.1 IONIZING IRRADIATION 11
1.4.2 THERMAL CURING 11
1.5 SCOPE AND OUTLINE OF THE THESIS 14
1.6 REFERENCES 15

CHAPTER 2 SOLUTION POLYMERIZATION OF SEMI-AROMATIC POLYAMIDE PA 10T 19

2.1 INTRODUCTION 20
2.2 EXPERIMENTAL 21
2.2.1 MATERIALS 21
2.2.2 PA 10T POLYMERIZATION 21
2.2.3 CHARACTERIZATION 22
2.3 OPTIMIZATION OF PA 10T SOLUTION POLYMERIZATION 23
2.4 THERMAL PROPERTIES 26
2.4.1 TGA 26
2.4.2 DSC 26
2.5 WAXD STUDY OF SOLUTION-POLYMERIZED PA 10T 30
2.6 THERMO-MECHANICAL PROPERTIES 33
2.7 CONCLUSIONS 35
2.8 REFERENCES 36

CHAPTER 3 SYNTHESIS AND CHARACTERIZATION OF REACTIVE PA 10T OLIGOMERS AND THERMOSETS THEREOF 39

3.1 INTRODUCTION 40
3.2 SYNTHESIS AND CHARACTERIZATION 42
3.2.1 MATERIALS 42

3.2.2 Characterization 42
3.2.3 Synthesis of reactive end-caps 43
3.2.4 Reactive model compounds 45
3.2.5 Synthesis of reactive PA 10T oligomers 48
3.2.6 Preparation of thermoset films 49
3.3 Study of reactive oligomers 50
3.3.1 Solution polymerization 50
3.3.2 Thermal properties 51
3.3.3 Cure behaviour 53
3.3.4 Network Characterization 55
3.4 Study of thermoset films 56
3.4.1 Melting and crystallization 56
3.4.2 WAXD analysis of thermoset films 58
3.4.3 Thermo-mechanical properties 61
3.4.4 Mechanical properties 64
3.5 Conclusions 65
3.6 References 66

CHAPTER 4 SYNTHESIS AND CHARACTERIZATION OF REACTIVE SIDE-GROUP FUNCTIONALIZED COPOLYAMIDES AND THERMOSETS THEREOF 69

4.1 Introduction 70
4.2 Experimental 72
4.2.1 Materials 72
4.2.2 Characterization 73
4.2.3 Synthesis of PE comonomers 74
4.2.4 Synthesis of PE side-group functionalized copolyamides 76
4.2.5 Preparation of thermoset films 77
4.3 Study of side-group functionalized copolyamides 77
4.3.1 Thermal behavior of PE comonomers 77
4.3.2 Copolyamide structures and molecular weights 78
4.3.3 Thermal properties 81
4.4 Thermal cure of copolyamides 84
4.4.1 Post-condensation 84
4.4.2 Thermal cure behavior 87
4.5 Morphology of the thermoset films 88
4.5.1 Melting and crystallization 88
4.5.2 WAXD analysis of thermoset films 91
4.6 Thermo-mechanical properties 93
4.7 Mechanical properties 94
4.8 Approaches towards PA 10T thermosets 96

4.9 CONCLUSIONS **98**
4.10 REFERENCES **99**

CHAPTER 5 HIGH-TEMPERATURE SHAPE MEMORY BEHAVIOR OF PA 10T THERMOSETS **101**

5.1 INTRODUCTION **102**
5.2 EXPERIMENTAL **106**
5.2.1 MATERIALS 106
5.2.2 CHARACTERIZATION 107
5.3 SHAPE MEMORY EFFECT IN TORSION MODE **108**
5.4 DUAL-SHAPE MEMORY BEHAVIOR **110**
5.5 TRIPLE-SHAPE MEMORY BEHAVIOR **117**
5.6 CONCLUSIONS **124**
5.7 REFERENCES **125**

SUMMARY **127**

SAMENVATTING **129**

APPENDIX **131**

ACKNOWLEDGEMENTS **137**

CURRICULUM VITAE **139**

LIST OF PUBLICATIONS AND PRESENTATIONS **141**

Chapter 1

Introduction

1.1 Polyamides

Polyamides (PAs) remain a topic of interest because of their complex internal structure and their commercial importance and versatility. The amide group, along with its essential role in joining the monomers, dictates most of the properties of PAs. Amide groups participate in hydrogen bonding, and consequently organize polymer chains into ordered crystalline regions in most PAs, as shown in Figure 1.1. The crystalline regions substantially augment the strength and heat-resistance of PAs, leading to their use in demanding engineering applications.[1]

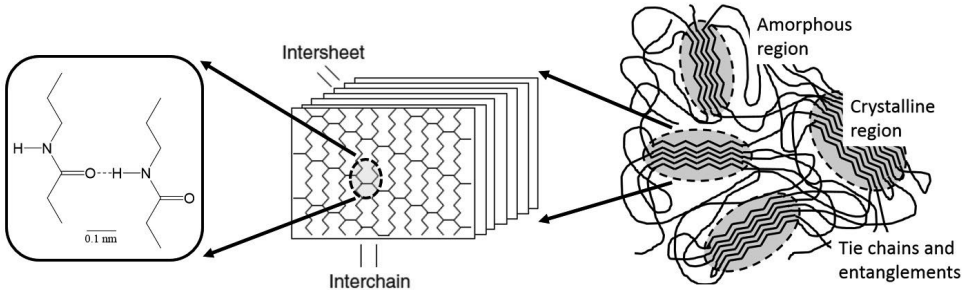

Figure 1.1 Structure of a semi-crystalline PA at different length scales. From left to right: hydrogen bonding between amides, stacked hydrogen-bonded sheets, crystalline and amorphous regions. Reproduced with permission from R. Rulkens, C. Koning, 5.18 Chemistry and Technology of Polyamides, Polymer Science: A Comprehensive Reference. Amsterdam: Elsevier, **2012**.[1]

1.2 Semi-aromatic polyamides

1.2.1 Monomer composition of semi-aromatic polyamides

According to the composition of PA chains, synthetic polyamides are generally classified into aliphatic, semi-aromatic and all-aromatic. Semi-aromatic PAs are polyamides in which part of the monomer molecules contain an aromatic structural unit. Semi-aromatic PAs were brought to market much later than aliphatic PAs, e.g. PA 6 and PA 66 (Scheme 1.1). The commercialization of semi-aromatic PAs was realized in 1980s to fulfil the requirements of engineering applications. Until now, a substantial amount of semi-aromatic PA resins and composites with different

compositions and formulations have been developed towards a wide range of applications.

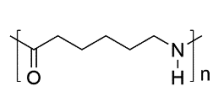

PA 6, T_g =50 ºC, T_m =225 ºC

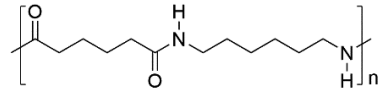

PA 66, T_g =60 ºC, T_m =265 ºC

Scheme 1.1 Molecular structures and thermal transition temperatures of PA 6 and PA 66.

As an intermediate between aliphatic and all-aromatic PAs, semi-aromatic PAs combine the melt processability of aliphatic PAs and part of the thermal and mechanical performance of fully aromatic PAs. Semi-aromatic PAs generally offer higher stiffness and strength, greater thermal and dimensional stability over most commonly used PA 6 and PA 66, leading to applications in complex electronic devices, domestic appliances and automotive thermal management components.[2, 3]

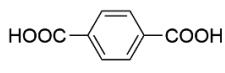

Terephthalic acid (TPA)

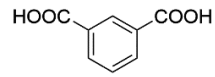

Isophthalic acid (IPA)

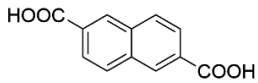

2,6-Naphthalic acid

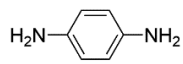

1,4-Phenylenediamine

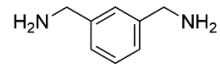

Meta-xylylenediamine (MXD)

Scheme 1.2 Examples of aromatic monomers in semi-aromatic polyamides.

Polyphthalamides (PPAs) are defined in ASTM D-5536 as a polyamide containing aliphatic diamines and at least 55 mol% of terephthalic acid (TPA) or isophthalic acid (IPA) or a combination of both (Scheme 1.2).[4] PPAs form the most important group of semi-aromatic PAs and were introduced into the market in the early 1990s and hold a dominant position in the family of commercial semi-aromatic PAs. They generally have low moisture absorption and moisture has little effect on their mechanical and electrical properties.[5] Most importantly, the carbonyl group of the amide functionality conjugates with the aromatic ring, leading to enhanced

molecular rigidity and consequently resulting in a much higher T_g of 100–125 °C compared to PA 6 and PA 66 (50 and 60 °C, respectively). PPAs can be semi-crystalline or amorphous, depending on the combination of the monomers. Linear TPA is the major component in commercial semi-crystalline PPAs. The kinked IPA, on the other hand, disrupts the linear progression of the polymer chains, therefore IPA is often used as a comonomer to control the crystallinity of the final PAs.

In addition to TPA and IPA, other types of monomers with aromatic moieties, such as 2,6-naphthalic acid,[6] 1,4-phenylenediamine[7, 8] and meta-xylenediamine (MXD),[9] have also been incorporated in semi-aromatic polyamides (Scheme 1.2). However, MXD seems to be the only monomer of interest for commercialization. PA MXD6, produced by Mitsubishi using MXD and adipic acid, has modest thermal properties with a T_m of 243 °C and a T_g of 110 °C. The success of MXD-based polyamide arises from its combination of good economics and outstanding oxygen barrier properties.[1]

1.2.2 Semi-crystalline polyphthalamides

PPAs are generally semi-crystalline when TPA is used as the main dicarboxylic acid monomer. The series of TPA-based PPAs, containing single straight-chain aliphatic 2-carbon to 13-carbon diamines, have been studied by different researchers.[7, 10-12] Figure 1.2 shows the T_m and T_g of these polymers as a function of the number of carbon atoms of the diamine monomer. Both T_g and T_m values tend to decrease with the increase in diamine length, which is due to the reduced density of stiff terephthalamide units. The resultant decrease in polymer chain stiffness leads to a decrease in T_g, and together with the weakened inter-chain hydrogen-bonding interaction reduces the T_m.

The T_m data show the well-known “odd-even” effect, which is consistent with the melting behaviour of aliphatic polyamides.[13] The PPAs with odd-carbon diamines show relatively lower T_ms compared to PPAs with even-carbon diamines, because the odd number of atoms results in less efficient packing of polymer chains and accordingly less energy is required to melt the crystals.

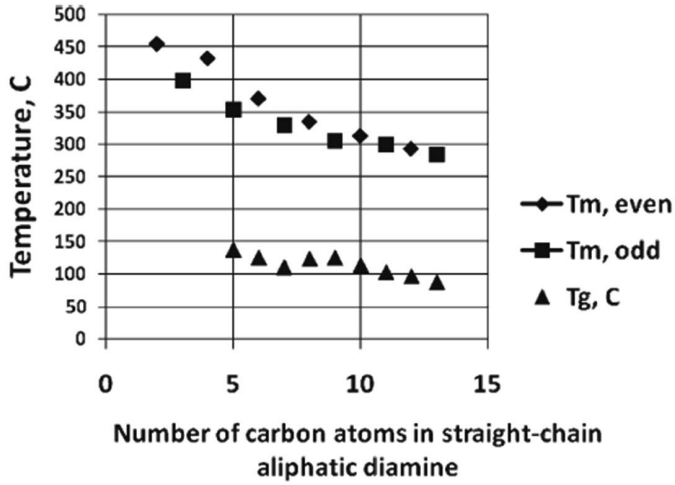

Figure 1.2 Melting points (T_m) and glass transition (T_g) temperatures of TPA-based PPAs. Reprinted with permission from K. Marchildon, *Macromol. React. Eng.* **2011**, 5, 32.[5]

Most commercial PPAs are based on poly(hexamethylene terephthalamide), PA 6T (Scheme 1.3). Homopolymer PA 6T exhibits a very high T_m of 370 °C, which complicates polymer preparation and processing. The high temperatures required during polycondensation promote side reactions such as branching and decomposition. Also, melt-processing is not possible due to severe decomposition at the processing temperature.[14] To overcome this problem, various comonomers, as shown in Scheme 1.3, have been introduced into PA 6T as chain modifiers to lower the T_m to an acceptable range of 280–330 °C. In practice, every comonomer will reduce T_m, so care has to be taken to select the comonomer such that the T_g is not decreased too much.[1]

The most utilized comonomer is adipic acid. TPA and adipic acid are of similar molecular length, so their repeating units can co-crystallize forming one crystalline phase at all compositions with minimal disruption in crystallinity.[15] Therefore, they display an almost linear trend of melting temperature with increasing the content of adipic acid comonomer, as shown in Figure 1.3. However, the T_g of the copolymer is greatly reduced to ~85 °C due to the aliphatic nature of adipic acid. Another comonomer introduced into PA 6T is caprolactam, which cannot co-crystallize with 6T units and disrupts the crystallinity to a great extent. It is also aliphatic and therefore reduces the T_g to ~100 °C. Partly replacing the linear TPA

monomer with kinked IPA has an effect of lowering T_m, while the T_g is only slightly affected, because the benzene ring of IPA is equally effective in immobilizing the amorphous regions. In order to keep the melt-crystallizability of the copolymer, the IPA content should not exceed 50 mol%.[16]

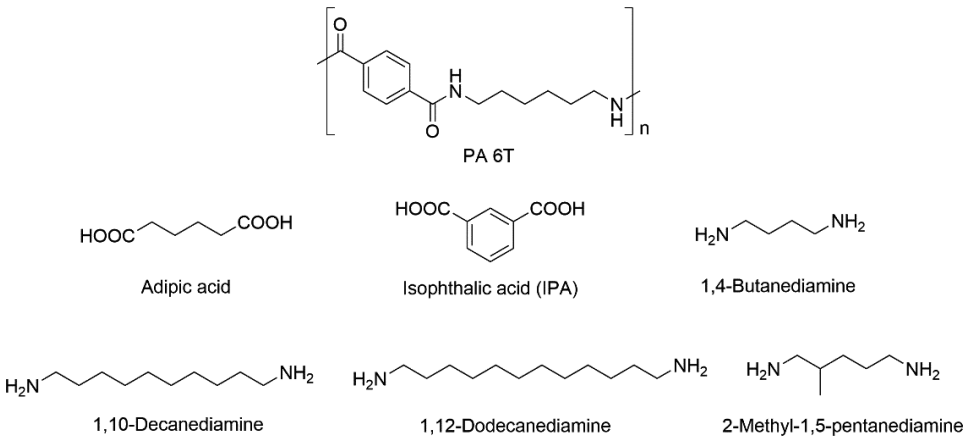

Scheme 1.3 Molecular structures of PA 6T and introduced comonomers to modify PA 6T

Some aliphatic diamines, such as 1,4-butanediamine, 1,10-decanediamine and 1,12-dodecanediamine,[17, 18] have been incorporated into PA 6T to partly replace 1,6-hexanediamine. Figure 1.3 shows the T_m of PA 6T-based copolyamides as a function of the molar amount of 6T units. The resultant random copolyamides, PA 4T/6T, PA 6T/10T and PA 6T/12T, show a eutectic melting behaviour, that is the T_ms pass through a minimum at a certain composition.[12] This is due to the formation of two different crystalline phases depending on the composition. This isodimorphic behaviour is different from the isomorphic behaviour of PA 6T/66 copolyamides. PA 4T/6T copolyamides show a minimal melting point of 331 °C at the composition of 40:60 mol% 4T:6T, which leads to a PPA with high T_g (125 °C) and acceptable melt-processability.[18] An asymmetric diamine comonomer, 2-methyl-1,5-pentanediamine (M5), has also been found to be effective in terms of modifying the melt behaviour of PA 6T.[19]

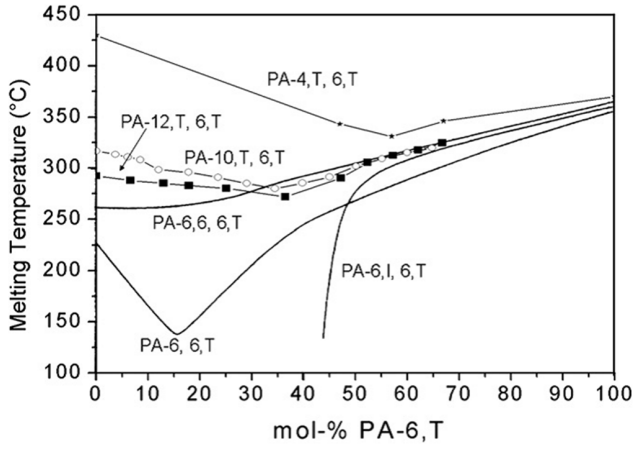

Figure 1.3 Melting behaviour of copolyamides PA 6T/10T, PA 6T/12T, PA 6T/66, PA 4T/6T, PA 6T/6I, PA 6T/6 versus PA 6T content in the copolyamides. Reprinted with permission from T. F. Novitsky; C. A. Lange; L. J. Mathias; et al. *Polymer* **2010**, 51, 2417.[12]

PA 9T and PA 10T based PPAs have also been introduced into the market place.[17, 20-22] Their longer diamine units reduce the density of amide groups, which in turn provides advantages in terms of low moisture absorption and dimensional stability. This makes them especially suitable for electrical and electronic applications. Some examples of commercial semi-crystalline PPA resins are listed in Table 1.1.

1.2.3 Amorphous polyphthalamides

Amorphous polyamides, usually amorphous PPAs, exhibit high transparency and high barrier properties against oxygen and carbon dioxide. In general, they exhibit excellent chemical resistance and environmental stress-cracking resistance compared to other transparent plastics such as poly(methyl methacrylate) or polycarbonate.[14] These amorphous PPAs have found application as automotive components, hollow fibers for semipermeable membranes, packaging materials, spectacles and sunglasses.

Table 1.1 Examples of commercial semi-crystalline PPA resins.

Entry	Structure	T_g (°C)	T_m (°C)	Common name (company)
1	PA 6T/6	100	295	Ultramid® T (BASF)
2	PA 6T/6I	125	320	Arlen® A (Mitsui)
3	PA 6T/6I/66	126	310	Amodel® AD1000 (Solvay)
4	PA 6T/66	90	310	Arlen® C (Mitsui)
5	PA 4T/X[a]	125	325	Stanyl® ForTii (DSM)
6	PA 6T/M5T	141	300	Zytel® HTN (DuPont)
7	PA 9T	125	300	Genestar® (Kuraray)
8	PA 10T/6T	116	295	Grivory® HT3 (EMS)
9	PA 10T/X[a]	125	285	Vestamid® M3000 (Evonik)
10	PA 10T	125	316	Vicnyl® (Kingfa)

[a] unreported component

The most significant physical properties of amorphous PPAs are T_g and water uptake.[1] T_g corresponds to the rigidity of polymer chains and becomes lower when polyamides pick up moisture. The water uptake ability is strongly dependent on the density of amide groups. High T_g (≥ 125 °C) and low water uptake (≤ 2% at 23 °C, 50% rel. humidity) are important selection criteria for the diamine monomers.

Disrupting monomer structures is necessary to prevent crystallization in these amorphous PPAs. The PPAs from IPA and linear aliphatic diamines tend to be amorphous due to the kinked structure of IPA. They do not crystallize from the melt, but do show solvent-induced crystallization.[23-25] PA 6I is one example of a commercial amorphous IPA-based PPA.[26] Diamine monomers containing methyl side-groups or cyclic structures also effectively disrupt the regularity of polymer

chains, and have found use in amorphous PPAs. Examples of these diamines are shown in Scheme 1.4.[27]

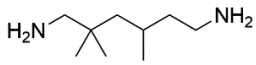

1,6-Diamino-2,2,4-trimethylhexane (NT)

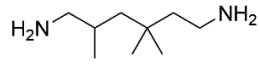

1,6-Diamino-2,4,4-trimethylhexane (IND)

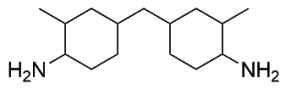

3,3'-Dimethyl-4,4'-diamino-dicyclohexylmethane (MACM)

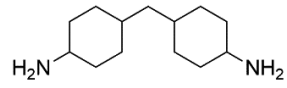

Bis-(p-aminocyclohexyl)-methane (PACM)

Scheme 1.4 Examples of aliphatic diamine monomers used in the design of amorphous PPAs.

1.3 Poly(decamethylene terephthalamide) (PA 10T)

Poly(decamethylene terephthalamide) (PA 10T) is an important member of the commercial PPA family, and has been produced by several companies such as EMS, Evonik and Kingfa. PA 10T has gained particular interest because the 10-CH_2 diamine can be obtained from castor beans without competing with the food chain. Compared with PA 6T based PPAs, PA 10T has a lower amide density due to the relatively higher molar mass of the 10-CH_2 diamine, which provides low moisture absorption (0.15% at 23 °C, 50% rel. humidity). However, the T_g of PA 10T remains fixed at ~125 °C, almost the same as that of PA 6T based PPAs.[5] This makes PA 10T more competitive for electrical and electronic applications.

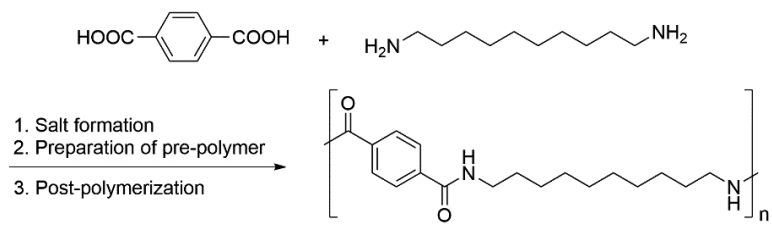

Scheme 1.5 Polymerization of PA 10T from TPA and 1,10-decanediamine.

In general, PA 10T is polymerized in a 3-stage polycondensation of TPA and 1,10-decanediamine.[11, 12, 28, 29] The reaction is shown in Scheme 1.5. The final stage is performed using the low molecular weight pre-polymer at high temperature (>250 °C) under reduced pressure. The polymer in this stage can be in the solid state,[11, 28] or in the molten state.[12, 29] In order to eliminate thermal decomposition and undesired side reactions during polymerization, solid-state polycondensation is expected to be the trend for the preparation of high T_m polyamides such as PA 10T.[1]

The thermal decomposition of PA 10T has been studied by analyzing the gaseous by-products produced from pyrolysis of PA 10T at 650 °C.[30] The results show that chain scission of PA 10T is mainly due to cleaving of the C-N bond, because it has a lower bond energy (285 kJ·mol^{-1}) compared to the C-C bond (356 kJ·mol^{-1}). The decomposition chemistry involves β-hydrogen transfer, free radical formation due to chain scission and hydrolysis of amide groups.

Double melting endotherms have been found for the PA 10T homopolymer.[11] The melting point of PA 10T, generally referring to the higher one, is reported to be around 315 °C. A study of crystallization kinetics of a PA 10T-based copolyamide indicates that the crystallization process is composed of primary and secondary stages. The crystallization rate of this PA 10T-based copolyamide was detected to be higher than that of common aliphatic polyamides.[31] To date, limited information has been reported on the crystalline structure of PA 10T.

Random copolyamides PA 10T/6T of various compositions have been investigated, and exhibit a eutectic melting behavior. A minimum T_m of 280 °C was observed when 30 wt% of 6T units exist in the copolyamide.[12] Since the 10T and 6T units are not able to co-crystallize, 10T-6T alternating units act as impurities that impede the formation of PA 10T crystals. Some commercial PA 10T based products are expected to contain 6T unit as a polymer modifier.

As a semi-crystalline engineering thermoplastic, PA 10T based PPAs are usually reinforced with glass fibers (15-60 wt%), achieving an elastic modulus of 6-20 GPa and tensile strength of 110-230 MPa depending on the wt% fiber used.[32] Carbon fibers are also used to reinforce PA 10T resins.[33]

1.4 Polyamide thermosets

To access PAs with better dimensional stability at elevated temperatures and better thermo-mechanical performance over time, researchers have explored the possibility of crosslinking PAs. Two crosslinking methods, ionizing irradiation and thermal curing, have been investigated to prepare PA thermosets.

1.4.1 Ionizing irradiation

Ionizing irradiation, especially electron beam irradiation, has been applied to crosslink aliphatic PAs, such as PA 66 and PA 6.[34-36] The ionizing irradiation generates reactive intermediates, which initiate the crosslinking reaction in the amorphous phase and at the PA crystallite interface.[36] An increase in yield strength and Young's modulus has been observed in an electron beam crosslinked PA 66.[35] The down side of this method is that degradation may take place, especially when high irradiation doses are used. This may lead to a deterioration in overall properties. Sometimes, a crosslinking agent, e.g. trially cyanurate, was used to promote crosslinking.[34]

Crosslinks can also be generated in the crystalline phase of PA with ionizing irradiation. Rubner et. al. have studied an aliphatic PA containing diacetylene functionalities in the polymer backbone (Scheme 1.6a).[37] The cross-polymerization of diacetylene is induced by electron beam irradiation, and mainly takes place in the crystalline regions. The generated bridges are perpendicular to the direction of the polymer backbone, and fix the polymer chains in the crystalline phase with complete retention of hydrogen bonds.[38] This results in a substantial increase in tensile strength and modulus of the polyamide fibers.[39]

1.4.2 Thermal curing

Thermal curing has also been explored to prepare PA thermosets. This approach essentially requires thermally curable groups, which should remain latent during polymer preparation and form crosslinks at elevated temperatures. A summary of curable groups used for PA thermosets are listed in Table 1.2.

Table 1.2 Curable groups used to prepare PA thermosets

Chemical structure	Name	Cure temp. (°C)	Position	References
	Cyano	300	pendant, end	40-44
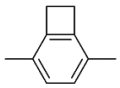	Benzocyclobutene	300	backbone	45, 46
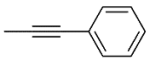	Phenylethynyl	350	pendant, end	47, 48
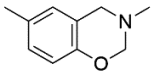	Benzoxazine	220	backbone	49
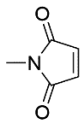	Maleimide	230	pendant, end	48, 50, 51

These groups are introduced into the PA chains and this results in processable curable precursors. The cure temperature should be high enough to guarantee a proper processing window, and should not exceed the decomposition temperature of the polymer. Additionally, producing volatiles during cure is not desired for void-free thermosets.[52] Thermosets can be prepared via direct cure of the precursor as a single-component system.[49] A second reactive component can also be introduced to promote crosslinking.[53-55]

Most research has focused on all-aromatic polyamides towards amorphous thermosets and liquid crystalline aramid fibers. The main route is to use monomers containing curable groups for polyamide preparation, some examples as shown in Scheme 1.6. These groups can be placed in the polymer backbone, or attached as pendant or end-groups at the polymer chains. Kim et. al. have explored cyano side-group functionalized all-aromatic polyamides (Scheme 1.6b) towards high-temperature thermosets.[44] Martin et. al. have studied poly(phenylene terephthalamide) (PPTA) copolymers containing benzocyclobutene in the polymer backbone (Scheme 1.6c).[46] A solid-state thermal treatment (>320 °C) of the as-spun aramid fibers triggers crosslinking between the polymer chains resulting in improved compressive and creep resistance.[45] By introducing a furanic component

to a maleimide side-group functionalized polyamide (Scheme 1.6d), the reversible Diels-Alder reaction between maleimide and furan groups can be used to prepare thermo-responsive gels,[50] and self-repairing films.[51]

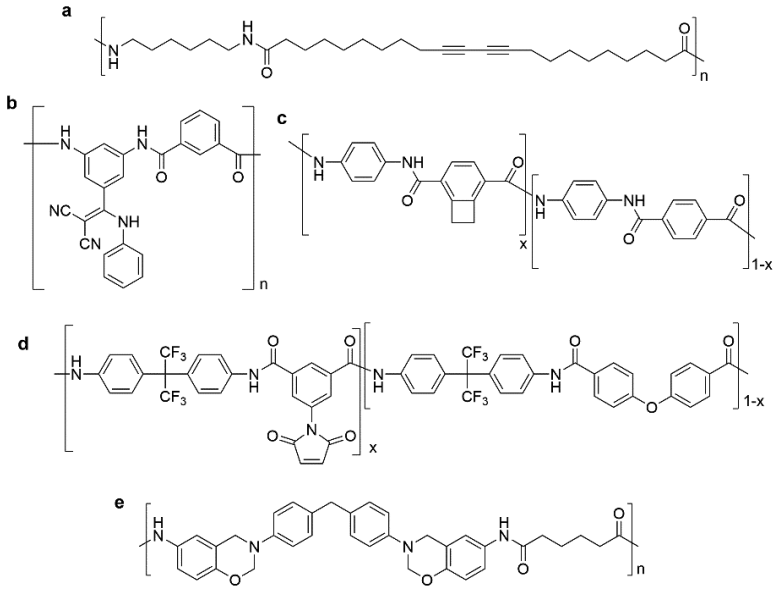

Scheme 1.6 Polyamide precursors containing curable groups (a) diacetylene;[38] (b) cyano;[44] (c) benzocyclobutene;[45] (d) maleimide;[50] (e) benzoxazine.[49]

One important approach towards high-performance thermosets is to cure reactive group end-capped oligomers, because the low molecular weight oligomers generally have better processability over their high molecular weight counterpart. This concept has been explored in all-aromatic liquid crystalline systems, such as polyesters,[56] and polyesterimides,[57] using phenylethynyl end-groups.[52] Knijnenberg et. al. have investigated phenylethynyl, maleimide and methacrylate end-capped PPTA oligomers towards compression-stable aramid fibers, which is one example of this concept used in polyamides.[58]

Little research has been done on crosslinking semi-aromatic polyamides. One example is based on a polyamide with benzoxazine groups in the polymer backbone (Scheme 1.6e). This route requires complicated synthetic procedures towards the benzoxazine-containing monomer, and leads to an amorphous

thermoset due to its low backbone symmetry and high crosslinking density.[49] Nevertheless, crosslinked semi-crystalline polymers are of great interest as structural polymers with added functionality as they can be used in single-component high temperature shape-memory applications.[59-61]

1.5 Scope and outline of the thesis

The work presented in this thesis describes a route towards PA 10T-based semi-crystalline thermosets. A mild-temperature solution polymerization method was developed to synthetize melt-processable PA 10T precursors with crosslinkable functionalities placed either in the polymer backbone or at the polymer chain-ends. The resulting precursors were thermally cured into single-component thermoset polymers. We have investigated how crosslinking affects polymer crystallinity and the thermo-mechanical properties of the final thermosets. Finally, the resulting semi-crystalline thermosets were evaluated as single-component high-temperature shape memory materials.

In **Chapter 2**, the solution polymerization conditions of PA 10T will be discussed. Synthetic parameters were optimized with the aim to prepare the highest molecular weight PA 10T possible under solution polymerization conditions. The thermal properties of the solution-polymerized PA 10T will be evaluated and contrasted with melt-processed PA 10T. Particularly, the melt and polymorphic behavior of the solution-polymerized PA 10T will be discussed in detail.

In **Chapter 3**, we will discuss the preparation of PA 10T thermoset films via a reactive oligomer precursor route. Crosslinkable PA 10T oligomers with thermally curable phenylethynyl end-groups were synthesized via solution polymerization. Rheological characterization was used to investigate the melt processability and cure behavior of the reactive oligomers. The morphology and thermo-mechanical properties of cured thermoset films will be discussed as function of cure time and temperature.

In **Chapter 4**, a different approach towards PA 10T-based thermosets will be discussed and is based on high molecular weight copolyamides with reactive phenylethynyl side-groups. Two phenylethynyl-based comonomers with different conformations were copolymerized with PA 10T, resulting in two series of high molecular weight copolyamides with various amounts of reactive pendant groups. The effect of the comonomer conformation and composition on the melting

behavior of the as-prepared precursors will be discussed. The thermo-mechanical and mechanical properties of the resultant thermoset films will be described.

In **Chapter 5**, the semi-crystalline polyamide thermosets as discussed in the previous chapters were investigated as high-temperature single-component shape memory films. A characterization method based on a torsion mode geometry was adopted in order to evaluate the shape fixity and recovery performance. The effect of semi-crystallinity on the shape memory properties of the thermoset films will be described in detail.

1.6 References

1. Rulkens, R.; Koning, C., 5.18 - Chemistry and Technology of Polyamides. In *Polymer Science: A Comprehensive Reference*, Matyjaszewski, K.; Möller, M., Eds. Elsevier: Amsterdam, 2012; pp 431-467.
2. Glasscock, D.; Atolino, W.; Kozielski, G.; Martens, M. *DuPont Engineering Polymers* **2008**.
3. Kemmish, D., *Practical guide to high performance engineering plastics*. ISmithers: 2011.
4. American Society for Testing and Materials, Standard Specification for Polyphthalamide (PPA) Injection Molded Materials, ASTM International, D 5336-03. In 2003.
5. Marchildon, K. *Macromolecular Reaction Engineering* **2011,** 5, (1), 22-54.
6. Yang, S.; Fu, P.; Liu, M.; Wang, Y.; Zhao, Q. *Journal of Applied Polymer Science* **2010,** 118, (2), 1094-1099.
7. Morgan, P. W.; Kwolek, S. L. *Macromolecules* **1975,** 8, (2), 104-111.
8. Deshmukh, Y. S.; Wilsens, C. H.; Verhoef, R.; Hansen, M. R.; Dudenko, D.; Graf, R.; Klop, E. A.; Rastogi, S. *Macromolecules* **2016**.
9. *Mitsubishi Gas Chemical Company, document "MGC-A History of Nylon-MXD6", 2009 April 9*; 2009.
10. Shashoua, V. E.; Eareckson, W. M. *Journal of Polymer Science* **1959,** 40, (137), 343-358.
11. Wang, W.; Wang, X.; Liu, B.; Li, R.; Wang, E.; Zhang, Y. *Journal of Applied Polymer Science* **2009,** 114, (4), 2036-2042.
12. Novitsky, T. F.; Lange, C. A.; Mathias, L. J.; Osborn, S.; Ayotte, R.; Manning, S. *Polymer* **2010,** 51, (11), 2417-2425.

13. Coffman, D.; Berchet, G.; Peterson, W.; Spanagel, E. *Journal of Polymer Science* **1947,** 2, (3), 306-313.
14. Kohan, M. I., *Nylon plastics handbook*. Hanser New York: 1995; Vol. 378.
15. Yu, A. J.; Evans, R. D. *Journal of Polymer Science* **1960,** 42, (139), 249-257.
16. Togashi, O.; Umetsu, H.; Iwamoto, M., EP0448221 A1. In Toray Industries, Inc.: 1991.
17. Hewel, M., EP1988113 B1. In Ems-Patent Ag: 2009.
18. Rulkens, R.; Crombach, R. C. B., US6747120 B2. In Dsm Ip Assets B.V.: 2004.
19. Mok, S. L.; Pagilagan, R. U., US5378800 A. In EI Du Pont De Nemours And Company, DuPont Canada Inc.: 1995.
20. Hayashihara, H.; Kashimura, T.; Oka, H.; Yokota, S., EP0659799 B1. In Kuraray Co., Ltd.: 1999.
21. Oka, H.; Matsuoka, H.; Kuki, T., US7009029 B2. In Kuraray Co., Ltd.: 2006.
22. Cao M., C. J., CN101456949 A. In Kingfa Sci&Tech Co. Ltd.: 2009.
23. Chapman, R.; Holmer, D.; Pickett, O.; Lea, K.; Saunders, J. *Textile Research Journal* **1981,** 51, (9), 564-573.
24. Laurati, M.; Arbe, A.; de Anda, A. R.; Fillot, L.-A.; Sotta, P. *Polymer* **2014,** 55, (12), 2867-2881.
25. Gaymans, R.; Van der Ham, A. *Polymer* **1984,** 25, (12), 1755-1758.
26. Nielinger, W. D. C. D.; Neuray, D. D. C. D.; Brassat, B. D. C. D., Polyamide aus isophthalsaeure und hexamethylendiamin. In Bayer Ag: 1979.
27. Dolden, J. G. *Polymer* **1976,** 17, (10), 875-892.
28. Wang, W. Z.; Zhang, Y. H. *Chinese Journal of Polymer Science* **2010,** 28, (4), 467-473.
29. Wang, Z.; Hu, G.; Zhang, J.; Xu, J.; Shi, W. *Chinese Journal of Chemical Engineering* **2016**.
30. A., Z. Y. P. J. Z. Z. W. W. L. In *Preparation and Pyrolysis Mechanism of Poly(decamethyleneterephthalamide)*, 7th China National Conference on Functional Materials and Applications, 2010; 2010.
31. Liu, H.; Yang, G.; He, A.; Wu, M. *Journal of Applied Polymer Science* **2004,** 94, (2), 819-826.
32. Evonik *VESTAMID® HTplus: PA 6T/X and PA 10T/X product range and main properties* 2012.
33. EMS *Grivory HT: Enhanced Performance at High Temperatures*; 2014.
34. Pramanik, N.; Haldar, R.; Bhardwaj, Y.; Sabharwal, S.; Niyogi, U.; Khandal, R. *Journal of Applied Polymer Science* **2011,** 122, (1), 193-202.

35. Sengupta, R.; Sabharwal, S.; Tikku, V.; Somani, A. K.; Chaki, T. K.; Bhowmick, A. K. *Journal of Applied Polymer Science* **2006,** 99, (4), 1633-1644.
36. Adem, E.; Burillo, G.; Del Castillo, L.; Vásquez, M.; Avalos-Borja, M.; Marcos-Fernández, A. *Radiation Physics and Chemistry* **2014,** 97, 165-171.
37. Beckham, H.; Rubner, M. F. *Macromolecules* **1989,** 22, (5), 2130-2138.
38. Beckham, H. W.; Rubner, M. F. *Macromolecules* **1993,** 26, (19), 5192-5197.
39. Beckham, H. W.; Rubner, M. F. *Polymer* **1991,** 32, (10), 1821-1825.
40. Mikroyannidis, J. A. *Journal of Polymer Science, Part A: Polymer Chemistry* **1995,** 33, (3), 381-387.
41. Mikroyannidis, J. A. *Polymer* **1994,** 35, (4), 839-844.
42. Diakoumakos, C. D.; Mikroyannidis, J. A. *Polymer* **1993,** 34, (10), 2227-2232.
43. Yu, G.; Wang, J.; Liu, C.; Lin, E.; Jian, X. *Polymer* **2009,** 50, (7), 1700-1708.
44. Kim, Y. J.; Chung, I. S.; In, I.; Kim, S. Y. *Polymer* **2005,** 46, (12), 3992-4004.
45. Jiang, T.; Rigney, J.; Jones, M.-C. G.; Markoski, L. J.; Spilman, G. E.; Mielewski, D. F.; Martin, D. C. *Macromolecules* **1995,** 28, (9), 3301-3312.
46. Jones, M. C. G.; Jiang, T.; Martin, D. C. *Macromolecules* **1994,** 27, (22), 6507-6514.
47. Sankaran, V.; Lin, S. C.; Marvel, C. *Journal of Polymer Science: Polymer Chemistry Edition* **1980,** 18, (2), 495-503.
48. Knijnenberg, A.; Bos, J.; Dingemans, T. J. *Polymer* **2010,** 51, (9), 1887-1897.
49. Agag, T.; Arza, C. R.; Maurer, F. H. J.; Ishida, H. *Journal of Polymer Science, Part A: Polymer Chemistry* **2011,** 49, (20), 4335-4342.
50. Liu, Y.-L.; Hsieh, C.-Y.; Chen, Y.-W. *Polymer* **2006,** 47, (8), 2581-2586.
51. Liu, Y. L.; Chen, Y. W. *Macromolecular Chemistry and Physics* **2007,** 208, (2), 224-232.
52. Dingemans, T., High-Temperature thermosets. In *Polymer Science: A Comprehensive Reference*, 1st ed.; M, M. K. M., Ed. Elsevier BV: Amsterdam, 2012; Vol. 5, pp 753-769.
53. Ivanov, D.; Gărină, C.; Grigoraş, C. *Journal of Applied Polymer Science* **2004,** 91, (2), 779-788.
54. Gupta, A.; Singhal, R.; Nagpal, A. K. *Journal of Applied Polymer Science* **2004,** 92, (2), 687-697.

55. Li, B.; Zhang, Y.; Wang, S.; Ji, J. *European Polymer Journal* **2009,** 45, (8), 2202-2210.
56. Iqbal, M. All-aromatic Liquid Crystal Thermosets and Composites Thereof. TU Delft, Delft, 2010.
57. Guan, Q. Design, Synthesis and Characterization of Novel (Multiblock) Copoly(esterimide)s and Their Shape-memory Properties. TU Delft, Delft, 2016.
58. Knijnenberg, A., *Compressive failure behaviour of novel aramid fibres*. TU Delft, Delft University of Technology: 2009.
59. Lendlein, A.; Kelch, S. *Angewandte Chemie International Edition* **2002,** 41, (12), 2034-2057.
60. Zhao, Q.; Qi, H. J.; Xie, T. *Progress in Polymer Science* **2015,** 49, 79-120.
61. Zhou, J.; Turner, S. A.; Brosnan, S. M.; Li, Q.; Carrillo, J.-M. Y.; Nykypanchuk, D.; Gang, O.; Ashby, V. S.; Dobrynin, A. V.; Sheiko, S. S. *Macromolecules* **2014,** 47, (5), 1768-1776.

Chapter 2 Solution Polymerization of Semi-aromatic Polyamide PA 10T

Abstract

In this chapter, we present the optimal conditions for the solution polymerization of poly(decamethylene terephthalamide) (PA 10T). A maximum M_n of 7.5 kg·mol^{-1} was achieved using NMP with 8 wt% $CaCl_2$ and triethylamine as acid scavenger. DSC analysis shows that the solution polymerized PA 10T oligomers exhibit two consecutive melt endotherms at 292 and 317 °C, respectively. The low temperature crystal form is reaction (solvent) induced and can be transformed into the high melting form after a heat treatment at 300 °C. After melt processing the oligomers into films, DMTA analysis show a glass transition temperature (T_g) of ~127 °C and the presence of an α' transition at 203 °C (0.1 and 1 Hz). This transition could be confirmed by DSC and variable-temperature WAXD experiments. The α' transition appears to be a reversible thermal process related to a sudden change in inter-sheet spacing.

2.1 Introduction

Semi-aromatic polyamides based on terephthalic acid and aliphatic diamines have been widely used in engineering applications because of their excellent heat resistance, fluid stability and thermo-mechanical properties.[1, 2] Crosslinked semi-aromatic PAs are of scientific and engineering interest because crosslinking can be used to control the degree of crystallinity of the final product, which in turn controls mechanical properties such as storage modulus (*E'*) and stress–strain behavior. Crosslinked semi-crystalline polymers have also attracted interest as functional polymers as they can be used in shape-memory applications.[3-5] As a model system for this study we have selected poly(decamethylene terephthalamide) or PA 10T. This semi-aromatic PA is of special interest because the 10-CH_2 diamine has a bio-based origin and improves the hydrophobicity of the polymer.[6] The hydrogen-bonded terephthalamide units provide a relatively stiff polymer backbone with a T_g of 127 °C and a high T_m of ~315 °C.[7, 8]

Crosslinkable PA 10T precursors intrinsically require reactive functionalities, which should remain latent during the polymerization step. Typically, PA 10T is prepared via a 3-stage high-temperature polycondensation procedure.[7-11] The high temperatures (>250 °C) employed during polycondensation will not be compatible with the reactive functionalities as they will start to react prematurely. For this reason we will adopt a solution polymerization method[7, 12, 13] in which we utilize a reactive diacyl chloride, in our case terephthaloyl chloride, and couple this under moderate heating conditions with the aliphatic 1,10-decanediamine monomer.

In this chapter, the solution polymerization of PA 10T was explored and optimized with the aim to obtain the highest molecular weight possible by varying the reaction conditions, such as temperature, salt concentration and acid scavenger. The melt behavior and solvent induced crystallization of PA 10T, of which little is known yet, has been investigated in detail. The highest molecular weight that can be reached via this route provides important guidelines for the synthesis of reactive PA 10T oligomers (Chapter 3).

2.2 Experimental

2.2.1 Materials

Terephthaloyl chloride was purchased from Sigma-Aldrich and purified via sublimation prior to use. 1,10-Decanediamine was generously supplied by DSM and dried under vacuum. Anhydrous LiCl (99%), anhydrous $CaCl_2$ (96%) was purchased from Sigma Aldrich and dried at 200 °C under vacuum. Extra dry NMP (water content <0.005%) and concentrated sulfuric acid (96%) were purchased from Acros Organic and used as received. Triethylamine (99%) was purchased from Sigma-Aldrich and distilled over CaH_2 before use.

2.2.2 PA 10T polymerization

All polymers were prepared according to the same synthetic procedure as shown in Scheme 2.1. A representative procedure is described below. Prior to the synthesis, all glassware was dried in a vacuum oven at 150 °C for at least 60 min.

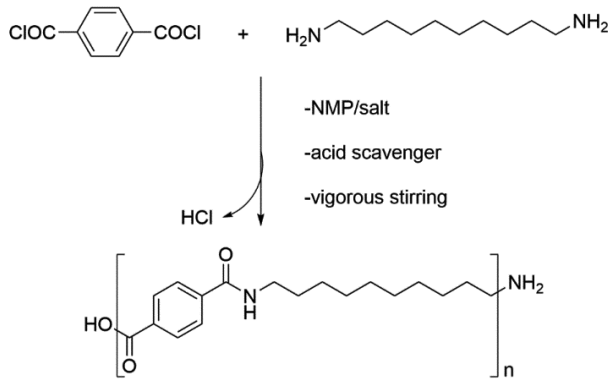

Scheme 2.1 Synthetic route towards PA 10T

In a 100 mL three-neck flask equipped with a mechanical stirrer, an argon inlet and a vacuum connection, 30 mL of NMP and 2.4 g of $CaCl_2$ were placed. Then 2.154 g (12.5 mmol) of 1,10-decanediamine were added. Vacuum was applied followed by an argon purge. This procedure was repeated 3 times to remove all traces of moisture. The mixture was stirred (100 rpm) and heated to 70 °C to allow

the 1,10-decanediamine to dissolve completely, and then cooled to 0 °C in an ice-bath. Triethylamine (5 mL) was injected into the flask with a syringe, followed by 2.538 g (12.5 mmol) of terephthaloyl chloride and the stirring rate was increased to 350 rpm. The reaction was kept at 0 °C for 30 min and at 55 °C for another 3 hours to obtain a viscous slurry. This slurry was precipitated in demineralized water and washed with demineralized water 3 times in a heavy duty blender. The final product was dried under vacuum at 60 °C, yielding 3.3 g PA 10T (88%). ^{1}H NMR (400 MHz, D_2SO_4, δ): 8.07 (s, 4H, Ar-H), 3.80 (s, 4H; CH_2), 1.85 (s, 4H; CH_2), 1.37 (s, 12H, CH_2).

2.2.3 Characterization

Solutions containing 0.5 g·dL^{-1} of polymer in concentrated sulfuric acid (96%) were prepared for single-point intrinsic viscosity measurements. Measurements were performed using an Ubbelohde viscometer in a 25 °C controlled water bath. The flow times reported are an average of three values that agreed within 0.2 seconds. Drop times of concentrated sulfuric acid and each of the polymer solutions were used to calculate the specific and relative viscosities. Single point intrinsic viscosities ([η]) were then determined using the Solomon and Ciuta equation (2.1).[14] The number average molecular weight was estimated using Mark-Houwink equation (2.2).

$$[\eta] = \frac{\sqrt{2*[\eta_{sp} - \ln(\eta_{rel})]}}{C} \qquad (2.1)$$

$$[\eta] = K\left(\frac{\mathrm{dL}}{\mathrm{g}}\right) * {M_\mathrm{n}}^{\alpha} \qquad (2.2)$$

where, η_{sp} is the specific viscosity, η_{rel} the relative viscosity and C the concentration. The Mark-Houwink constants K=5.58*10^{-4} dL·g^{-1} and α=0.81 as determined for poly(dodecamethylene terephthalamide) (PA 12T), were used to determine the number average molecular weight (M_n) for PA 10T as their molecular structures are very similar.[15]

Thermogravimetric analysis (TGA) was performed on a Perkin-Elmer Pyris diamond TG/DTA under a nitrogen atmosphere with a heating rate of 10 °C·min^{-1}.

Differential scanning calorimetry (DSC) was performed using a Perkin-Elmer Sapphire DSC under a nitrogen atmosphere at a heating/cooling rate of 20 °C·min^{-1}. Dynamic mechanical thermal analysis (DMTA) was performed on a Perkin-Elmer Diamond DMTA with film samples (0.2-0.3 mm thick) at a heating rate of 2 °C·min^{-1} under a nitrogen atmosphere. Data was collected at a frequency of 0.1, 1, and 10 Hz. Films were prepared via melt-compression at 340 °C for 5 min with a heating rate of 5 °C·min^{-1} and cooling rate of 20 °C·min^{-1}.

Wide angle X-ray diffraction (WAXD) studies were performed using a Bruker-AXS D5005 diffractometer with a CuKα-radiation source. The data were collected in the 2θ range of 3-30° at a rate of 2°·min^{-1} using a step size of 0.04°. The temperature of the sample was controlled with a PID controller within ±0.1 °C. FTIR spectra were collected in the range of 400 and 600 cm^{-1} at room temperature using a Perkin-Elmer Spectrum 100 FT-IR spectrophotometer.

2.3 Optimization of PA 10T solution polymerization

Solution polymerization is widely used to prepare fully aromatic polyamides (aramids), e.g. poly(p-phenylene terephthalamide),[16, 17] for which melting temperatures are usually too high to perform a high temperature polycondensation. This method can be extended towards the preparation of semi-aromatic polyamides with aliphatic diamine and highly reactive diacyl chlorides as monomers.

Morgan et. al. found that a tertiary amide is a better solvent medium for PAs than halogenated hydrocarbons.[12] Therefore we selected NMP for the synthesis of PA 10T and we used a salt (5 wt% LiCl or 8 wt% $CaCl_2$) to disrupt hydrogen-bond formation between the amide groups. As a consequence, the solubility of the polymer is increased, and this promotes growth of the polymer chains. The use of an acid scavenger is necessary, because the aliphatic diamine is deactivated by the HCl side-product, which in turn disrupts the stoichiometry.[16] Triethylamine and pyridine were chosen as the acid scavenger. Triethylamine can react with aromatic acid chlorides to form a non-reactive monoamide group and an alkyl halide. This reaction rate, compared to the amide-forming condensation reaction, can be suppressed significantly by decreasing the reaction temperature to 0 °C.[18] Therefore, the polymerization reactor was kept in an ice-bath at the start of the polymerization. The reaction mixture became opaque within seconds after the

addition of terephthaloyl chloride, which indicated a quick formation of PA 10T crystals precipitating from the reaction mixture.

Conditions for PA 10T solution polymerization, such as temperature, salt, acid scavenger and solvent, were explored through a series of experiments, as shown in Table 2.1. The M_n was found to be fairly sensitive to the reaction temperature and monomer concentration. Higher M_n was achieved using $CaCl_2$ instead of LiCl. Triethylamine was found to be a more effective acid scavenger than pyridine, and the lowest M_n was obtained without using any acid scavenger. The highest M_n of 7.5 kg·mol^{-1} was reached using 8 wt% $CaCl_2$, triethylamine as acid scavenger and a temperature of 0-55 °C. These conditions are considered as the optimal conditions for the solution polymerization of PA 10T, and used for all polymerizations, except when stated otherwise. An M_n value of 19.7 kg·mol^{-1} was reported for a PA 10T sample prepared using melt polycondensation.[7] The relatively lower M_n obtained from solution polymerization can be explained by the solubility limitation of the solvent system. During solution polymerization, the growing polymer chains tend to crystallize and precipitate, which greatly reduces the chance of end-groups (-COCl and -NH_2) to react.

After polymer work-up and drying, the obtained PA 10T appeared insoluble in common organic solvents, such as NMP, tetrahydrofuran and hexafluoro-2-propanol, which preclude solvent-based GPC analyses.[8] Concentrated sulfuric acid and trifluoroacetic acid can break the inter-chain hydrogen bonding and dissolve PA 10T, and therefore said solvents were used to characterize our PA 10T polymers.

Table 2.1 Intrinsic viscosity, estimated M_n, and yield of PA 10T samples polymerized under different conditions.

Sample	$[\eta]$ ($dL \cdot g^{-1}$)	M_n [a] ($kg \cdot mol^{-1}$)	Yield (%)	Conditions of solution polymerization[b]			
				Salt (wt%)	Acid scavenger	NMP (mL)	Temperature (°C)
PA 10T-1	0.11	0.65	88	$CaCl_2$ (8)	no	30	0-30
PA 10T-2	0.26	2.0	87	$CaCl_2$ (8)	Pyridine	30	0-55
PA 10T-3	0.48	4.2	88	LiCl (5)	Triethylamine	30	0-55
PA 10T-4	0.77	7.5	88	$CaCl_2$ (8)	Triethylamine	30	0-55
PA 10T-5	0.65	6.1	86	$CaCl_2$ (11)	Triethylamine	30	0-55
PA 10T-6	0.42	3.5	76	$CaCl_2$ (8)	Triethylamine	30	0-30
PA 10T-7	0.71	6.8	86	$CaCl_2$ (8)	Triethylamine	30	0-80
PA 10T-8	0.73	7.1	94	$CaCl_2$ (8)	Triethylamine	60	0-55

[a] M_n is obtained using Equation (2.2)

[b] The reaction time for all polymerizations was fixed at 3 hours.

2.4 Thermal properties

2.4.1 TGA

Four PA 10T samples (PA 10T-1, -2, -3 and -4) with distinctively different M_n values were selected for thermal analysis experiments. TGA was used to evaluate the dynamic thermal stability of the PA 10T samples under N_2 atmosphere, as shown in Figure 2.1. PA 10T-1, with the lowest M_n of 0.65 kg·mol^{-1}, shows two steps of weight loss. The first step appearing at 250-280 °C may be caused by post-condensation. The other samples with higher M_n values undergo a one-step decomposition from 430 °C to 500 °C, and reach almost 100% weight loss at 500 °C. The temperature of the maximum decomposition rate is about 478 °C for all samples, which is in agreement with literature.[8] As shown in Table 2.2, with the increase of M_n, the $T_d^{5\%}$ increases to 425 °C which is much higher than what is reported for aliphatic polyamides.[1]

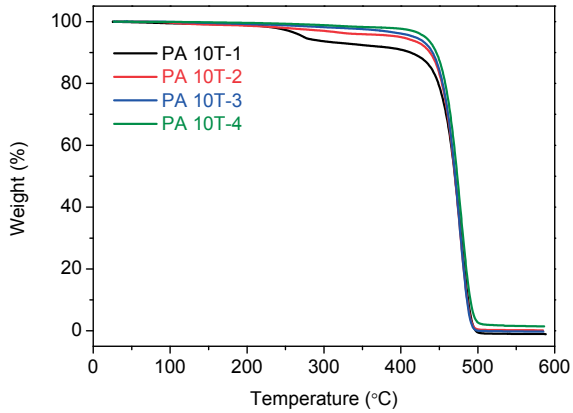

Figure 2.1 TGA thermograms of PA 10T under N_2 atmosphere with a heating rate of 10 °C·min^{-1}.

2.4.2 DSC

DSC was used to investigate the melt and crystallization behaviour of the PA 10T samples. Figure 2.2 depicts the 1st heating, cooling and the 2nd heating scans of PA 10T-1, -2, -3 and -4 samples using a heating/cooling rate of 20 °C·min^{-1}. The DSC results are summarized in Table 2.2.

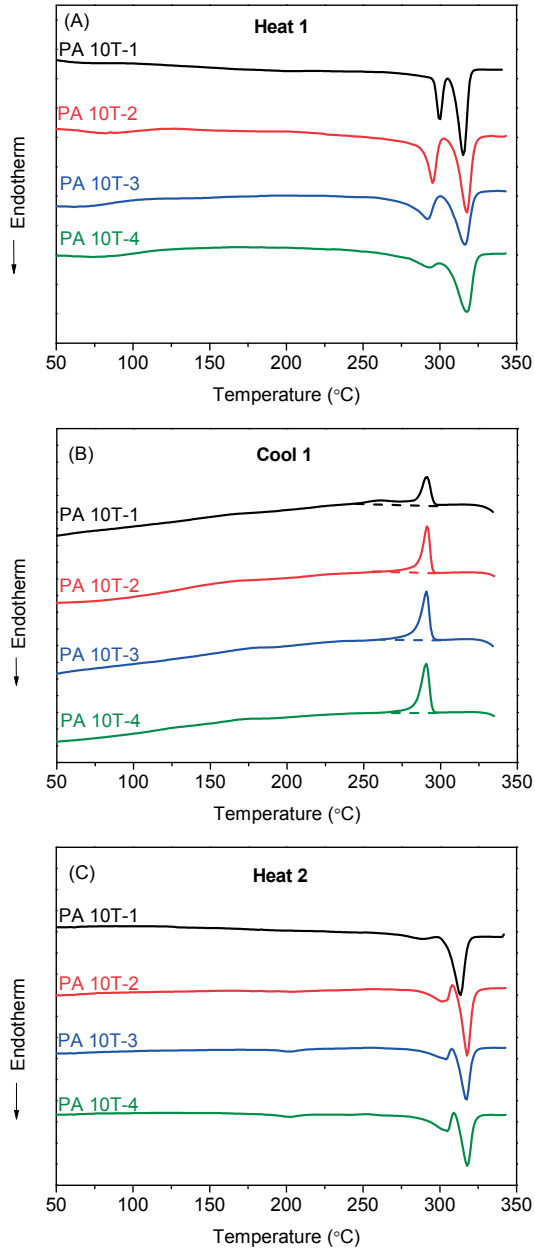

Figure 2.2 DSC traces of PA 10T 1-4 series using a heating/cooling rate of 20 °C·min^{-1}. (A) The 1st heating scans; (B) cooling scans; (C) the 2nd heating scans. Curves are normalized to sample weight and are offset for clarity.

Table 2.2 Thermal properties of the solution-polymerized PA 10T series 1-4

Sample	$T_d^{5\%}$ (°C)[a]	1st heating			T_c (°C)[e]	2nd heating		
		T_{m1} (°C)[b]	T_{m2} (°C)[c]	ΔH_m (J·g^{-1})[d]		T_{m1} (°C)[b]	T_{m2} (°C)[c]	ΔH_m (J·g^{-1})[d]
PA 10T-1	262	300	315	98	261, 291	289	314	80
PA 10T-2	400	295	317	95	291	302	318	82
PA 10T-3	418	292	316	93	291	304	318	80
PA 10T-4	425	292	317	89	291	305	318	81

[a] T_d is reported at 5 wt% weight loss under N_2.

[b] T_{m1} refers to the peak temperature of the 1st melting endotherm.

[c] T_{m2} refers to the peak temperature of the 2nd melting endotherm.

[d] ΔH_m is reported as the melting enthalpy of the double melting endotherms.

[e] T_c refers to the peak temperature of the crystallization exotherm.

None of the samples shows a glass transition by DSC. This means the fraction of the mobile amorphous phase, which contributes to the change in C_p associated with the glass transition, is too low to be detected.[19] The ΔH_m for a 100% crystallized PA 10T is not known, so the absolute degree of crystallinity for the PA 10T samples cannot be determined via DSC.

Double melting endotherms are observed for all PA 10T samples upon the 1st heating as shown in Figure 2.2 (A), which are separated by a crystallization exotherm, suggesting a recrystallization process in which the lower-melting crystals (T_{m1}) convert to the higher-melting crystals (T_{m2}). The lower melting crystals may be reaction(solvent)-induced crystallization, which is not uncommon for polymers prepared in solution.

Figure 2.2 (B) shows the crystallization exotherms obtained during the cooling scans. All samples exhibit similar crystallization behaviour with a well-defined exotherm at 291 °C. It is interesting to note that the exotherms have a long tail, which may be associated with a secondary crystallization process.[20] For PA 10T-1 with the lowest M_n, a small but discernible crystallization exotherm is shown at 261 °C. It should be noted that the PA 10T samples have to be considered as reactive pre-polymers (oligomers), which continue to polymerize when they melt. PA 10T-1, -2, -3 and -4 samples show an increase in M_n after the first heating scan. The molecular weight increased to 1.6, 3.9, 5.7 and 7.7 kg·mol^{-1}, respectively as measured by intrinsic viscosity.

Double melting endotherms are also detected in the 2nd heating traces of all samples, as shown in Figure 2.2 (C), suggesting that a fraction of the low temperature crystals still exists after the first heating scan. The T_{m2} of all samples is rather similar to what was observed in the 1st heating scans. PA 10T-1 with the lowest M_n exhibits the lowest T_{m1} (289 °C), which may be due to the large number of disrupting end-groups (-NH_2 or –COOH). The T_{m1} of PA 10T-2, -3 and -4 shifts to higher temperatures (302-305 °C) compared to that in the 1st heating scans (295-292 °C). This is contradictory as we observed an increase in M_n upon heating, which should not induce an increase in T_{m1}. Based on the DSC experiments, we propose that the crystal forms of the reaction(solution)-crystallized and melt-crystallized PA 10T samples are different. This crystalline behaviour is not unique and has been reported for a variety of semi-crystalline polyamides.[1, 6]

To gain more insights into the double melt behavior of PA 10T, the PA 10T-3 sample was used as a model compound. A thermal treatment was performed at

300 °C using the as-prepared PA 10T-3 sample, which is exactly between the double melting endotherms. The sharp crystallization exotherm observed in Figure 2.2(B) did not appear during Cool 1 in Figure 2.3 (A), indicating the lower-melting crystals do not crystallize during cooling. Upon reheating, only one sharp melting endotherm appeared at 317 °C (T_{m2}) with a higher ΔH_m (87 J·g^{-1}) than that for the second melting endotherm (65 J·g^{-1}) of the PA 10T-3. This indicates that the lower-melting crystals were erased in Heat 1, and converted into higher-melting crystals.

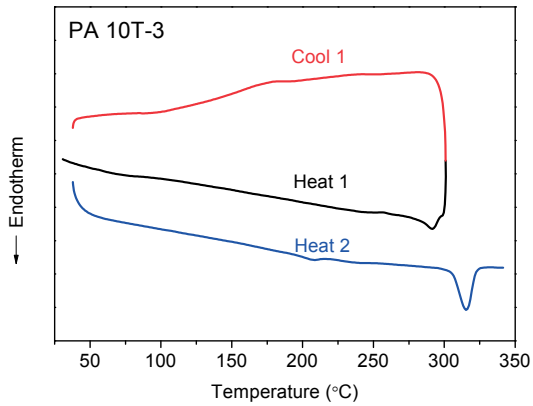

Figure 2.3 DSC traces of as-prepared PA 10T-3 sample, heated to 300 °C, cooled and reheated at 20 °C·min^{-1}.

The small exotherm appearing at 181°C during cooling and the endotherm at 209 °C during reheating will be discussed later in detail.

2.5 WAXD study of solution-polymerized PA 10T

Temperature-dependent WAXD was used to investigate the temperature variation of the solution polymerized PA 10T crystalline structure. Figure 2.4 (A) and (B) show the temperature dependence of the WAXD patterns of the as-prepared PA 10T-3 upon heating and cooling, respectively. The sample was measured up to 300 °C which lies between the double melting endotherms shown in DSC curve (Figure 2.2 A).

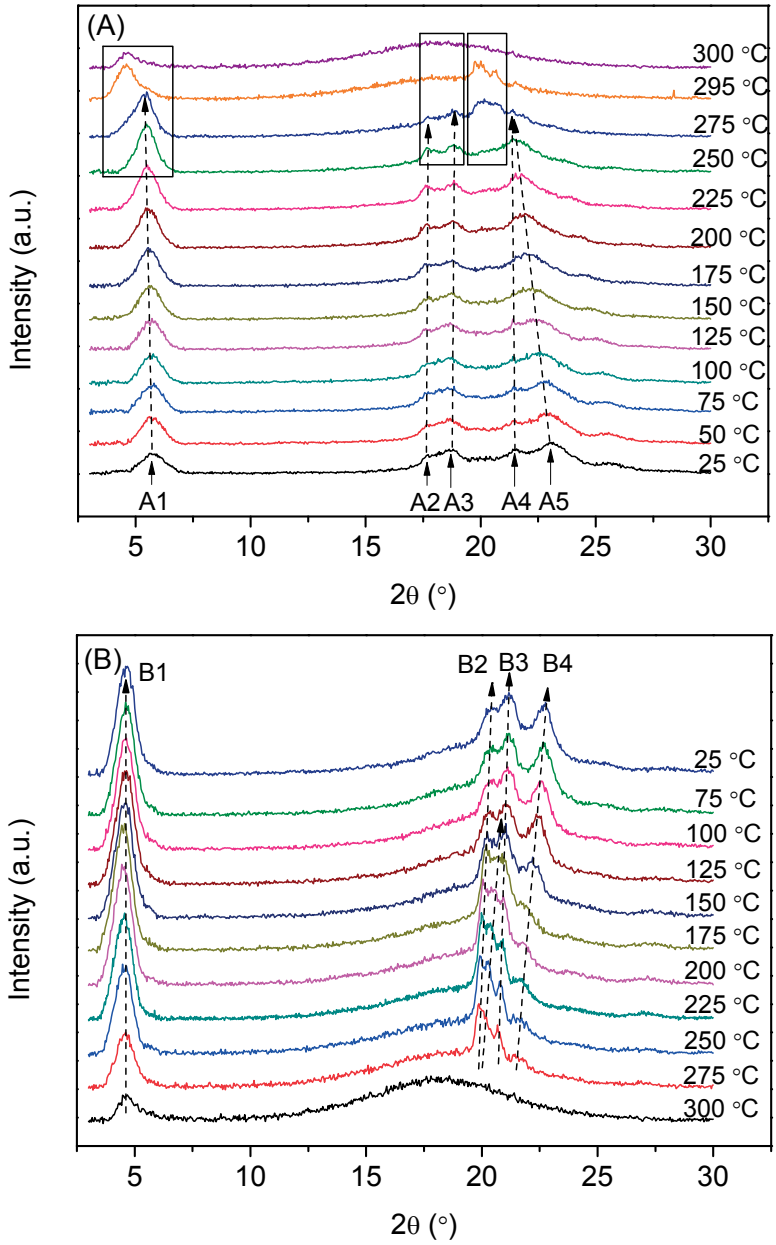

Figure 2.4 The temperature dependence of WAXD patterns of the as-prepared PA 10T-3 (A) heating process; (B) cooling process. The arrows point out the development of the reflections.

The major observed reflections for the as-prepared PA 10T-3 are labelled as A1 to A5 as shown in Figure 2.4 (A) and listed in Table 2.3. The 2θ of A1, A2, A3 and A4 reflections stay almost constant until 275 °C, while the A5 reflection shifts to lower 2θ, indicating an increase of intersheet distance. This phenomenon is often observed when heating an aliphatic polyamide sample up to its Brill transition temperature, e.g. 220 °C for PA 66.[21, 22] One explanation could be the increased conformational disorder of the methylene sequences upon heating, thereby pushing the hydrogen-bonded sheets further away from each other.[23]

Substantial variations take place in the WAXD patterns when the sample is heated above 250 °C, as shown in the rectangles in Figure 2.4 (A). The A2 and A3 reflections gradually vanish and disappear at 295 °C, whereas new reflections appear at 2θ 19.5-21°. Additionally, the A1 reflection shifts to lower 2θ. These changes clearly indicate a formation of a new crystal form. This crystalline transformation happens between 250 °C and 300 °C, in the temperature range of the first melting endotherm as shown in Figure 2.2 (A).

Table 2.3 Observed major 2θ reflections and *d*-spacings for as-prepared and heat-treated PA 10T-3

As-prepared PA 10T				**Heat-treated PA 10T**			
No.	**2θ (°)**	***d* (Å)**	**Index**	**No.**	**2θ (°)**	***d* (Å)**	**Index**
A1	5.76	15.34	$00l$	B1	4.84	18.26	$00l$
A2	17.74	5.00		B2	20.26	4.38	
A3	18.63	4.76		B3	21.29	4.17	
A4	21.53	4.13		B4	23.03	3.86	$0k0$
A5	23.13	3.85	$0k0$				

When the sample is subsequently cooled from 300 °C to 25 °C, we obtained a different WAXD pattern than the pattern of the as-prepared sample. The major

reflections of the heat-treated sample are labelled as B1 to B4 as shown in Figure 2.4 (B) and listed in Table 2.3. The newly developed WAXD pattern agrees with the literature results of a melt-polymerized PA 10T.[7] This demonstrates a complete crystalline transformation from the reaction(solution)-induced crystal form to the melt-crystallized crystal form. The general reason for the crystalline transformation of polyamides lies in the optimization of local packing preferences. Such crystalline transformations have been intensively studied in various aliphatic polyamides,[20, 24-29]

2.6 Thermo-mechanical properties

DMTA measurements were performed to characterize the thermo-mechanical properties of the melt-processed PA 10T films. We could not obtain defect-free films from PA 10T-1 and -2 due to their low melt viscosity, which precludes DMTA measurements on these samples. PA 10T-3 and -4 films were obtained using a standard melt-compression technique, and their DMTA results were summarized in Table 2.4. The DMTA curves for these two samples are rather similar, therefore, PA 10T-3 is shown as a representative sample. Figure 2.5 depicts the storage modulus (E'), loss modulus (E'') and tan δ as a function of temperature at frequencies of 0.1, 1 and 10 Hz.

Table 2.4 DMTA results of PA 10T

sample	T_g (°C) [a]	E' (GPa) [b] at 25 °C	$T_{\alpha'}$ (°C) [c]
PA 10T-3	127	4.1	203
PA 10T-4	128	4.4	203

[a] T_g is reported as the peak temperature of E'' at 1 Hz.

[b] E' at 25 °C is reported at 1 Hz.

[c] $T_{\alpha'}$ is reported as the peak temperature of tan δ.

The glass transition of PA 10T shows broad peaks of *E*" and tan *δ*. The peak temperature of *E*" at 1 Hz is taken as T_g, which is 127 °C. The broad glass transition suggests a wide mobility distribution of the amorphous chain segments.

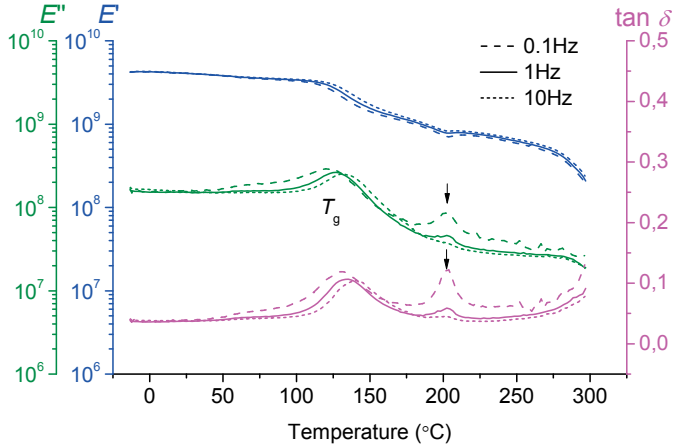

Figure 2.5 DMTA results of the PA 10T-3 film. Frequencies of 0.1, 1, and 10 Hz were used. The arrows point to the peaks of *E*" and tan *δ* at 203 °C.

The *E*" and tan *δ* curves show α' peaks at 203 °C, which is much higher than T_g. A similar α' peak at around 130 °C has been reported for annealed PA 66 and is associated with a sharp increase of the intersheet distance. Unlike the T_g which shifts with frequency, the temperature of these α' peaks is independent of frequency, which rules out the possibility of dynamic relaxation. The α' peaks show higher intensity at 0.1 Hz, while they are almost invisible at 10 Hz, suggesting that this transition is only observable at larger time scales. This points to a melting-like behaviour. The DSC results (Figure 2.3) present an exotherm (181 °C) and endotherm (209 °C) during the cooling and reheating scans, respectively, which are believed to be related to this transition. In addition, a change of slope in *E*' is observed when this α' transition takes place, suggesting that this transition in the crystals may have significant contributions on the E' between T_g and T_m.

This α' transition can also be detected via temperature-dependent WAXD. Figure 2.1S (A) and (B) show the temperature variation of the WAXD patterns of the melt-pressed PA 10T-3 film upon heating and cooling, respectively. The B4 reflection is associated with the intersheet distance in the crystals. Figure 2.6 (A)

and (B) show the associated *d*-spacing and intensity of the B4 reflection as a function of temperature, respectively. We found that the *d*-spacing values go through a sharp increase during heating from 150 to 225 °C, accompanied with a sharp decrease of the intensity. The reverse change is observed during cooling from 200 to 125 °C. The reason of this transition may lie in the mobility change of the 10-carbon-methylene segments between rigid hydrogen-bonded aromatic units. These short aliphatic chains may gain energy during heating to become more mobile and more disorder until an energetically stable state is achieved.

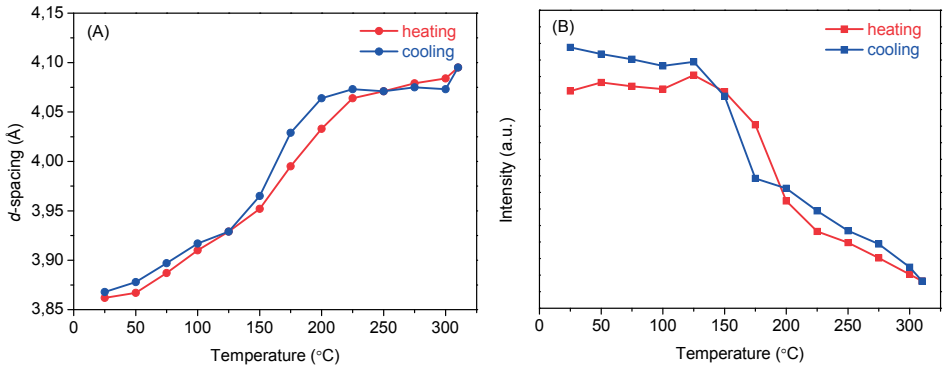

Figure 2.6 Evolution of (A) *d*-spacing corresponding to B4 reflection; (B) intensity of B4 reflection, during heating up to 310 °C and cooling down to 25 °C.

2.7 Conclusions

We have explored the solution polymerization of PA 10T, and investigated the thermal, morphological and thermo-mechanical properties of the as-prepared polymer and melt-pressed films. A maximum M_n of 7.5 kg·mol^{-1} was achieved using NMP with 8 wt% $CaCl_2$ and triethylamine as acid scavenger. The as-prepared PA 10T shows double melting endotherms at 292 and 317 °C, respectively. This behaviour is associated with a crystalline transformation as confirmed by DSC and WAXD. The reaction(solution)-induced crystals transform into the melt-crystallized crystals upon a thermal treatment at 300 °C. Moreover, a reversible α' transition is detected exclusively for the melt-pressed PA 10T film, which is the result of a sharp change in the intersheet distance as confirmed by DSC and WAXD. In DMTA, this transition is visible as a peak at 203 °C in *E*" and tan *δ*. This transition is

temperature independent but frequency dependent, which is in contrast with the glass transition (ca. 127 °C). The solution-polymerization conditions of PA 10T will be used for the synthesis of reactive PA 10T oligomers and copolymers as will be discussed in the following chapters.

2.8 References

1. Kohan, M. I., *Nylon plastics handbook*. Hanser New York: 1995; Vol. 378.
2. Marchildon, K. *Macromolecular Reaction Engineering* **2011,** 5, (1), 22-54.
3. Lendlein, A.; Kelch, S. *Angewandte Chemie International Edition* **2002,** 41, (12), 2034-2057.
4. Zhao, Q.; Qi, H. J.; Xie, T. *Progress in Polymer Science* **2015,** 49, 79-120.
5. Zhou, J.; Turner, S. A.; Brosnan, S. M.; Li, Q.; Carrillo, J.-M. Y.; Nykypanchuk, D.; Gang, O.; Ashby, V. S.; Dobrynin, A. V.; Sheiko, S. S. *Macromolecules* **2014,** 47, (5), 1768-1776.
6. Rulkens, R.; Koning, C., 5.18 - Chemistry and Technology of Polyamides. In *Polymer Science: A Comprehensive Reference*, Matyjaszewski, K.; Möller, M., Eds. Elsevier: Amsterdam, 2012; pp 431-467.
7. Novitsky, T. F.; Lange, C. A.; Mathias, L. J.; Osborn, S.; Ayotte, R.; Manning, S. *Polymer* **2010,** 51, (11), 2417-2425.
8. Wang, W. Z.; Zhang, Y. H. *Chinese Journal of Polymer Science* **2010,** 28, (4), 467-473.
9. Kim, Y. J.; Yohana, K. E.; Lee, H.-s.; Kim, J. *Industrial & Engineering Chemistry Research* **2012,** 51, (49), 15801-15810.
10. Wang, W.; Wang, X.; Liu, B.; Li, R.; Wang, E.; Zhang, Y. *Journal of Applied Polymer Science* **2009,** 114, (4), 2036-2042.
11. Wang, Z.; Hu, G.; Zhang, J.; Xu, J.; Shi, W. *Chinese Journal of Chemical Engineering* **2016**.
12. Morgan, P. W.; Kwolek, S. L. *Macromolecules* **1975,** 8, (2), 104-111.
13. Deshmukh, Y. S.; Wilsens, C. H.; Verhoef, R.; Hansen, M. R.; Dudenko, D.; Graf, R.; Klop, E. A.; Rastogi, S. *Macromolecules* **2016**.
14. Solomon, O.; Ciută, I. *Journal of Applied Polymer Science* **1962,** 6, (24), 683-686.

15. Novitsky, T.; Lange, C.; Jarrett, W.; Mathias, L.; Osborn, S.; Ayotte, R.; Manning, S. *Journal of Applied Polymer Science* **2010,** 116, (6), 3388-3395.
16. de Ruijter, C.; Jager, W. F.; Groenewold, J.; Picken, S. J. *Macromolecules* **2006,** 39, (11), 3824-3829.
17. Knijnenberg, A.; Bos, J.; Dingemans, T. J. *Polymer* **2010,** 51, (9), 1887-1897.
18. Hess, O. *Berichte der deutschen chemischen Gesellschaft* **1885,** 18, (1), 685-688.
19. Li, L.; Curran, G. *Thermal Analysis Application Note, Perkin Elmer Inc* **2006**.
20. Morales-Gámez, L.; Soto, D.; Franco, L.; Puiggalí, J. *Polymer* **2010,** 51, (24), 5788-5798.
21. Jones, N.; Atkins, E.; Hill, M.; Cooper, S.; Franco, L. *Macromolecules* **1996,** 29, (18), 6011-6018.
22. Jones, N.; Atkins, E.; Hill, M.; Cooper, S.; Franco, L. *Polymer* **1997,** 38, (11), 2689-2699.
23. Tashiro, K.; Yoshioka, Y. *Polymer* **2004,** 45, (18), 6349-6355.
24. Nakagawa, T.; Nozaki, K.; Maeda, S.; Yamamoto, T. *Polymer* **2015,** 57, 99-104.
25. Atkins, E.; Hill, M.; Hong, S.; Keller, A.; Organ, S. *Macromolecules* **1992,** 25, (2), 917-924.
26. Laurati, M.; Arbe, A.; de Anda, A. R.; Fillot, L.-A.; Sotta, P. *Polymer* **2014,** 55, (12), 2867-2881.
27. Murase, S. K.; Casas, M. T.; Martínez, J. C.; Estrany, F.; Franco, L.; Puiggalí, J. *Polymer* **2015,** 76, 34-45.
28. Puiggalí, J.; Franco, L.; Alemán, C.; Subirana, J. *Macromolecules* **1998,** 31, (24), 8540-8548.
29. Villaseñor, P.; Franco, L.; Subirana, J.; Puiggali, J. *Journal of Polymer Science Part B: Polymer Physics* **1999,** 37, (17), 2383-2395.

Chapter 3 Synthesis and Characterization of Reactive PA 10T Oligomers and Thermosets Thereof

Abstract

We have explored the synthesis of semi-crystalline polyamide (PA) thermosets via a reactive PA oligomer precursor route. Poly(decamethylene terephthalamide) (PA 10T) oligomers with a target M_n of 1K and 3K g·mol^{-1} were synthesized via solution polymerization and end-capped with reactive phenylethynyl (PE) groups. The reactive oligomers could be cured in a stepwise manner using successive high temperature treatment steps. Depending on the concentration of PE end-groups, the degree of crystallinity of the final thermosets can be controlled and depressed by 60% for the crosslinked 3K precursor and completely eliminated for the crosslinked 1K precursor. From the calculated molecular weight between crosslinks, we estimated that 35–41% of the PE end-groups form crosslinking functionalities, and the remainder of the PE end-groups contribute to chain extension. All thermoset films are stable up to ~400 °C in DMTA experiments due to network formation, which effectively increases the maximum use temperature of PA 10T by 100 °C.

3.1 Introduction

Semi-aromatic and aliphatic polyamides (PAs) have been widely used in demanding engineering applications because of their excellent heat resistance, fluid stability and thermo-mechanical properties.[1] To access PAs with better dimensional stability at elevated temperatures, researchers have explored the possibility of crosslinking PAs. Ionizing irradiation and thermal curing protocols have been used to prepare semi-aromatic and aliphatic PA thermosets. Ionizing irradiation, especially electron beam irradiation, was used to crosslink aliphatic PAs, such as PA 66 and PA 6.[2-4] The ionizing irradiation initiates crosslinking in the amorphous phase and the crystallite interface of the PAs.[3] An increase in yield strength and Young's modulus was observed for electron beam crosslinked PA 66.[4] The downside of this method is that degradation may take place, especially when high irradiation doses are used. Also, this method is only suitable for thin film applications due to the limited penetrating depth of the radiation. Little research has been reported on crosslinked semi-aromatic PAs. One example is based on the thermal cure of a PA precursor with benzoxazine groups placed in the polymer backbone.[5] This route requires complicated synthetic procedures and results in an amorphous thermoset (T_g = 169 °C) due to the high crosslinking density.

Crosslinked semi-aromatic PAs are of scientific and engineering interest because crosslinking can be used to control the degree of crystallinity of the final product, which in turn controls mechanical properties such as storage modulus (*E'*) and stress-strain behavior. Crosslinked semi-crystalline polymers have also attracted interest as functional polymers as they can be used in shape-memory applications.[6-8] When the reactive functionalities are placed at both polymer chain-ends, a reactive oligomer or macro-monomer can be obtained, which has the additional advantage of a low melt viscosity (ease of processing).

As a model system for this study we have selected poly(decamethylene terephthalamide) or PA 10T. This semi-aromatic PA is of special interest because the 10-CH_2 diamine has a bio-based origin and improves the hydrophobicity of the polymer.[9, 10] Three crosslinkable functionalities, phenylethynyl (PE), maleimide (MI) and methylethynyl (ME), have been selected as potential end-groups because of their accessibility and cure characteristics. In order to prevent premature reaction of the end-groups during high-temperature polycondensation, a mild-temperature solution polymerization method described in Chapter 2 will be adopted for the synthesis of the reactive PA 10T oligomers.

Phenylethynyl (PE) is well-known and used as chain extender/crosslinker in a variety of all-aromatic high-performance polymers.[11-15] PE is known for its excellent thermal stability, volatile-free polymerization and high cure temperature. MI-based functionalities have also found extensive use in high-performance thermosets.[16] It should be noted that the amine-maleimide Michael addition takes place during solid state curing (<180 °C) in systems containing aromatic amines.[17] The aliphatic diamine used in PA 10T may promote this side-reaction due to its stronger nucleophilicity.[18] Undesired branching or crosslinking may take place if Michael addition occurs during solution polymerization, which will preclude the use of MI. The use of ME-based functionalities is only found in a few recent patents about polyamide[19] and polyimide[20] thermosets. The cure temperature for ME seems to be between that for PE and ethynyl, however, the cure mechanism and after-cure properties are not well understood.

In this chapter we will discuss the synthesis and properties of a semi-aromatic crosslinked PA model system PA 10T. MI, ME and PE-based end-caps, as shown in Table 3.1, have been evaluated in model compounds with regard to preparation chemistry and cure behavior. Thermosets were prepared from reactive PA 10T oligomers with a target M_n of 1K and 3K g·mol^{-1}. The cure behavior, the thermo-mechanical and morphological properties of the final semi-crystalline thermosets were investigated and will be discussed in detail.

Table 3.1 Molecular structures of MI, ME, and PE-based end-caps.

Type	Molecular structure
MI-COCl	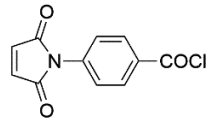
ME-COCl	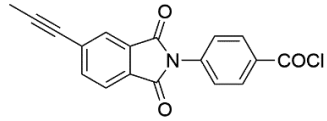
PE-COCl	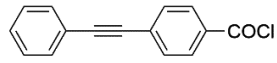

3.2 Synthesis and characterization

3.2.1 Materials

Terephthaloyl chloride was purchased from Sigma-Aldrich and purified via sublimation prior to use. 1,10-Decanediamine was generously supplied by DSM and dried under vacuum. $CaCl_2$ (96%) was purchased from Acros Organic and dried at 200 °C under vacuum. Triethylamine (99%) was purchased from Sigma-Aldrich and distilled over CaH_2 before use. Extra dry N-methyl-2-pyrrolidone (NMP, water content <0.005%) was purchased from Acros Organic and used as received. Trifluoroacetic acid (TFA, 99%), thionyl chloride (99%), 4-aminobenzoic acid (99%), anhydrous chloroform (99%), anhydrous sodium acetate (99%) and anhydrous N,N-dimethylformamide (99.8%) were purchased from Sigma-Aldrich. Acetic anhydride (98%) and maleic anhydride (99%) were purchased from Merck. 4-Methylethynyl phthalic anhydride (MEPA) was received from Nexam and used as received. 4-Phenylethynyl benzoic acid was purchased from Fluorochem and recrystallized from ethanol. The solution-polymerized homopolymer PA 10T-4 sample described in Chapter 2 was used as the reference sample, and denoted as PA 10T-ref.

3.2.2 Characterization

^{1}H and ^{13}C NMR spectra were recorded using a 400 MHz Bruker WM-400 at 25 °C. Mass spectra (MS) were recorded using a Shimadzu QP2010S over the m/z range of 45-900. The oven of MS was heated from 50-300 °C at 10 °C·min^{-1} under high vacuum (0.055 mbar). WAXD studies were performed using a PANalytical X'Pert Pro PW3040/60 diffractometer with CuKα-radiation. Data was collected in an angular 2θ range of 3-30° at a rate of 2°·min^{-1} and a step size of 0.008°.

The density of the thermoset films was measured using a Mettler Toledo AG204 Delta-Range scale equipped with a density measurement kit (gravimetric method according to Archimedean principle). The gel fraction of the thermoset films was determined using the Equation (3.1)

$$gel\ fraction = \frac{W_g}{W_0} \times 100\% \quad (3.1)$$

where W_g and W_0 are the sample weight before and after extraction with TFA, respectively.

Uniaxial tensile tests were performed on an Instron Model 3365 universal testing system equipped with a 1 kN load cell. Tensile specimens having approximate width of 2.5 mm, thickness of 0.25 mm and length of 20 mm between the clamps were stretched at 25 °C at a tensile rate of 0.2 mm·min^{-1}. The elastic modulus was measured by calculating the slope of the stress-strain curve between 0.1 and 0.3% strain. Data reported represent the average value of 3 specimens.

The rheological behaviour of the oligomers was investigated using a ThermoFisher Haake MARS III rheometer equipped with a force-rebalanced transducer in a parallel plate geometry (8 mm in diameter). Pelletized samples of 8 mm in diameter and ~0.5 mm in thickness were prepared by compression at room temperature. The samples were tested under N_2 with temperature ramping (5 °C·min^{-1}) from 200 °C to 350 °C followed by an isothermal hold at 350 °C for 50 min. Measurements were performed at a frequency of 1.0 Hz and a strain amplitude of 0.1%, which lies within the linear viscoelastic range of the material.

TGA was performed on a Perkin-Elmer Pyris diamond TG/DTA under a nitrogen atmosphere with a heating rate of 10 °C·min^{-1}. DSC was conducted on a Perkin-Elmer Sapphire DSC under a nitrogen atmosphere at a heating/cooling rate of 20 °C·min^{-1}. DMTA was performed on a Perkin-Elmer Diamond DMTA with film samples (0.2-0.3 mm thick) at a heating rate of 2 °C·min^{-1} under a nitrogen atmosphere. Data was collected at a frequency of 1 Hz.

3.2.3 Synthesis of reactive end-caps

4-Maleimidobenzoyl chloride (MI-COCl). The title compound was prepared and purified according to a literature procedure[21] as shown in Scheme 3.1. T_m = 157 °C (157-158 °C [22]). ^{1}H NMR ($CDCl_3$) δ(ppm): 6.91 (s, 2H), 7.63-7.65 (d, *J*=8.8 Hz, 2H), 8.20-8.22 (d, *J*=8.8 Hz, 2H). ^{13}C NMR ($CDCl_3$) δ(ppm): 125.1, 131.7, 132.2, 134.6, 137.6, 167.5, 168.5. MS m/z (relative intensity): 234.90 (M+, 3.6), 200.05 (100.0), 172.10 (24.3), 144.10 (17.5), 116.15 (34.9), 90.10 (40.9), 82.05 (22.8), 63.05 (37.6), 54.10 (51.8).

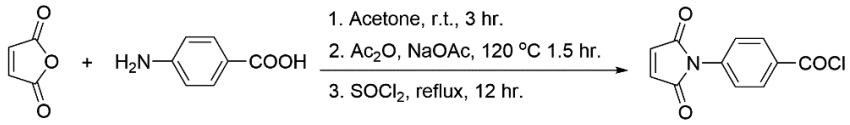

Scheme 3.1 Synthetic route towards MI-COCl

4-(methylethynyl phthalimido) benzoyl chloride (ME-COCl). According to Scheme 3.2, a 100 mL round bottom flask equipped with a reflux condenser was charged with 250 mL acetic acid and MEPA 18.6 g (0.1 mol). The mixture was heated to ~120 °C until all solids were dissolved. 4-Aminobenzoic acid 13.7 g (0.1 mol) was added and this mixture was refluxed for 4 hours. After cooling to room temperature, the precipitated product was filtered, washed with acetic acid and ethanol, and dried under vacuum at 60 °C, yielding 25.9 g (85%) of the intermediate as off-white powder. The intermediate (10 g) was treated with 25 mL $SOCl_2$ in a 100 mL round bottom flask. The reaction mixture was refluxed for 12 hours under an argon purge before the excess $SOCl_2$ was distilled off. The crude product was purified via recrystallization from dry chloroform, yielding 7.6 g (72%) of the title compound. T_m = 183 °C. ^{1}H NMR ($CDCl_3$) δ(ppm): 2.12 (s, 3H), 7.71-7.73 (d, J=8.4 Hz, 2H), 7.77-7.79 (d, *J*=7.6 Hz, 1H), 7.87-7.89 (d, *J*=8.0 Hz, 1H), 7.93 (s, 1H), 8.24-8.26 (d, J=8.4 Hz, 2H). ^{13}C NMR ($CDCl_3$) δ(ppm): 4.6, 78.4, 92.4, 123.9, 125.9, 126.8, 129.4, 131.5, 131.6, 131.8, 132.1, 137.7, 138.1, 166.0, 167.6. MS m/z (relative intensity): 323.10 (M+, 6.9), 288.15 (100.0), 260.10 (24.5), 142.10 (20.5), 114.15 (40.6), 113.10 (24.4), 88.05 (26.1), 63.10 (37.0).

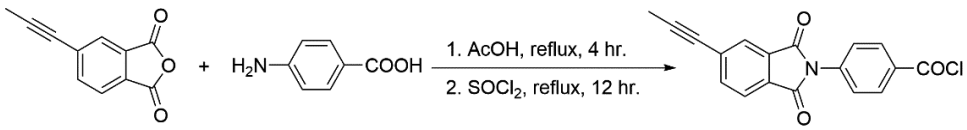

Scheme 3.2 Synthetic route towards of ME-COCl

4-phenylethynyl benzoyl chloride (PE-COCl). The title compound was prepared from 4-phenylethynyl benzoic acid as illustrated in Scheme 3.3. A mixture of 4-phenylethynyl benzoic acid (10 g, 45 mmol) in 25 mL $SOCl_2$ was refluxed at 80 °C for 12 hours under an argon purge before the excess $SOCl_2$ was distilled off. The crude product was purified via recrystallization from dry hexane, yielding 8.1 g (75%) of

the title compound. T_m = 85 °C (89-90 °C[23]) ^{1}H NMR ($CDCl_3$) δ(ppm): 7.37-7.38 (m, 3H), 7.54-7.56 (m, 2H), 7.62-7.64 (d, *J*=8.0 Hz, 2H), 8.08-8.10 (d, *J*=8.0 Hz, 2H). ^{13}C NMR ($CDCl_3$) δ(ppm): 88.0, 94.6, 122.2, 128.5, 129.2, 130.7, 131.3, 131.8, 131.9, 132.1, 167.7. MS m/z (relative intensity): 240.00 (M+, 26.9), 205.05 (100.0), 176.00 (53.0), 151.10 (27.3), 88.10 (48.2).

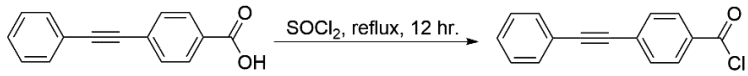

Scheme 3.3 Synthetic route towards PE-COCl

3.2.4 Reactive model compounds

We tried to synthesize well-defined model compounds to evaluate the end-groups in terms of chemistry and processing window. The reactions were performed using 1,10-decanediamine and each end-cap in a 1:2 molar ratio. The preparation procedure is depicted in Scheme 3.4.

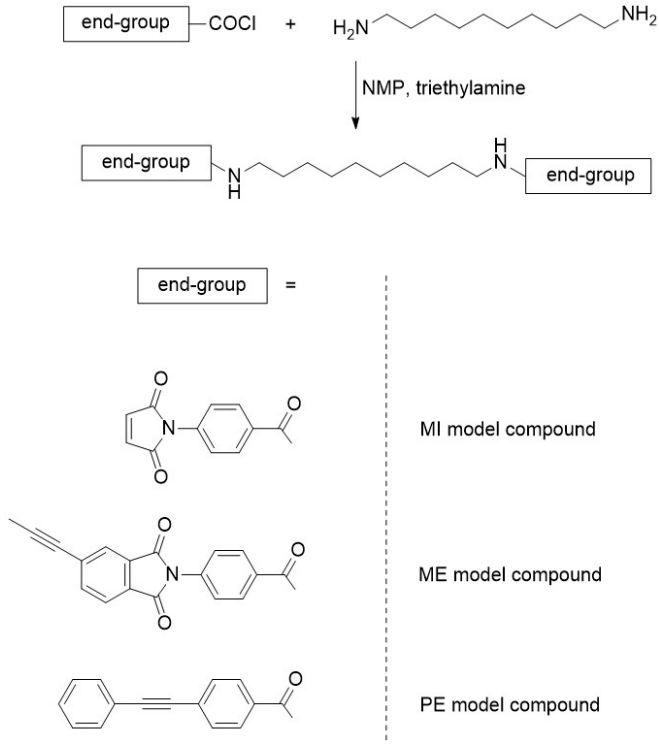

Scheme 3.4 Preparation of MI, ME and PE model compounds

MI model compound. In a 100 mL dry flask with argon purge, 30 mL of NMP was placed followed by 1,10-decanediamine 0.431 g (2.5 mmol). The mixture was stirred and heated to 70 °C to allow the 1,10-decanediamine to dissolve completely, and then cooled to 0 °C on an ice-bath. Triethylamine (1 mL) was added to the flask, followed by MI-COCl 1.178 g (5 mmol). The reaction was stirred at 0 °C for 30 min and 3 h at 55 °C. A cloudy mixture was formed, which was precipitated in water and the collected solids were washed 3 times with water. The title compound was obtained after drying under vacuum at 60 °C overnight.

The obtained model compound was characterized using ^{1}H NMR in TFA-d solvent. The peak area ratio of maleimide protons (=C-H) to phenyl protons (ϕ-H) is 1:2 for the MI-COCl end-cap, however, this value is reduced to 0.7:2 for the MI model compound. This indicates that a Michael-type addition takes place rapidly under the used conditions and consumes ~30% of the maleimide groups. This side reaction results in a product that is a partially reacted (chain-extended) maleimide as shown in Figure 3.1, and is expected to induce undesired branching and premature crosslinking when used in the polymerization of PA 10T oligomers. Therefore, the use of MI-COCl as an end-cap is discontinued.

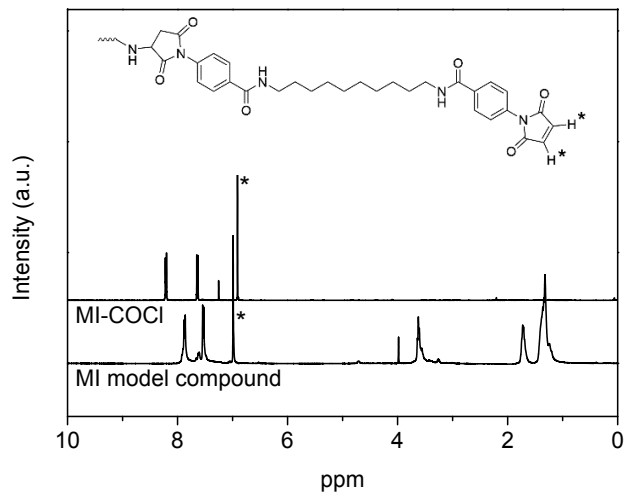

Figure 3.1 ^{1}H NMR spectra of MI-COCl (in $CDCl_3$) and MI model compound (in TFA-d). The peak associated with the maleimide proton is marked with an asterisk (*).

ME model compound. The preparation of the title compound follows the same procedure as reported for the MI model compound. ME-COCl 1.618 g (5 mmol) was used for the reaction. ^{1}H NMR (TFA-d) δ(ppm): 1.35 (br, 12H), 1.75 (br. 4H), 2.02 (s, 3H), 3.65 (t, 4H), 7.61-7.63 (d, *J*=7.6 Hz, 4H), 7.79-7.81 (d, *J*=8.0 Hz, 2H), 7.86-7.93 (m, 8H).

PE model compound. The preparation of the title compound follows the same procedure as reported for the ME model compound. PE-COCl 1.204 g (5 mmol) was used for the reaction. ^{1}H NMR (TFA-d1) δ(ppm): 1.38 (br, 12H), 1.80 (br, 4H), 2.02 (s, 3H), 3.71 (t, 4H), 7.30-7.32 (m, 6H), 7.47-7.49 (d, *J*=6.4 Hz, 4H), 7.65-7.67 (d, *J*=8.0 Hz, 4H), 7.73-775 (d, *J*=8.0 Hz, 4H).

DSC was performed to investigate the thermal behaviour of the ME and PE model compounds as shown in Figure 3.2. The ME model-compound shows a much higher T_m and ΔH_m (296 °C, 151 J·g^{-1}) than the PE model compound (227 °C, 84 J·g^{-1}), which may be due to the additional interactions between imide groups in the ME model-compound. The cure of the ME model-compound reveals a broad exotherm with an onset temperature of ~300 °C, which is about 40 °C lower than that of the PE model compound. This is probably because the methyl group in ME displays lower steric hindrance than the bulky phenyl ring in PE, which in turn results in a lower required energy to activate the cure of ME.

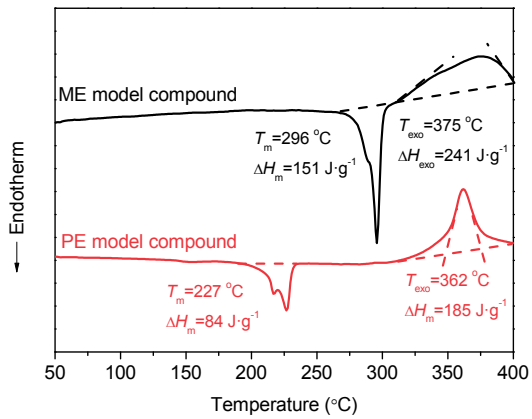

Figure 3.2 DSC heating scan (1st heat) of ME and PE model compounds (N_2 atmosphere and heating rate was 20 °C·min^{-1})

One important aspect of selecting reactive end-groups is that they should provide a proper processing window. The cure temperature should be higher than the T_m of the reactive PA 10T oligomer. PA10T homopolymer shows a melting endotherm at ~317 °C, which lies in the cure temperature range of ME, so a premature cure is anticipated leading to narrow processing window. In this sense, the ME end-cap is not optimal for PA 10T oligomers. In contrast, the cure reaction of the PE model compound is revealed as an exotherm at the temperature range of 340–380 °C. This is well above the melting temperature of PA 10T, and therefore, PE will be used as the end-group for the study of PA 10T oligomers and thermosets.

3.2.5 Synthesis of reactive PA 10T oligomers

Carothers theory was used to calculate the monomer to reactive PE end-cap ratio.[24, 25] The general form of Carothers equation is expressed as Equation (3.2)

$$\overline{x}_n = \frac{1+r}{1+r-2rp} \qquad (3.2)$$

where p is the extent of the reaction and approaches 1 at complete polymerization; $\overline{x}_n$ is the number average degree of polymerization; and r is stoichiometric monomer ratio. For a given polymer, $\overline{x}_n$ can be calculated from the pre-determined number average molecular weight $\overline{M}_n$ and the mean molar mass of the monomer units $\overline{M}_0$ using Equation (3.3)

$$\overline{x}_n = \frac{\overline{M}_n}{\overline{M}_0} \qquad (3.3)$$

Then the stoichiometric ratio r is determined using $p = 1$ (full conversion) in Equation (3.2). In the case of using a mono-functional end-cap with an A functionality to control the $\overline{M}_n$ of an AA-BB type of polycondensation, the molar amount of the two reacting groups should be equal, that is to say

$$2N_A + N_{A'} = 2N_B \quad (3.4)$$

where N_A, N_B and $N_{A'}$ are the molar amount of A monomer, B monomer and end-cap. Together with the expression of r

$$r = \frac{N_A}{N_B} \quad (3.5)$$

the molar ratio of the two AA and BB monomers can be obtained.

PE oligomers. PE oligomers with a target M_n of 1K and 3K g·mol^{-1} were prepared as shown in Scheme 3.5 and denoted as PA 10T-PE-1K and PA 10T-PE-3K, respectively. The synthetic procedure of PA 10T-PE-3K is described as an example:

In a dry 100 mL three-neck flask equipped with a mechanical stirrer, an argon inlet and a vacuum connection, 30 mL of NMP, 2.4 g of $CaCl_2$ (21.6 mmol) and 1.785 g (10.36 mmol) of 1,10-decanediamine were placed. The mixture was heated to 70 °C to allow the 1,10-decanediamine to dissolve completely, and then cooled to 0 °C on an ice-bath. Triethylamine (4 mL) was added to the flask followed by a 10 mL NMP solution of terephthaloyl chloride 1.900 g (9.36 mmol) and PE-COCl 0.481 g (2 mmol). The mixture was stirred at 350 rpm for 30 min at 0 °C and for another 3 hours at 55 °C to obtain a viscous slurry. This slurry was precipitated into demineralized water and the solids were washed 3 times with demineralized water in a heavy-duty blender before being collected by filtration. The oligomer was obtained after drying under vacuum at 60 °C overnight.

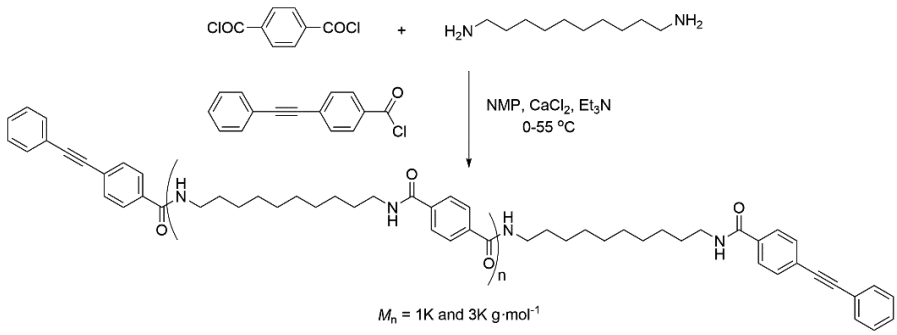

Scheme 3.5 Preparation of PE end-capped PA 10T oligomers, PA 10T-PE-1K and PA 10T-PE-3K, via solution polymerization.

3.2.6 Preparation of thermoset films

Thermoset films were prepared using standard melt compression techniques. The oligomer was ground to a fine powder, placed between two Kapton™ films and consolidated in a Joos hot press using a 5 kN force. The temperature program was set as heating to 350 °C at 5 °C·min^{-1}, hold for 15 min, and cool to 50 °C at 20 °C·min^{-1}.

3.3 Study of reactive oligomers

3.3.1 Solution polymerization

The solution-polymerized PA 10T-ref polymer shows an M_n of 7.5K g·mol^{-1}, as confirmed by intrinsic viscosity measurements.[26] Since we aim to produce reactive oligomers with an M_n of 1K and 3K g·mol^{-1}, solution polymerization conditions seems to work perfectly for the preparation of our target oligomers.

After work-up and drying, the reactive oligomers appeared unstable in concentrated sulfuric acid and insoluble in common organic solvents, such as NMP, tetrahydrofuran and hexafluoro-2-propanol [27, 28]. This precludes solvent-based GPC analyses. However, trifluoroacetic acid (TFA) can dissolve the oligomers without destroying the PE reactive end-groups. The reference polymer, the PE model compound and the reactive oligomers were dissolved in TFA-d and analyzed using ^{1}H NMR. As shown in Figure 3.3, the ^{1}H NMR spectra of the PE model compound and oligomers in TFA-d show clearly distinguished peaks associated with the PE end-group and the polymer backbone, which confirms the structure of the oligomers and the integrated area under the peaks can be used to estimate M_n.

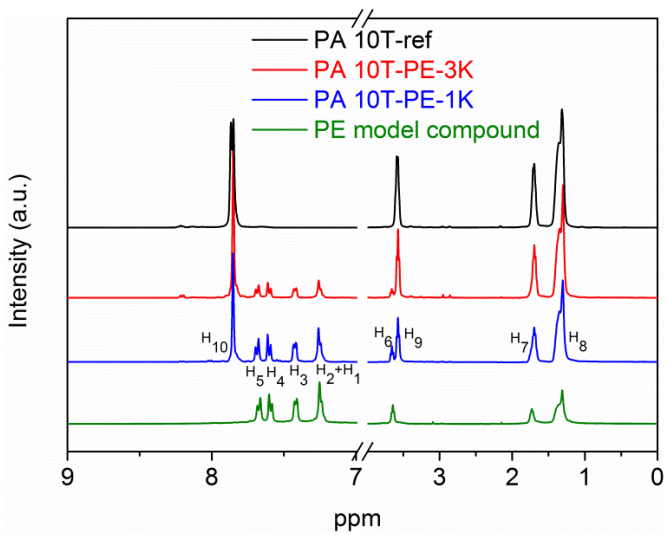

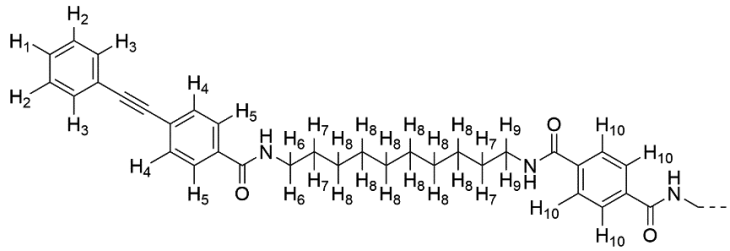

Figure 3.3 ^{1}H NMR spectra of the PA 10T reference polymer, the PE model compound and the 1K and 3K reactive oligomers.

In principal, a conversion rate of 100% is required to obtain the targeted M_n, however, trace amounts of moisture may deactivate –COCl groups, and therefore the M_n might be lower than targeted. The small peak at 8.2 ppm can be assigned to the protons adjacent to the –COOH functionality at the end of oligomer chain, but the area of this peak is negligible compared to the total integrated area of PE end-groups (H_1-H_5), especially for the 1K oligomer. Therefore, based on the integrated peak area of protons in PE end-groups and the polymer backbone, the obtained M_n of the oligomers is in agreement with the targeted M_n, as shown in Table 3.2.

3.3.2 Thermal properties

Thermal properties of the oligomers and PA 10T-ref obtained from TGA and DSC are listed in Table 3.2. TGA analysis shows that the reactive oligomers start to undergo severe thermal degradation at around 400 °C. As investigated in Chapter 2, the PE model compound cures at 340–380 °C. Based on these results, we selected 350 °C as the maximum cure temperature of our oligomers.

Table 3.2 Molecular weight data and thermal properties of reactive oligomers.

Sample	M_n (kg·mol^{-1})	T_d [c] (°C)	$T_{m\ onset}$ (°C)	T_{m1} (°C)	T_{m2} (°C)	$T_{m\ end}$ (°C)	ΔH_m (J·g^{-1})
PA 10T-ref	7.5 [b]	425	275	292	317	324	89
PA 10T-PE-3K	2.9 [a]	408	266	293	310	315	74
PA 10T-PE-1K	1.1 [a]	393	280	-	302	311	39
PE model compound	–	322	210	217	227	232	84

[a] Values are calculated by ^{1}H NMR analysis.

[b] Value calculated from intrinsic viscosity measurements.[26]

[c] T_d is reported as the 5% weight loss point using TGA (N_2 atmosphere and heating rate of 10 °C·min^{-1}).

As shown in Figure 3.4, the 3K-reactive oligomer shows double melting endotherms similar to that of PA 10T-ref, however, the double melting endotherms of the 3K-reactive oligomer are less distinct. Compared to PA 10T-ref, the 3K-reactive oligomer shows a similar T_{m1} (293 °C), but lower T_{m2} (310 °C), which indicates that the PE reactive functionalities disrupt the formation of the high-melting crystals. The 1K-reactive oligomer shows one single broad melting endotherm only, which may be due to merging of both melting endotherms or formation of the high melting crystals are suppressed by the large concentration of PE end-groups. Introducing PE reactive functionalities at the polymer chain-ends also has a disrupting effect on the overall degree of crystallinity. Whereas PA10T-ref exhibits a melt endotherm of 89 J·g^{-1} (Table 1), the 3K- and 1K-reactive oligomers show melting endotherms of 74 and 39 J·g^{-1}, respectively. In addition, a melting event (220–235 °C) was detected in the DSC scan for both oligomers. This event is reminiscent of the melt behaviour of the PE model compound (Figure 3.2). This makes sense as the 3K- and 1K-reactive oligomers have a substantial concentration (9.2 mol% and 23.6 mol%) of the phenylethynyl end-group (PE-COCl) in the monomer feed, which increases the chance of forming PE end-capped diamine trimers.

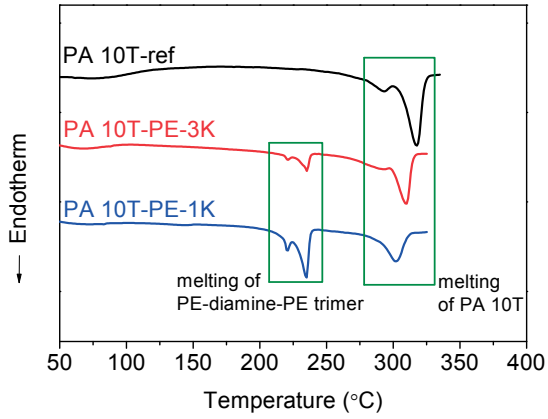

Figure 3.4 DSC heating scan (1st heat) of PA 10T-ref, PA 10T-PE-3K and PA 10T-PE-1K (N_2 atmosphere and heating rate of 20 °C·min^{-1}).

3.3.3 Cure behaviour

Rheology experiments were performed to study the cure behaviour of the oligomers. Both the 1K- and 3K-reactive oligomers show a minimum complex melt viscosity in the range of 10–100 Pa·s, as shown in Figure 3.5. This low viscosity makes it difficult to prepare well consolidated, defect free films using compression moulding techniques. In order to obtain free-standing thermoset films that are suitable for DMTA and tensile testing, a pre-cure treatment was applied prior to the final cure process. This treatment was performed at 260 °C for a specified period with the aim to increase the melt viscosity of the precursors. After the pre-cure, the oligomers become insoluble in TFA, which indicates that crosslinking has taken place. For the 1K oligomer, a 6 hour pre-cure is able to bring the melt viscosity up to ~10^4 Pa·s, which becomes suitable for compression moulding. The 3K oligomer has a lower concentration of PE end-group than the 1K oligomer and as a result, a longer pre-cure time of 14 hours was needed.

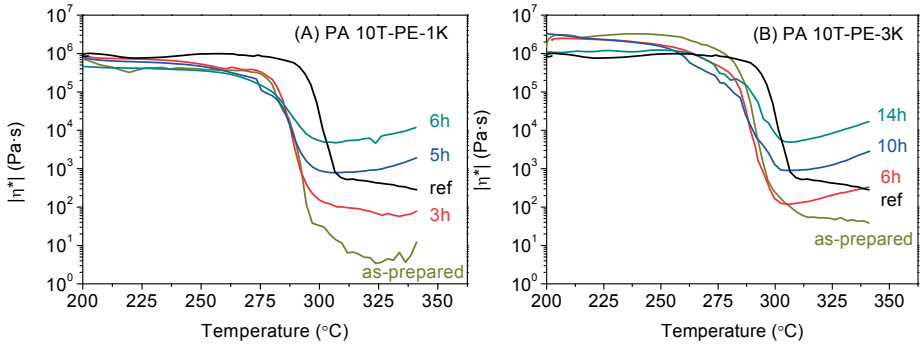

Figure 3.5 $|\eta^*|$ as a function of temperature for the PE reactive oligomers (A) PA 10T-PE-1K as-prepared and pre-cured for 3, 5 and 6 hours at 260 °C; (B) PA 10T-PE-3K as-prepared and pre-cured for 6, 10 and 14 hours at 260 °C. A PA 10T-ref sample without pre-cure treatment is included as a reference. Experiments were performed using a frequency of 1 Hz, a heating rate of 5 °C·min^{-1} and a N_2 atmosphere.

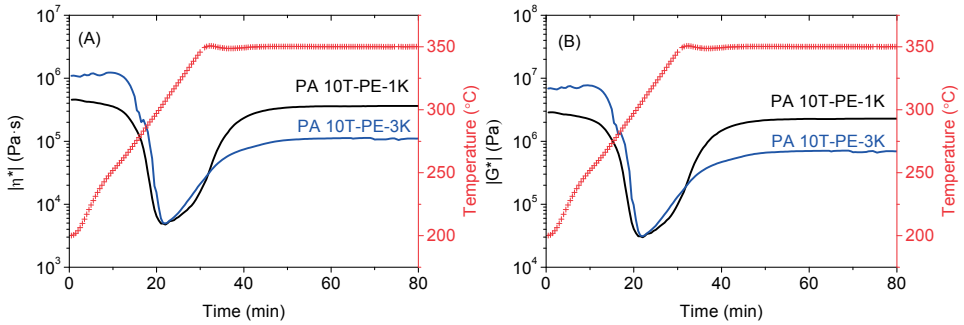

Figure 3.6 Rheology measurements of pre-cured PE oligomers. (A) $|\eta^*|$ and (B) $|G^*|$ as a function of temperature and a 50 min. isothermal hold at 350 °C. Experiments were performed using a frequency of 1 Hz and a heating rate of 5 °C·min^{-1} (N_2 atmosphere). The test specimens were prepared after a pre-cure at 260 °C under vacuum for 6 hours for PA 10T-PE-1K, and 14 hours for PA 10T-PE-3K.

The cure behavior of the two pre-cured oligomers is shown in Figure 3.6. The temperature program for the rheology test was set to mimic the film pressing conditions. The $|\eta^*|$ and $|G^*|$ start to increase at around 300 °C, and reach a plateau after a 15 minutes hold at 350 °C. Little change on $|G^*|$ and $|\eta^*|$was observed when extending the cure time, indicating that the oligomers are close to

being fully cured in the first 15 minutes at 350 °C. Therefore, these conditions were used as the cure conditions for preparing the thermoset films. This result is in agreement with the kinetic study of an *N*-phenyl[(4-phenylethynyl)-phthalimide] model compound as reported by Takekoshi, et al. They found that the half-life of their model compound was approximately 50, 20, and 6 min at 320 °C, 340 °C, and 360 °C, respectively.[29]

3.3.4 Network Characterization

In order to get insight in the network formation and crosslink density we used classical rubber elasticity theory (Equation 3.6) to characterize the polymer networks prepared from the 1K and 3K reactive precursors,[30] the equilibrium shear modulus (G_e) is given by,

$$G_e = \frac{\rho RT}{M_c} \quad (3.6)$$

where ρ is the density of the crosslinked material, T the absolute temperature in Kelvin (K), and R the universal gas constant. M_c is the molecular weight between chemical crosslinks, which demonstrates the degree of crosslinking. G_e is taken from the rheology experiments (Figure 3.6B) at t= 60 min and T = 350 °C (623 K). At this point the reactive precursors are fully crosslinked and the modulus $|G^*|$ has reached a stable plateau value.

As shown in Table 3.3, the M_c for the cured 1K and 3K oligomers are estimated to be 2.7 and 8.4 kg·mol^{-1}, respectively, which are values that exceed the initial M_n of the starting oligomers. In this sense, one can say that PE end-groups only partly participate in crosslinking. Roberts et al. have studied the cure chemistry of PE groups,[31] and proposed after-cure structures of both chain extension (f=2) and crosslinking (f=3). Previous studies have shown that the PE cure is strongly affected by temperature, time, and PE concentration. Rheology studies by Iqbal et al. have shown that chain extension reactions of PE groups predominate at lower temperatures (310–340 °C) and crosslinking is the major reaction at higher temperatures (370–400 °C).[14]

If we assume that every PE end-group undergoes either chain extension (f=2) or crosslinking (f=3), and only the formed crosslinks contribute to the G_e of the network, the percentage of both chain extension and crosslinking can be roughly estimated as shown in Table 2. 35~41% of PE end-groups contribute to crosslinking,

and 59-65% contribute to chain extension. The number average functionality ($\bar{f}$) of PE end-groups is calculated to be 2.35 and 2.41, respectively. In practice, the cure chemistry will be more complicated. Trapped entanglements may be formed that contribute to G_e in a similar fashion as chemical crosslinks,[32] especially for the 3K sample which has longer oligomer chains. Also, there might be unreacted PE end-groups leftover and polymer chain scission might take place during cure. All these factors grouped together will have to be factored in when one wants to establish a more accurate M_c value.

Table 3.3 Calculated molecular weight values between crosslinks (M_c) and crosslinking/chain extension estimations.

Sample	M_n [a] (kg·mol^{-1})	G_e [b] (Pa)	ρ [c] (kg·m^{-3})	M_c [d] (kg·mol^{-1})	Crosslinking/chain extension (%)	$\bar{f}$ [e]
PA 10T-PE-1K	1.1	2.3*10^6	1.21*10^6	2.7	41/59	2.41
PA 10T-PE-3K	2.9	7.1*10^5	1.15*10^6	8.4	35/65	2.35

[a] M_n was calculated by NMR analysis (Table 3.2).

[b] G_e was taken as the $|G^*|$ at the plateau region (Figure 3.6B).

[c] ρ is the density of the thermoset films when cured at 350 °C for 15 min.

[d] M_c was calculated based on the classical rubber elasticity theory.

[e] $\bar{f}$ stands for the mean functionality of PE end-groups

3.4 Study of thermoset films

3.4.1 Melting and crystallization

Figure 3.7 and Table 3.4 summarize the DSC results of after-cure film samples. The thermoplastic PA 10T-ref film is included as a reference. For both cured thermoset films, the melting endotherm associated with the PE-diamine-PE trimer is no longer present as it reacts (cures) and becomes part of the final thermoset.

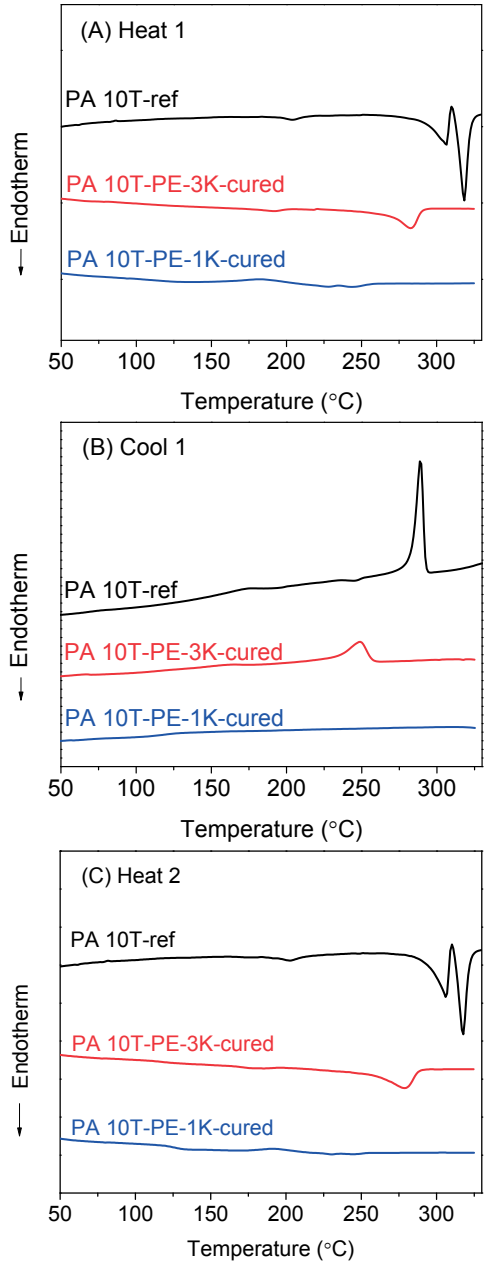

Figure 3.7 DSC curves of (A) Heat 1, (B) Cool 1 and (C) Heat 2 of PA 10T-ref thermoplastic film, PA 10T-PE-1K and PA 10T-PE-3K thermoset films. Heating and cooling rates were 20 °C·min^{-1} under N_2 atmosphere

Table 3.4 DSC results of the PA 10T-ref thermoplastic film, PA 10T-PE-1K-cured and PA 10T-PE-3K-cured thermoset films

Sample	Heat 1			Cool 1	Heat 2		
	T_m [a] (°C)	ΔH_m (J·g^{-1})	T_{cc} [b] (°C)	T_c [c] (°C)	T_m [a] (°C)	ΔH_m (J·g^{-1})	T_{cc} [b] (°C)
PA 10T-ref	318	82	-	289	318	74	-
PA 10T-PE-3K-cured	283	33	-	249	279	29	-
PA 10T-PE-1K-cured	244	8	182	-	-	3	191

[a] T_m is reported as the peak temperature of the second peak if there are double melting endotherms present.

[b] T_{cc} is reported as the peak temperature of the cold crystallization exotherm during heating.

[c] T_c is reported as the peak temperature of the crystallization exotherm during cooling.

The T_m and ΔH_m of thermoset films are substantially reduced when compared to the PA 10T reference polymer, which shows reversible melting and crystallization behaviour. For the reactive precursors, crystallization of the polymer chains is to a large extent hindered by the cure of the PE reactive end-groups (formation of f=3 functionalities). PA10T-PE-3K-cured film has the lowest crosslinking density and is still able to crystallize upon cooling. The degree of crystallinity is reduced by 60% when compared to PA 10T-ref (Table 3.4). Also, crosslinking has supressed the melting temperature from 310 °C for the reactive oligomer to 283 °C for the thermoset. For the PA 10T-PE-1K film we don't observe a crystallization exotherm during cooling (Cool 1). However, upon the first and second heat a small but discernable cold crystallization exotherm can be detected at 182 °C.

3.4.2 WAXD analysis of thermoset films

Room temperature WAXD experiments were performed to study the crystalline structure of the after-cure thermoset films and the results are shown in Figure 3.8.

The thermoplastic PA 10T-ref film was also included for reference purposes. The cured 1K film shows a broad halo in the WAXD pattern indicating it is fully amorphous. This means that the 1K polymer chains in the thermoset network are no longer able to crystallize during processing. These results are in agreement with the DSC results. The cured 3K film shows the same WAXD reflections as the PA 10T-ref film, which means the crystal form of the 3K film and the thermoplastic PA 10T reference polymer are the same. As shown in Figure 3.8 (B) and (C), the WAXD patterns of PA 10T-ref and PA 10T-PE-3K films could be deconvoluted into an amorphous halo and 5 crystalline reflections using a Gaussian curve-fitting procedure. The crystallinity index (*CI*) was calculated according to Equation (3.7) and the results are listed in Table 3.5.

$$CI\ (\%) = \frac{Area_{crystalline}}{Area_{crystalline} + Area_{amorphous}} \quad (3.7)$$

PA 10T-PE-3K shows lower *CI* value than PA 10T-ref indicating a lower degree of crystallinity.

The *d*-spacings corresponding to the 2θ peaks are calculated using Bragg's law and shown in Figure 3.8 (B) and (C). The reflection at around 4.7° is marked with asterisk (*), and is associated with the projection length of one repeating unit in the crystalline unit cell. The mean size of the crystallites in this direction, *D**, is calculated via the Scherrer equation (4).

$$D^* = \frac{0.9\lambda}{\beta \cos\theta} \quad (3.8)$$

where λ is the X-ray wavelength, θ is half of the scattering angle, and β is the Gaussian's full width at half-height (in radians). This crystal size estimate corresponds to the lamellar thickness, and the ratio *D**/*d** represents the average number of repeating units within one crystal lamella in the lamellar thickness direction.[33] As shown in Table 3.5, the results show that the lamellar thickness of PA 10T-ref is approximately composed of 5 repeating units, which is typically in the range of 3-6 for polyamides.[34] The lower *D** and *D**/*d** for PA 10T-PE-3K-cured is a clear indication that the crystallization is strongly hindered by crosslinking.

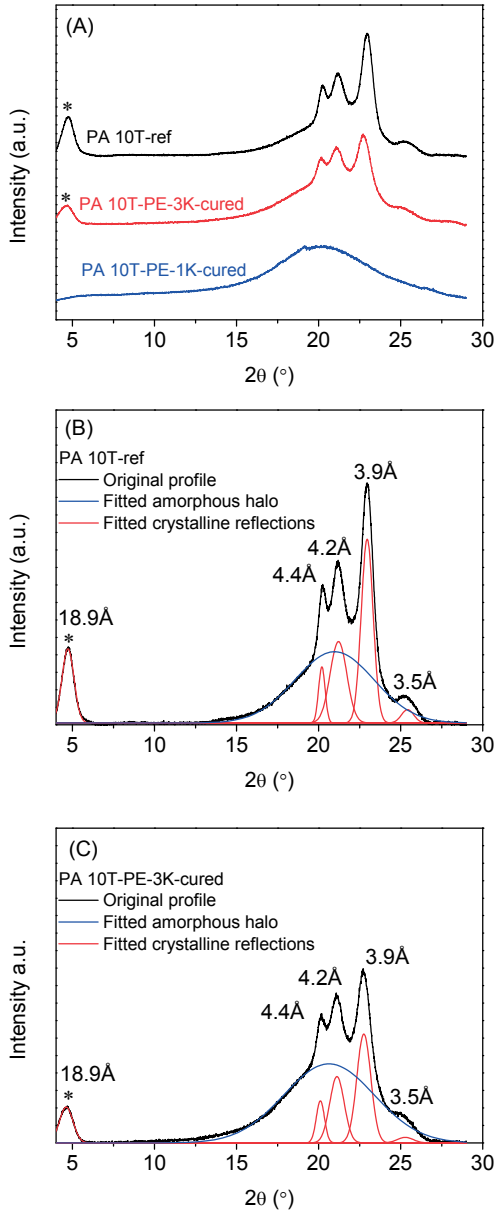

Figure 3.8 WAXD intensity as a function of the scattering angle 2θ (A) film samples of PA10T-ref, PA 10T-PE-3K-cured and PA 10T-PE-1K-cured. (B) Peak-fitting of PA 10T-ref WAXD pattern. (C) Peak-fitting of PA 10T-PE-3K-cured WAXD pattern. The *d*-spacing values are shown above the corresponding peak. The peak at around 4.7° is marked with asterisk (*).

Table 3.5 *CI*, *d** and *D** based on the fitted WAXD reflections

Sample	PA 10T-ref	PA 10T-PE-3K-cured
CI (%) [a]	47	32
d* (Å) [b]	18.9	18.9
D* (Å) [c]	92.7	81.3
D*/d*	4.9	4.3

[a] *CI* values were obtained according to Equation 3.7.

[b] *d** is the *d*-spacing of the * peak.

[c] *D** is the lamellar thickness as calculated using Equation 3.8.

The melting point of a semi-crystalline polymer can be described by the Hoffmann-Weeks equation (Equation 3.9)[35]

$$T_m = T_m^o \left(1 - \frac{2\gamma_e}{\Delta H_f l_c}\right) \quad (3.9)$$

where T_m and T_m^o are the observed and equilibrium melting point, γ_e the surface free energy, ΔH_f the heat of fusion, and l_c the lamellar crystal thickness. The T_m^o and ΔH_f values should be the same for both PA 10T-ref and PA 10T-PE-3K-cured, because they have the same crystal structure. The lamellar thickness of the PA 10T-PE-3K-cured is lower than that of PA 10T-ref, which can be one reason for the relatively lower T_m of PA 10T-PE-3K-cured according to Equation (3.9). Moreover, the γ_e between the amorphous and crystalline phase should be higher in a matrix that also contains heterogeneous crosslinks than in a homopolymer matrix,[36] which may also contribute to the T_m depression of PA 10T-PE-3K-cured.

3.4.3 Thermo-mechanical properties

DMTA experiments were performed to study the thermo-mechanical properties of PA 10T-ref thermoplastic film and cured thermoset films. The storage modulus (*E*') and loss modulus (*E*") as a function of temperature are shown in Figure 3.9.

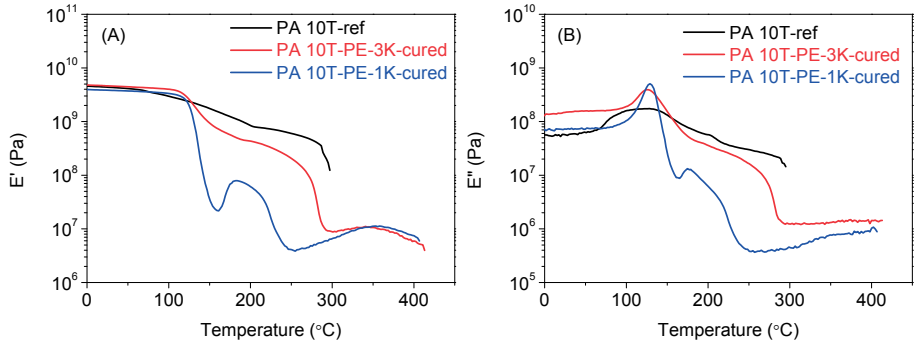

Figure 3.9 DMTA of PA 10T-ref thermoplastic film, PA 10T-PE-1K-cured and 3K-cured thermoset films. (A) Storage modulus (*E'*) as a function of temperature; (B) loss modulus (*E"*) as a function of temperature. Experiments were performed using a frequency of 1 Hz and heating rate of 2 °C·min^{-1} (N_2 atmosphere).

Table 3.6 lists the DMTA results and the gel fractions of all samples. PA 10T-ref displays typical thermo-mechanical behavior of a semi-crystalline thermoplastic with a temperature at break (T_{break}) of 297 °C because of melting. The thermoset analogs, on the other hand, are stable to temperatures well above 400 °C, which is about 100 °C higher than the melting point of PA 10T. The cured films can maintain their shape in TFA, and the gel fraction of the cured 1K and 3K films are 88% and 80%, respectively, which means that most oligomers are crosslinked and formed a network structure.

Table 3.6 Summary of DMTA results and gel fraction results.

Sample	$E'_{at\ 25\ °C}$ (GPa)	T_g [a] (°C)	T_{break} [b] (°C)	T_c (°C)	Gel fraction (%)
PA 10T-ref	4.4	127	297	-	0
PA 10T-PE-3K-cured	4.6	127	407	-	80
PA 10T-PE-1K-cured	3.8	129	407	182	88

[a] T_g is reported at the maximum of *E"*.

[b] T_{break} is reported at the temperature where the sample fails.

For the amorphous PA 10T-PE-1K-cured film, cold crystallization was observed when the polymer film passed through the T_g event. The peak maximum of E' appears at 182 °C, which is consistent with the DSC results. Subsequent melting gives a ΔH_m of 8 $J \cdot g^{-1}$ (Table 3.4), which corresponds to a relative degree of crystallinity of ~10%. In a separate experiment, a PA 10T-PE-1K-cured film was allowed to crystallize using a thermal annealing step at 182 °C for 10 min. In a consecutive DMTA experiment, the film shows a T_g, T_m and a following plateau only, as shown in Figure 3.10.

At the temperature range below T_g, the polymer chain segments are rigid for all samples, as a result, a similar E' of ~4 GPa is obtained. However, in the temperature range between T_g and T_m, the thermoset films show a lower E' than PA 10T-ref due to the lower degree of crystallinity. In this sense, crystallinity has a more significant effect on the E' within this temperature range than the crosslinking. Above the melting temperature, both thermoset films show an increase in E' until ~350 °C, which might be caused by the post-cure of leftover curable groups or alignment of the mobile chains within the network. Above 350 °C, the E' starts to decrease until the sample fails, which is probably due to the start of thermal scission of polymer chains.

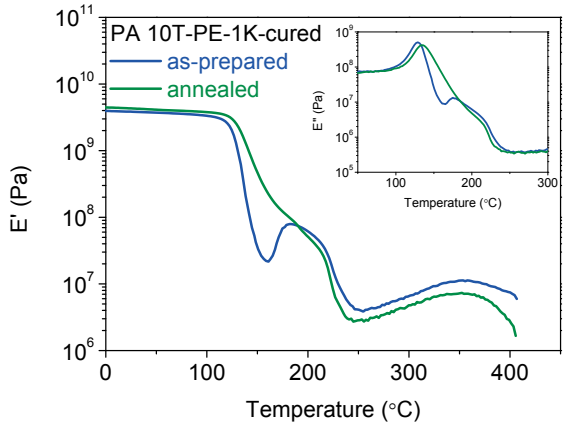

Figure 3.10 DMTA of PA 10T-PE-1K-cured film before and after an annealing treatment at 182 °C. Heating rate of 2 $°C \cdot min^{-1}$ under N_2 atmosphere and a frequency of 1 Hz. The insets show the E'' at the glass transition temperature.

The loss modulus (*E*”) peaks of the thermoset films, and especially E” of the amorphous 1K film, are much narrower than that of the PA 10T-ref film. This confirms the fact that the mobility of the amorphous chains becomes more restricted in the thermosets.

By changing the M_n of the reactive PA 10T oligomers, that is to say the concentration of PE end-groups, the crosslinking density of the thermosets can be controlled, consequently leading to adjustable crystallinity. This strongly affects the morphology and the thermo-mechanical properties of the obtained thermosets. DMTA experiments confirm that semi-crystalline thermosets with a crosslinked amorphous phase can be prepared via a reactive oligomer approach. A molecular representation of the PA 10T semi-crystalline network structure is shown in Figure 3.11.

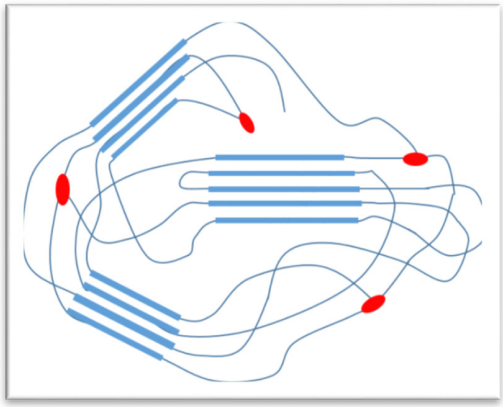

Figure 3.11 Schematic illustration of the semi-crystalline thermoset molecular structure. Blue curvy lines represent the amorphous chain segments, the straight blue (bold) lines represent the crystalline chain segments and the red dots represent the crosslinks in the amorphous phase.

3.4.4 Mechanical properties

Stress-stain measurements were performed to investigate the mechanical properties of the PA 10T thermosets. Figure 3.12 shows the tensile strength, elastic modulus and elongation at break of the PA 10T-ref, PA 10T-PE-3K-cured and PA 10T-PE-1K-cured polymers. All samples show brittle fracture without yielding. The cured 1K sample has the lowest elastic modulus due to the loss of crystallinity.

Although the thermoset samples are crosslinked in the amorphous phase, they still display an elongation at break of 6.5-7%, which exceeds that of other thermoset polymers (typically ε <5%). We may conclude that the mechanical properties of the PA 10T thermosets are not significantly deteriorated compared to the thermoplastic PA 10T reference polymer.

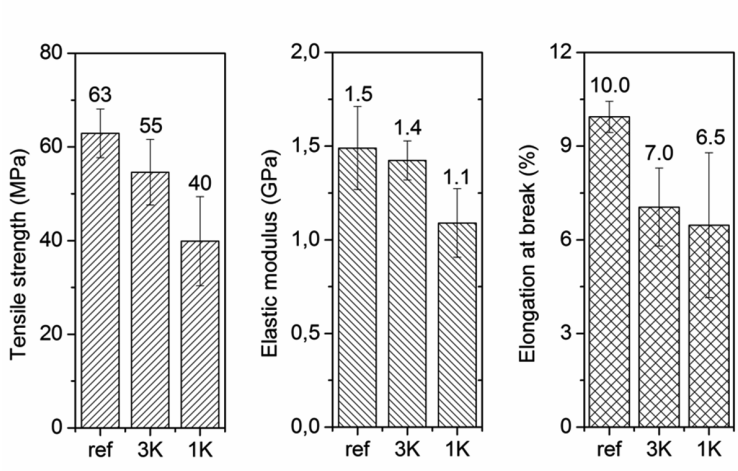

Figure 3.12 Tensile strength, elastic modulus and elongation at break of PA 10T-ref (ref), PA 10T-PE-3K-cured (3K) and PA 10T-PE-1K-cured (1K) films. Data shown is the average of 3 experiments.

3.5 Conclusions

We have demonstrated that phenylethynyl (PE) reactive end-groups can be used to prepare semi-aromatic oligomeric polyamides with excellent melt processability. Two reactive PA 10T oligomers with an M_n of 1K and 3K g· mol^{-1} were successfully synthesized via a solution polymerization method. The oligomer precursors exhibit low complex melt viscosities in the range of 10-100 Pa·s. Melt rheology experiments show that reactive oligomers can be polymerized in multiple thermal treatment steps. When crosslinked, a stable rubber plateau is observed with a complex melt viscosity of 3.6×10^5 and 1.1×10^5 Pa·s for PA 10T-1K-cured and PA 10T-3K-cured, respectively. Based on the theory of rubber elasticity we conclude that 35-41% of the PE end-groups contribute to crosslinking and the remainder of the PE functionalities undergoes chain extension reactions. DMTA

measurements showed that 3K and 1K thermoset films are stable up to ~400 °C as a result of network formation. The melt transition and degree of crystallinity in the final thermoset films are strongly depressed by the thermal cure process. The PA 10T-1K-cured film is remarkable in that the fully amorphous thermoset film is able to exhibit cold crystallization upon heating above T_g. Stress-strain experiments show very little difference between the PA 10T reference polymer and the thermoset analogs. In conclusion, we have demonstrated that a semi-aromatic polyamide, PA 10T, can be crosslinked using phenylethynyl reactive end-groups. This approach can be used to expand the thermal use window of semi-aromatic polyamides. The presence of two plateau regions ($T_g - T_m$ and $> T_m$) is of interest, as this will enable the design of polyamides with high-temperature shape-memory capabilities.

3.6 References

1. Kohan, M. I., *Nylon plastics handbook*. Hanser New York: 1995; Vol. 378.
2. Pramanik, N.; Haldar, R.; Bhardwaj, Y.; Sabharwal, S.; Niyogi, U.; Khandal, R. *Journal of Applied Polymer Science* **2011,** 122, (1), 193-202.
3. Adem, E.; Burillo, G.; Del Castillo, L.; Vásquez, M.; Avalos-Borja, M.; Marcos-Fernández, A. *Radiation Physics and Chemistry* **2014,** 97, 165-171.
4. Sengupta, R.; Sabharwal, S.; Tikku, V.; Somani, A. K.; Chaki, T. K.; Bhowmick, A. K. *Journal of Applied Polymer Science* **2006,** 99, (4), 1633-1644.
5. Agag, T.; Arza, C. R.; Maurer, F. H. J.; Ishida, H. *Journal of Polymer Science, Part A: Polymer Chemistry* **2011,** 49, (20), 4335-4342.
6. Lendlein, A.; Kelch, S. *Angewandte Chemie International Edition* **2002,** 41, (12), 2034-2057.
7. Zhao, Q.; Qi, H. J.; Xie, T. *Progress in Polymer Science* **2015,** 49, 79-120.
8. Zhou, J.; Turner, S. A.; Brosnan, S. M.; Li, Q.; Carrillo, J.-M. Y.; Nykypanchuk, D.; Gang, O.; Ashby, V. S.; Dobrynin, A. V.; Sheiko, S. S. *Macromolecules* **2014,** 47, (5), 1768-1776.
9. Rulkens, R.; Koning, C., 5.18 - Chemistry and Technology of Polyamides. In *Polymer Science: A Comprehensive Reference*, Matyjaszewski, K.; Möller, M., Eds. Elsevier: Amsterdam, 2012; pp 431-467.

10. Marchildon, K. *Macromolecular Reaction Engineering* **2011,** 5, (1), 22-54.
11. Dingemans, T., High-Temperature thermosets. In *Polymer Science: A Comprehensive Reference*, 1st ed.; M, M. K. M., Ed. Elsevier BV: Amsterdam, 2012; Vol. 5, pp 753-769.
12. Dingemans, T.; Knijnenberg, A.; Iqbal, M.; Weiser, E.; Stclair, T. *Liquid Crystals Today* **2006,** 15, (4), 19-24.
13. Knijnenberg, A.; Weiser, E.; StClair, T.; Mendes, E.; Dingemans, T. *Macromolecules* **2006,** 39, (20), 6936-6943.
14. Iqbal, M.; Norder, B.; Mendes, E.; Dingemans, T. J. *Journal of Polymer Science Part A: Polymer Chemistry* **2009,** 47, (5), 1368-1380.
15. Hergenrother, P. M. *High Performance Polymers* **2003,** 15, (1), 3-45.
16. Mison, P.; Sillion, B., Thermosetting oligomers containing maleimides and nadimides end-groups. In *Progress in Polyimide Chemistry I*, Springer: 1999; pp 137-179.
17. Mather, B. D.; Viswanathan, K.; Miller, K. M.; Long, T. E. *Progress in Polymer Science* **2006,** 31, (5), 487-531.
18. Kossmehl, G.; Nagel, H. I.; Pahl, A. *Die Angewandte Makromolekulare Chemie* **1995,** 227, (1), 139-157.
19. Rosenberg, J. E.; Persson, D.; Kiraly, E.; Deriss, M. J., US8492507 B2. In Nexam Chemical Ab: 2013.
20. Nishino, H. Thermally moldable imide oligomers and polyimide resins made by thermally curing the oligomers. JP 2013256549, 2013.
21. Cava, M.; Deana, A.; Muth, K.; Mitchell, M. *Organic Syntheses* **1961**, 93-93.
22. Cianga, L. *High Performance Polymers* **2005,** 17, (1), 117-134.
23. Peter, L. D.; Kurt, W. D.; Emil, S. D. A., DE1594835 A1. In Ciba Geigy: 1971.
24. Carothers, W. H. *Chemical Reviews* **1931,** 8, (3), 353-426.
25. Flory, P. J. *Chemical Reviews* **1946,** 39, (1), 137-197.
26. Novitsky, T.; Lange, C.; Jarrett, W.; Mathias, L.; Osborn, S.; Ayotte, R.; Manning, S. *Journal of Applied Polymer Science* **2010,** 116, (6), 3388-3395.
27. Knijnenberg, A.; Bos, J.; Dingemans, T. J. *Polymer* **2010,** 51, (9), 1887-1897.
28. Wang, W. Z.; Zhang, Y. H. *Chinese Journal of Polymer Science* **2010,** 28, (4), 467-473.
29. Takekoshi, T.; Terry, J. *Polymer* **1994,** 35, (22), 4874-4880.
30. Ferry, J. D., *Viscoelastic properties of polymers*. John Wiley & Sons: 1980.

31. Roberts, C. C.; Apple, T. M.; Wnek, G. E. *Journal of Polymer Science Part A: Polymer Chemistry* **2000,** 38, (19), 3486-3497.
32. De Rosa, M.; Winter, H. *Rheologica acta* **1994,** 33, (3), 220-237.
33. Telen, L.; Van Puyvelde, P.; Goderis, B. *Macromolecules* **2016**.
34. Dreyfuss, P. *Journal of Polymer Science: Polymer Physics Edition* **1973,** 11, (2), 201-216.
35. Hoffman, J. D.; Weeks, J. J. *J Res Natl Bur Stand A* **1962,** 66, (1), 13-28.
36. de Ruijter, C.; Jager, W. F.; Li, L.; Picken, S. J. *Macromolecules* **2006,** 39, (13), 4411-4417.

Chapter 4 Synthesis and Characterization of Reactive Side-group Functionalized Copolyamides and Thermosets Thereof

Abstract

We have explored the synthesis of semi-crystalline polyamide (PA) thermosets using side-group functionalized copolyamides as reactive precursors. A *meta*-based phenylethynyl diacid chloride (IPE) and a *para*-based phenylethynyl diacid chloride (TPE) were synthesized and incorporated in poly(decamethylene terephthalamide) (PA 10T) using a solution polymerization method. The PE-based comonomers disrupt crystallization of the final copolyamides. Copolyamides containing 5, 10 and 15 mol% of the reactive comonomer could be cured into PA thermoset films at 350 °C. All thermoset films are stable up to ~400 °C as confirmed by DMTA, which is the result of network formation. The thermosets exhibit both a crystalline phase and a crosslinked amorphous phase. Depending on the concentration of the PE side-groups, the degree of crystallinity of the final thermosets can be controlled and depressed by 52-76% compared to the PA 10T reference polymer. The IPE-15 thermoset film shows outstanding elongation at break (~19%) and toughness (791 $MJ \cdot m^{-3}$), which is the highest elongation and toughness reported for a semi-aromatic PA to date.

4.1 Introduction

Side-group functionalized all-aromatic polymers have been studied for heat-resistant applications.[1-4] The preparation of such reactive polymers essentially require monomers containing crosslinkable side-groups. Phenylethynyl (PE) is a well-known reactive functionality showing excellent thermal stability, volatile-free polymerization and high cure temperature (310–400 °C). PE has found use as chain extender/crosslinker in a variety of all-aromatic high-performance polymers.[5, 6] Scheme 4.1 shows some examples of PE-containing monomers, which have been used as comonomers for the preparation of PE side-group functionalized all-aromatic polyesters,[7] polyamides,[8] polyimides,[9] and other polymers.[10-17] Thermal curing of these copolymer precursors results in amorphous thermosets with high glass transition temperatures (>200 °C).

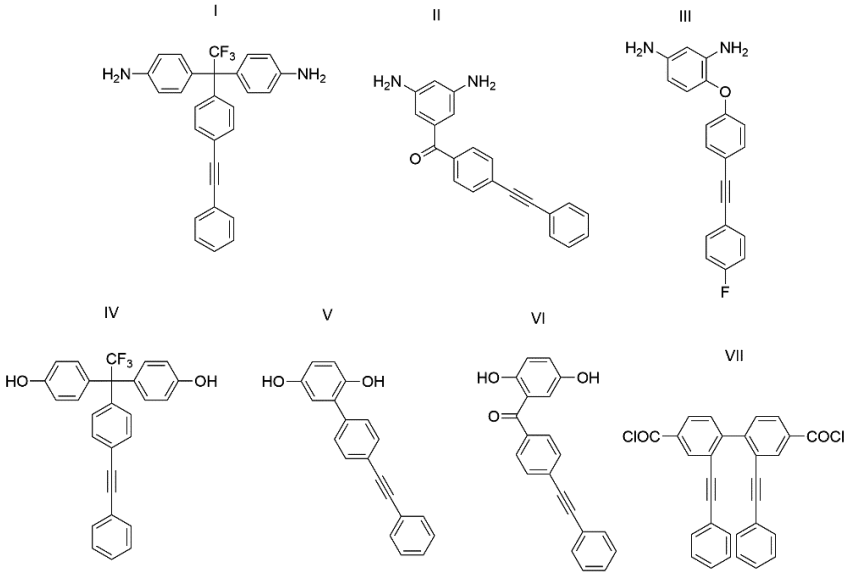

Scheme 4.1 PE-containing monomers used to prepare PE side-group functionalized polymers. Diamines (I-III), diols (IV-VI) and a diacid chloride (VII).[7-17]

Little research has been reported on crosslinkable semi-aromatic polymers containing PE side-groups. One example is a PE side-group functionalized poly(ethylene terephthalate) (PET), as shown in Scheme 4.2, which was designed to

be self-extinguishing and non-dripping in case of a fire.[18, 19] The PE side-groups distributed along the polymer chains remain latent during polymerization and melt-processing, but crosslinking takes place rapidly when exposed to temperatures > 300 °C but prior to combustion.[20]

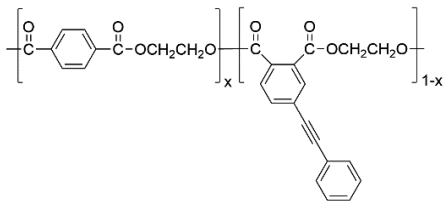

Scheme 4.2 Semi-aromatic copolyester with PE side-groups for flame retardant applications.[18-20]

Crosslinked semi-aromatic polymers are of scientific and engineering interest because crosslinking can be used to control the degree of crystallinity of the final product, which in turn controls mechanical properties such as storage modulus (*E*') and stress-strain behavior. We have described semi-crystalline poly(decamethylene terephthalamide) (PA 10T) thermosets prepared from PE end-capped PA 10T oligomers in Chapter 3. Inspired by the above mentioned copolymer examples, an alternative approach towards PA 10T thermosets can be explored using PE side-group functionalized copolyamides as precursors.

In the oligomer approach, as discussed in the previous chapters, the concentration of the PE end-groups is only controlled by varying the molecular weights of the oligomers. However, in the side-group functionalized copolymer approach, the effect of the PE concentration can be investigated independent of the precursor molecular weight. PE undergoes both chain extension (f=2) and crosslinking (f=3) reactions during cure,[21] and we have found that the chain extension is the major reaction (59-65%). Crosslinking of PE end-capped oligomers can only be realized via f=3 chemistries, whereas both f=2 and f=3 chemistries lead to crosslinking when PE groups are distributed along the polymer chain.

In this chapter, we will discuss the synthesis and properties of PA 10T-based thermosets using PE side-group functionalized copolyamides as reactive precursors. Isophthalic and terephthalic monomers with PE functionalities, as shown in Scheme 4.3, were incorporated using a solution-based polymerization

method. The cure behavior, the thermo-mechanical properties and morphological properties of the final semi-crystalline thermosets were investigated and discussed in detail.

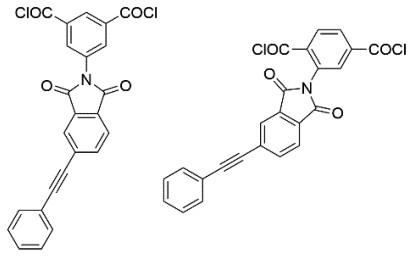

Scheme 4.3 The diacid chloride PE-based comonomers. Left: the isophthalic-based PE monomer IPE-COCl; Right: the terephthalic-based PE monomer TPE-COCl.

4.2 Experimental

4.2.1 Materials

Terephthaloyl chloride was purchased from Sigma-Aldrich and purified via sublimation prior to use. 1,10-Decanediamine was generously supplied by DSM and dried under vacuum. $CaCl_2$ (96%) was purchased from Acros Organic and dried at 200 °C under vacuum. Triethylamine (99%) was purchased from Sigma-Aldrich and distilled over CaH_2 before use. Extra dry N-methyl-2-pyrrolidone (NMP, water content <0.005%), 5-aminoisophthalic acid (98%) and 2-aminoterephthalic acid (99%) was purchased from Acros Organic and used as received. Trifluoroacetic acid (TFA, 99%), thionyl chloride (99%), anhydrous chloroform (99%), acetic acid (99%) and anhydrous N,N-dimethylformamide (DMF, 99.8%) were purchased from Sigma-Aldrich. Phenylethynyl phthalic anhydride (PEPA) was obtained from Hangzhou Chempro Tech Co., Ltd. The solution-polymerized PA 10T-4 sample discussed in Chapter 2 was used as the reference sample in this chapter, and denoted as PA 10T-ref.

4.2.2 Characterization

^{1}H and ^{13}C NMR spectra were recorded using a 400 MHz Bruker WM-400 at 25 °C. Mass spectra (MS) were recorded using a Shimadzu QP2010S over the m/z range of 45-900. The oven of MS was heated from 50-300 °C at 10 °C·min^{-1} under high vacuum (0.055 mbar). WAXD studies were performed using a PANalytical X'Pert Pro PW3040/60 diffractometer with CuKα-radiation. Data was collected in an angular 2θ range of 4-30° at a rate of 2°·min^{-1} and a step size of 0.008°. FTIR spectra were collected in the range of 400 and 600 cm^{-1} at room temperature using a Perkin-Elmer Spectrum 100 FT-IR spectrophotometer.

The rheological behavior of the oligomers was investigated using a ThermoFisher Haake MARS III rheometer equipped with a force-rebalanced transducer in a parallel plate geometry (8 mm in diameter). Pellets samples of 8 mm in diameter and ~0.5 mm in thickness were prepared by compression at room temperature. The samples were tested under N_2 with temperature ramping (5 °C·min^{-1}) from 200 °C to 350 °C followed by an isothermal hold at 350 °C for 30 min. Measurements were performed at a frequency of 1.0 Hz and a strain amplitude of 0.1%, which lies within the linear viscoelastic range of the material.

TGA was performed on a Perkin-Elmer Pyris diamond TG/DTA under a nitrogen atmosphere with a heating rate of 10 °C·min^{-1}. DSC was conducted on a Perkin-Elmer Sapphire DSC under a nitrogen atmosphere at a heating/cooling rate of 20 °C·min^{-1}. DMTA was performed on a Perkin-Elmer Diamond DMTA with film samples (0.2-0.3 mm thick) at a heating rate of 2 °C·min^{-1} under a nitrogen atmosphere. Data was collected at a frequency of 1 Hz.

Uniaxial tensile tests were performed on an Instron Model 3365 universal testing system equipped with a 1 kN load cell. Tensile specimens having approximate width of 2.5 mm, thickness of 0.25 mm and length of 20 mm between the clamps were stretched at 25 °C at a tensile rate of 0.2 mm·min^{-1}. The elastic modulus was measured by calculating the slope of the stress-strain curve between 0.1 and 0.3% strain. The area under the stress-strain curve was used to calculate the tensile toughness (MJ·m^{-3}). Data reported represent the average value of 3 specimens.

4.2.3 Synthesis of PE comonomers

5-(Phenylethynyl phthalimido) isophthaloyl chloride (IPE-COCl)

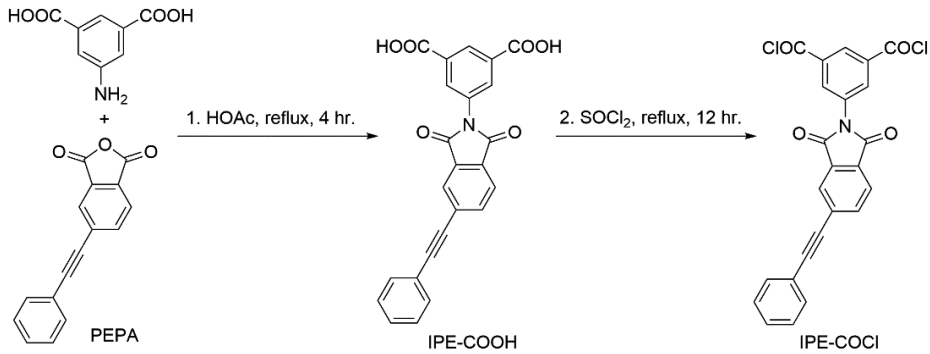

Scheme 4.4 Synthetic route towards IPE-COCl.

As shown in Scheme 4.4, a 250 mL round bottom flask equipped with a reflux condenser was charged with 100 mL acetic acid and PEPA 12.4 g (50 mmol). The mixture was heated to 120 °C until all solids were dissolved. 5-aminoisophthalic acid 9.0 g (50 mmol) was added to the flask and this reaction mixture was refluxed for 4 hours. After cooling to room temperature, the precipitated product was filtered, washed with acetic acid and ethanol, and dried under vacuum at 60 °C, yielding 17.5 g (85%) of the intermediate (IPE-COOH) as an off-white product. The intermediate 10 g (24 mmol) was used without further purification and added into a 100 mL round bottom flask containing 25 mL $SOCl_2$ and 2 drops of DMF. The mixture was refluxed for 12 hours under an argon blanket before the excess $SOCl_2$ was distilled off. The solid was purified via recrystallization from dry chloroform, yielding 7.6 g (70%) of off-white needle-shaped crystals. T_m = 229 °C; ΔH_{fus} =100 J·g^{-1} (DSC); ^{1}H-NMR ($CDCl_3$) δ(ppm): 7.41 (m, 3H), 7.58 (m, 2H), 7.97 (d, *J*=7.8 Hz 1H), 7.98 (d, *J*=7.8 Hz, 1H), 8.11 (s, 1H), 8.61 (s, 2H), 8.84 (s, 1H); ^{13}C-NMR ($CDCl_3$) δ(ppm): 87.39, 95.17, 121.79, 124.29, 127.00, 128.58, 129.50, 129.59, 130.99, 131.47, 131.91, 132.01, 133.62, 133.88, 135.20, 137.86, 165.58, 165.60, 166.57; MS m/z (relative intensity): 446.95 (M+, 25.2), 411.95 (52.6), 206.00 (24.6), 204.00 (24.8), 176.05 (43.4), 126.10 (100.0), 102.10 (25.63), 88.05 (37.1), 75.10 (23.8); FTIR υ/cm^{-1}: 3091, 2209, 1781, 1759, 1722, 1612, 1594.

2-(Phenylethynyl phthalimido) terephthaloyl chloride (TPE-COCl)

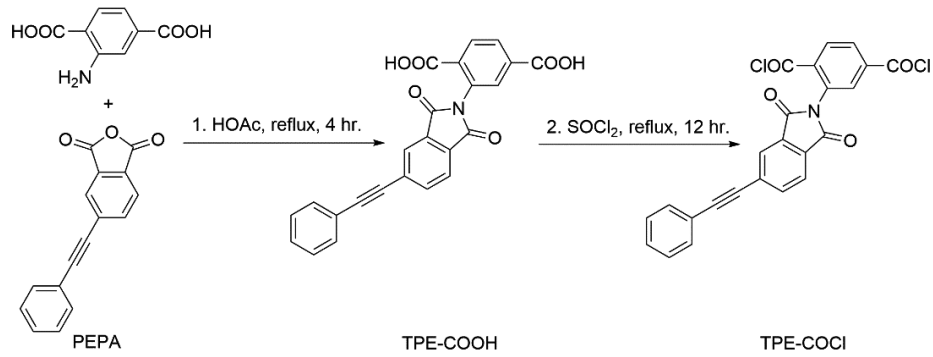

Scheme 4.5 Synthetic route towards TPE-COCl.

As shown in Scheme 4.5, a 250 mL round bottom flask equipped with a reflux condenser was charged with 100 mL acetic acid and PEPA 12.4 g (50 mmol). The mixture was heated to 120 °C until all solids were dissolved. 2-aminoterephthalic acid 9.0 g (50 mmol) was added to the flask and this reaction mixture was refluxed for 4 hours. After cooling to room temperature, the precipitated product was filtered, washed with acetic acid and ethanol, and dried under vacuum at 60 °C, yielding 16.5 g (80%) of the intermediate (TPE-COOH) as an off-white product. The intermediate 10 g (24 mmol) was used without further purification and added into a 100 mL round bottom flask containing 25 mL $SOCl_2$ and 2 drops of DMF. The mixture was refluxed for 12 hours under an argon blanket before the excess $SOCl_2$ was distilled off. The obtained crude product could not be recrystallized from chloroform, acetone, tetrahydrofuran, acetonitrile, ethyl acetate or toluene, which excludes purification via recrystallization. The crude product was dissolved in dry chloroform and filtered through a PTFE membrane (0.45 µm) to remove possible insoluble impurities. The crude product was used without additional purification. Yield: 9.9 g (91%) of yellowish solid. ^{1}H-NMR ($CDCl_3$) δ(ppm): 7.41 (m, 3H), 7.57 (m, 2H), 7.95 (s, 2H), 8.09 (s, 1H), 8.20 (s, 1H), 8.33 (d, *J*=8.4 Hz, 1H), 8.36 (d, *J*=8.2 Hz, 1H); ^{13}C-NMR ($CDCl_3$) δ(ppm): 87.47, 94.95, 121.88, 124.30, 127.07, 128.56, 129.41, 129.97, 130.81, 131.01, 131.81, 131.88, 131.91, 132.08, 133.10, 136.59, 137.68, 138.11, 165.65, 165.67, 165.70, 166.56; MS m/z (relative intensity): 447.10 (M+,

19.2), 412.10 (100.0), 176.10 (28.2), 126.15 (81.9); FTIR υ/cm^{-1}: 3058, 2212, 1778, 1755, 1722, 1614, 1569.

4.2.4 Synthesis of PE side-group functionalized copolyamides

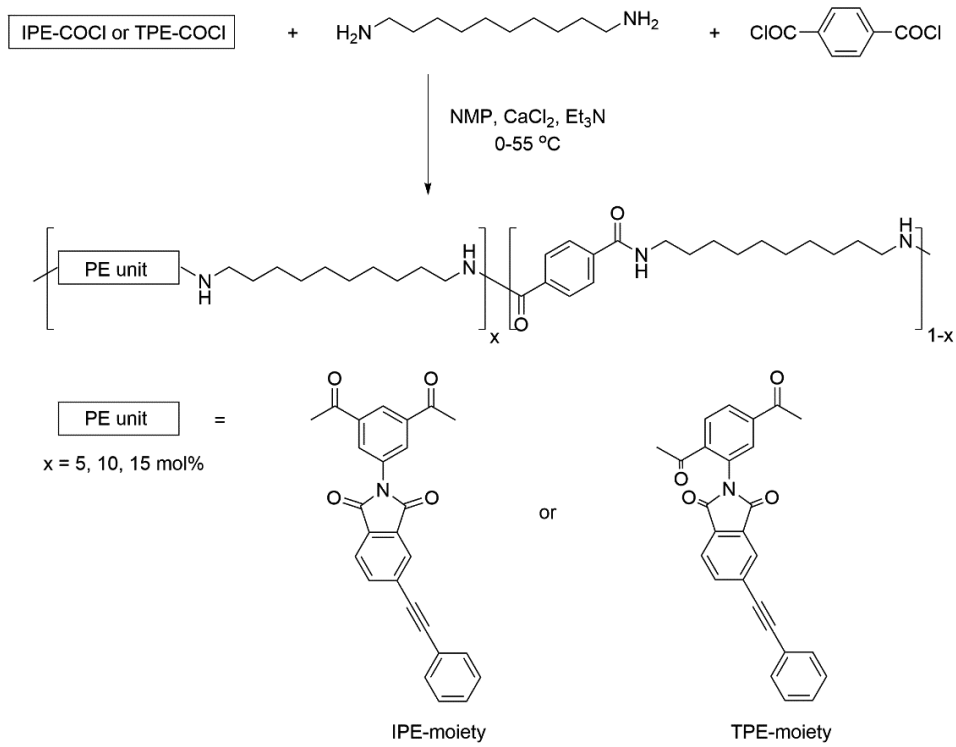

Scheme 4.6 Preparation of PE side-group functionalized copolyamides. The PE-comonomer concentration was selected to be 5, 10 or 15 mol%.

All polymerization variations were prepared according to the same synthetic procedure as shown in Scheme 4.6. The molar ratio of the diacid chloride and diamine monomers was kept at 1:1 to reach the highest M_n. The optimal polymerization conditions described in Chapter 2 was used for the synthesis. The PE-comonomer concentration was selected to be 5, 10 or 15 mol%. The IPE-copolyamides are denoted as IPE-5, IPE-10 and IPE-15, and the TPE-copolyamides

are denoted as TPE-5, TPE-10 and TPE-15, respectively. The synthetic procedure of IPE-5 is described as an example.

IPE-5. All glassware was pre-dried in a vacuum oven at 150 °C for at least 60 minutes. In a 100 mL three-neck flask equipped with a mechanical stirrer, an argon inlet and a vacuum connection, 30 mL of NMP, 2.4 g of $CaCl_2$ and 1.723 g (10 mmol) of 1,10-decanediamine was placed. The mixture was heated to 70 °C to allow the 1,10-decanediamine to dissolve completely, and then cooled to 0 °C on an ice-bath. Triethylamine (5 mL) was added to the flask followed by a 10 mL NMP solution of terephthaloyl chloride 1.929 g (9.5 mmol) and IPE-COCl 0.224 g (0.5 mmol). The mixture was stirred at 350 rpm for 30 min at 0 °C and for another 3 hours at 55 °C to obtain a viscous slurry. This slurry was precipitated into demineralized water and the solids were washed 3 times with water in a heavy-duty blender before being collected by filtration. The copolyamide IPE-5 was obtained as an off-white product after drying under vacuum at 60 °C overnight.

4.2.5 Preparation of thermoset films

Thermoset films were prepared using standard melt compression techniques. The precursor powder was placed inside a Kapton™ mold between two Kapton™ films and consolidated in Joos hot press under 5 kN force. The temperature program is ramping up to 350 °C with 5 °C·min^{-1}, holding for 15 min, and cooling to 50 °C at 5 °C·min^{-1}.

4.3 Study of side-group functionalized copolyamides

4.3.1 Thermal behavior of PE comonomers

DSC was performed to investigate the thermal behavior of the PE comonomers. Figure 4.1 (A) shows the DSC curves of the two intermediates, IPE-COOH and TPE-COOH. The intermediates are carboxylic acids with strong hydrogen bonds between the molecules, and thus show high melting points of 377 °C and 370 °C for IPE-COOH and TPE-COOH, respectively. Followed by the melting endotherm, an exotherm is revealed due to curing of the PE end-groups.

Figure 4.1 (B) shows the DSC curves of the acid chloride compounds, IPE-COCl and TPE-COCl, which are used for the copolymerization. TPE-COCl shows a small

but discernable second order phase transition at about 60 °C where the compound becomes liquid, whereas IPE-COCl exhibits a sharp melting endotherm at 229 °C. This means that the TPE-COCl has the characteristics of a glass, which is probably due to its higher steric hindrance and lower molecular symmetry.

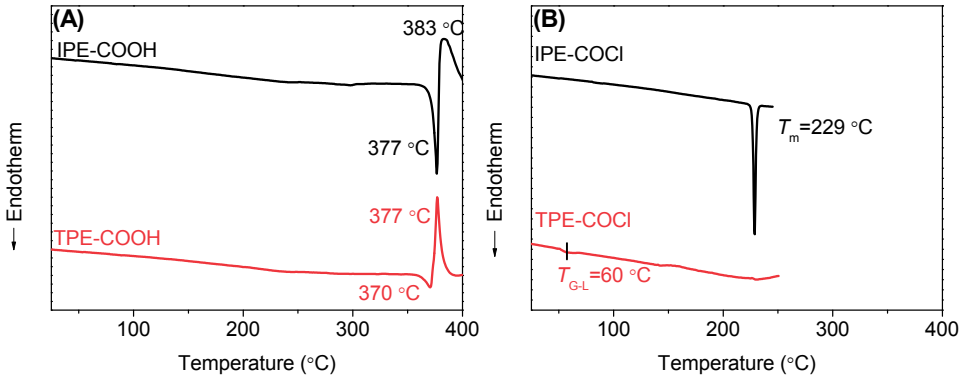

Figure 4.1 DSC heating scans of (A) IPE-COOH and TPE-COOH; (B) IPE-COCl and TPE-COCl. Curves obtained with a heating rate of 10 °C·min^{-1}, first heat. Curves are normalized to sample weight and are offset for clarity.

4.3.2 Copolyamide structures and molecular weights

After work-up and drying, the obtained copolyamides appeared unstable in concentrated sulfuric acid and insoluble in common organic solvents, such as NMP, tetrahydrofuran and hexafluoro-2-propanol.[22, 23] This precludes solvent-based analyses with these solvents. However, trifluoroacetic acid (TFA) can dissolve the copolyamides without destroying the PE reactive side-groups.

The reference polymer and PE-containing copolymers were dissolved in TFA-d and analyzed using ^{1}H NMR, as shown in Figure 4.2. The two clearly distinguished peaks at 7.28 and 7.45 ppm can be attributed to the five labeled PE-protons shown in the scheme in Figure 4.2. The composition of the copolyamides was determined by the peak area of these two peaks (A1) and the rest Ar-H peaks (A2). The molar amount (mol%) of the IPE or TPE commoner can be estimated using Equation (4.1) and are listed in Table 4.1. These values are close to the feed ratios of the monomers, confirming the target copolyamide structures.

$$IPE\ or\ TPE\ (mol)\% = \frac{A1/5}{(A2-6A1/5)/4+A1/5} * 100\% \quad (4.1)$$

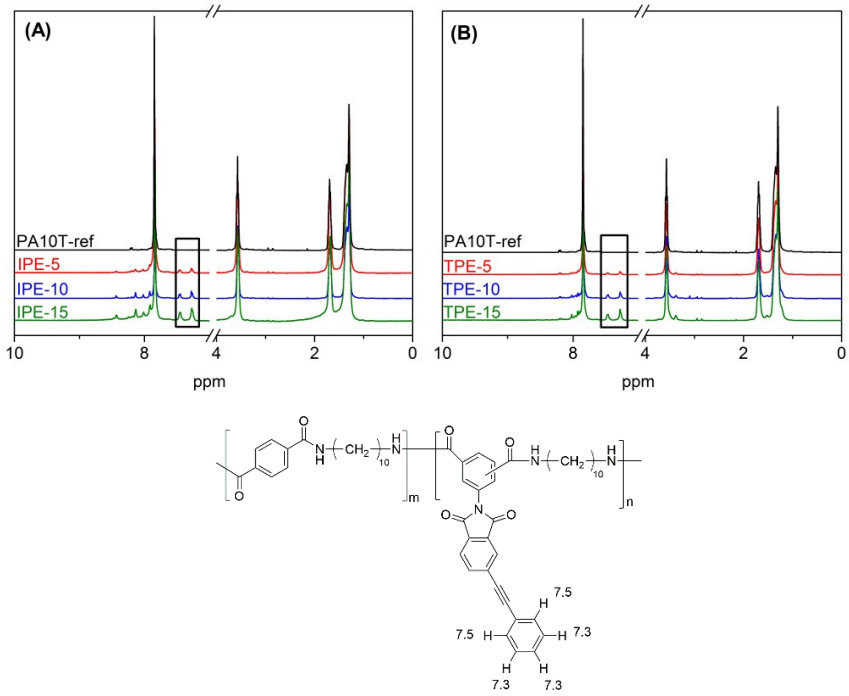

Figure 4.2 ^{1}H NMR spectra of (A) IPE-copolyamides; (B) TPE-copolyamides. The peaks in the rectangular frames are attributed to the labeled protons in the scheme.

The intrinsic viscosity of the copolyamides in TFA solvent was used for the determination of their molecular weights. The Mark-Houwink constants for PA 10T in TFA solvent were determined using 5 PA 10T homopolymer samples with different M_n, as shown in Figure 4.1S. The M_n of the copolyamides were calculated using the obtained Mark-Houwink constants as we assume that they are valid for the copolyamides due to their similar molecular structures to PA 10T.

Table 4.1 shows the M_n of the PA 10T-ref and the copolyamides. The M_n of the copolyamides range from 5.6 to 9.8 kg·mol^{-1}, which are comparable to the M_n of the PA 10T-ref (7.5 kg·mol^{-1}). Copolyamides containing higher concentrations of IPE or TPE comonomers show lower M_n, which might be due to the lower purity of the PE comonomers, especially TPE-COCl, which cannot be recrystallized.

Table 4.1 Overview of PA 10T-ref and the as-prepared copolyamides.

Sample	IPE or TPE (mol %)[a]	[η] (dL·g^{-1})[b]	M_n (kg·mol^{-1})[c]	T_d (°C)[d]	W_{350} (%)[e]	T_{m1} (°C)[f]	T_{m2} (°C)[g]	ΔH_m (J·g^{-1})[h]
PA 10T-ref	0	0.62	7.5	425	2.7	292	317	89
IPE-5	5.2	0.74	9.8	408	3.4	288	312	82
IPE-10	9.4	0.66	8.1	406	3.1	286	308	73
IPE-15	15.7	0.59	6.9	415	2.5	283	303	58
TPE-5	4.5	0.62	7.4	412	3.1	293	307	81
TPE-10	11.2	0.56	6.3	405	3.0	-	291	70
TPE-15	14.7	0.52	5.6	400	3.2	-	286	53

[a] The IPE or TPE comonomers concentration is calculated using ^{1}H NMR analysis.

[b] [η] is the intrinsic viscosity in TFA (99%) at 25 °C.

[c] M_n is calculated using Mark-Houwink constants K and α developed for PA 10T in TFA. K=2.7*10^{-3} dL·g^{-1}, and α=0.61.

[d] T_d is reported at the 5% weight loss under N_2 with a heating rate of 10 °C·min^{-1}.

[e] W_{350} is reported as the weight loss (%) at 350 °C under N_2.

[f] T_{m1} is reported as the peak temperature of the first melting endotherm.

[g] T_{m2} is reported as the peak temperature of the second melting endotherm.

[h] ΔH_m is reported as the melting enthalpy of the combined double melting endotherms.

4.3.3 Thermal properties

The thermal stability of the copolyamides were studied using TGA. All copolyamides start to undergo severe degradation at ≥400 °C as shown in Table 4.1. This is the same temperature range as for the PA 10T-ref homopolymer. The weight loss of the copolyamides at 350 °C is about 3%, which may be due to removal of residual NMP and/or the release of H_2O produced as result of post condensation. This weight loss is too high for film preparation via melt-compression, and therefore, a solid-state post-condensation is required prior to melt-compression.

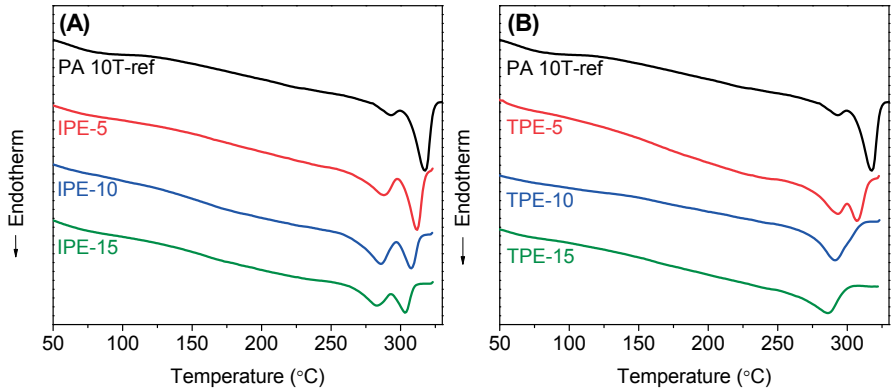

Figure 4.3 DSC heating scans of as-prepared samples (A) IPE-copolyamides, (B) TPE-copolyamides. Curves obtained with a heating rate of 20 °C·min^{-1}, first heat. Curves are normalized to sample weight and are offset for clarity.

DSC was used to investigate the melting behavior of the PA 10T-ref and copolyamides. As shown in Figure 4.3, the IPE copolyamides show similar double melting endotherms as the PA 10T-ref, which has been reported in Chapter 2. The double melting endotherms are also detected for TPE-5, but the difference between the two melting endotherms is smaller than that for the IPE copolyamides. Only one broad melting endotherm is found for TPE-10 and TPE-15, which is most likely because the high T_m crystal form is destabilized by introducing TPE and the melt transition is depressed as the concentration increases. The overal degree of crystallinity, as quantified by ΔH_m, decreases as the concentration of non-

linear IPE and TPE moieties increases. Both comonomers effectively disrupt polymer chain packing.

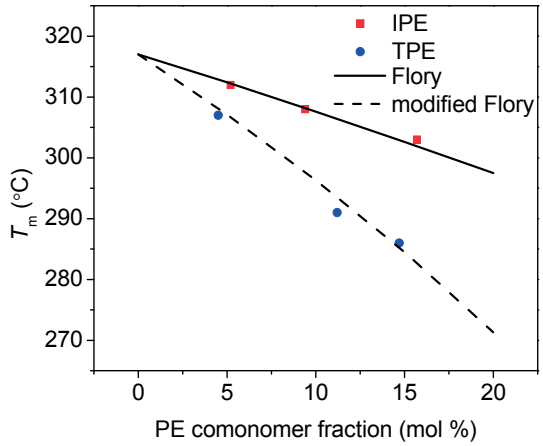

Figure 4.4 Experimental and predicted melting points as a function of PE comonomer fraction (mol%) for IPE- and TPE-copolyamides.

The T_{m2} of each sample is taken as the melting point, which is well below the cure temperature (350 °C) for the PE groups. The melting points are plotted as a function of PE comonomer content as shown in Figure 4.4. Clearly, a depression of melting points with increasing PE comonomer concentration is observed for both copolyamide series. Several theories have been developed to describe the melting point depression of random copolymers. The Flory theory is the most basic theory based on a comonomer exclusion model in which the minor comonomer is excluded from the polymer crystals.[24] Considering the bulky PE side-groups, they should not be able to fit into the crystal lattice formed by the PA 10T homopolymer sequences. Therefore, the exclusion model should be valid for both IPE and TPE copolyamides. The Flory theory is expressed as Equation 4.2.

$$\frac{1}{T_m^0} - \frac{1}{T_{m(X_B)}} = \frac{R}{\Delta H_m^0} \ln(1 - X_B) \quad (4.2)$$

where X_B is the concentration of the minor monomer B units in the copolymers and $\ln(1 - X_B)$ equals the collective activities of A sequences in the limit of the upper bound of the melting temperature. T_m^0 and ΔH_m^0 are the equilibrium melting temperature and enthalpy, respectively, and R is the gas constant. In this case, B is

the IPE or TPE comonomer, which is randomly distributed between the PA 10T homopolymer sequences. The T_m^0 and ΔH_m^0 of PA 10T homopolymer have not been reported to the best of our knowledge, however, the T_{m2} of PA 10T-ref (317 °C) can be approximately taken as the T_m^0 of PA 10T, and the ΔH_m^0 is estimated being 32 kJ·mol^{-1} based on literature data.[25]

The solid line in Figure 4.4 represents the predicted T_m of the copolyamides according to Flory theory and is a good fit with the experimental T_m values of the IPE copolyamides. However, the T_m of the corresponding TPE copolyamides are much lower. We proposed a modified Flory equation to fit the T_m of the TPE copolyamides, as shown in Equation 4.3. A coefficient A is introduced to correct for the effective length of the homopolymer sequences.

$$\frac{1}{T_m^0} - \frac{1}{T_m(X_B)} = \frac{R}{\Delta H_m^0}[\ln(1 - AX_B)] \quad (4.3)$$

The value of A is fitted to be 2.11, which is higher than 1 in the Flory equation 4.2, indicating that the TPE comonomer has a strong disrupting effect on the crystallizable length of the PA 10T homopolymer sequences. This may be due to the low structural symmetry of the TPE comonomer. The PE side-groups in the IPE copolyamides have only one possible direction, while they may point towards two directions in the TPE copolyamides. This, as a consequence, creates more conformational freedom (Scheme 4.7) and strongly disturbs the regularity of the polymer chains. The kinked structure (120° exocyclic bond angle) of the *meta*-substituted IPE comonomer also plays a negative role on crystallization,[26] however, it seems that this effect is not as significant as the conformational diversity of the PE side-groups. Also, the PE groups of TPE comonomer are in *ortho*-position to one direction of the polymer chains, from which the steric proximity creates more disturbance than the *meta*-position. Altogether, the IPE comonomer displays less hindrance to the crystallization of the polymer chains, and therefore, the IPE copolyamides show higher T_m and ΔH_m than their TPE counterparts.

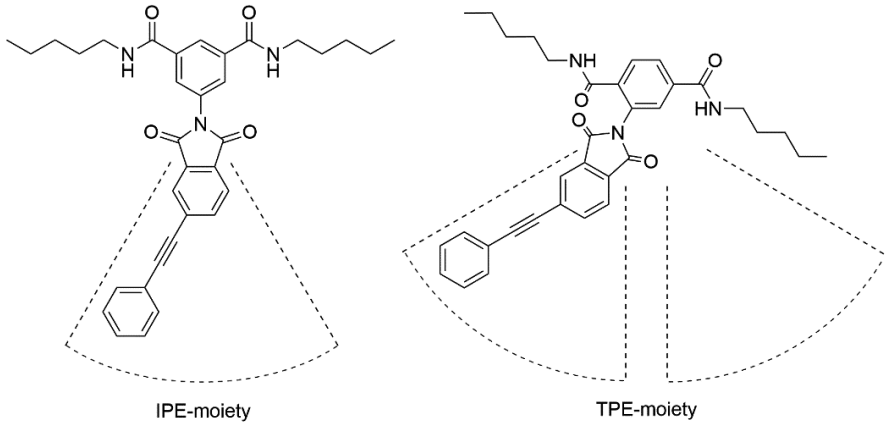

Scheme 4.7 Possible conformations of IPE- and TPE- moieties in the PA 10T polymer backbone. The (3D) cones represent the volume elements in which the IPE- and TPE- moeities may reside.

4.4 Thermal cure of copolyamides

4.4.1 Post-condensation

As discussed in Chapter 3, PE groups can be cured at 350 °C, but the weight loss of the as-prepared copolyamides at 350 °C is about 3% as shown in Table 4.2, which is too high for film preparation via melt-compression. Therefore, a solid-state post-condensation was performed at 250 °C for 6 hours under vacuum. A weight loss of not higher than 1.6% at 350 °C was found for the post-condensed samples, which allows subsequent melt-pressing.

The post-condensed copolyamides appear more yellowish, and cannot be completely dissolved in TFA, which is different from the as-prepared polymers. This change indicates that the copolyamides have already undergone a certain degree of crosslinking during post-condensation. Compared with the PA 10T-ref sample, which remains soluble in TFA after post-condensation, it seems clear that the PE side groups of the copolyamides contribute to the formation of a polymer network. The imide ring of the side-groups is expected to be stable during post-condensation, and this leads us to speculate that a pre-cure of PE groups takes place.

Table 4.2 TGA results and solubility of the copolyamides before and after post-condensation at 250 °C for 6 hours.

Sample	Before post-condensation			After post-condensation		
	T_d (°C)[a]	W_{350} (%)[b]	Solubility in TFA [c]	T_d (°C)[a]	W_{350} (%)[b]	Solubility in TFA [c]
PA 10T-ref	425	2.7	+	430	1.1	+
IPE-5	408	3.4	+	424	1.6	-
IPE-10	406	3.1	+	423	1.2	-
IPE-15	415	2.5	+	422	1.0	-
TPE-5	412	3.1	+	423	1.4	-
TPE-10	405	3.0	+	416	1.1	-
TPE-15	400	3.2	+	407	1.6	-

[a] T_d is reported at the 5% weight loss under N_2 with a heating rate of 10 °C·min^{-1}.

[b] W_{350} is reported as the weight loss (%) at 350 °C under N_2.

[c] Test of 10 mg sample in 1 mL TFA overnight, "+" dissolved at room temperature; "-" not dissolved at room temperature

The PE groups are usually cured above 300 °C in all-aromatic systems.[5] There is strong evidence that the thermal cure of PE proceeds via a free-radical mechanism,[27] and it has been reported that the free radicals formed by the thermolysis of polyethylene glycol can initiate the cure of PE groups and reduce the cure temperature of a phenylethynyl-terminated polyimide–PEG blend to 200-250 °C.[28] In semi-aromatic polyamides, thermal decomposition may result in the formation of benzamide and alkylamide radicals.[29] We speculate that free radicals generated during post-condensation initiate the pre-cure of the PE groups to form crosslinks. For the copolyamides with PE side-groups distributed along the polymer

chains, the combination of two PE groups results in a crosslinking point, which promotes the formation of networks. This is different from the linear end-capped systems where the end-groups are able to chain extend and crosslink. To collect evidence for this hypothesis, spectroscopic techniques were employed to prove that the reactive PE groups are consumed, but without success. Raman spectroscopy failed to observe signals for the post-condensed polyamides due to a strong fluorescence background which maybe due to the conjugated moieties formed by the pre-cure of PE groups, and also FTIR cannot detect the acetylene bond of PE because of IR insensitivity. Hence, direct evidence is not available to confirm that the PE functionalities are consumed during post-condensation. The change in polymer solubility after post condensation, however, does suggest that crosslinking is taking place.

Figure 4.5 shows the DSC traces of the post-condensed PA 10T-ref and reactive copolyamides. All post-condensed samples (Table 4.3) show a higher ΔH_m than the corresponding as-prepared samples. As we have studied in Chapter 3, crosslinking depresses the degree of crystallinity, which should have resulted in a lower ΔH_m. However, the high temperature used during post-condensation allows the amorphous polymer segments to become mobile and crystallize. This annealling effect seems to dominate over crosslinking, resulting in an overal increase in crystallinity by 21-37%. However, the T_m of post-condensed IPE-15 and TPE-15 are depressed by crosslinking because of the high PE concentration.

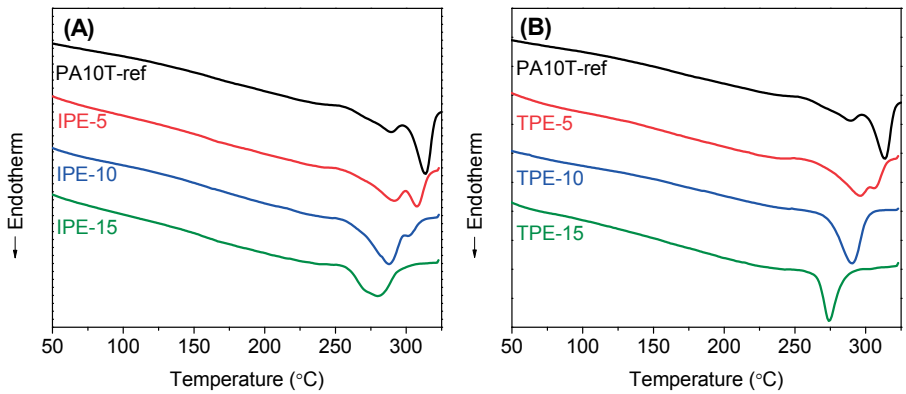

Figure 4.5 DSC scans of post-condensed samples (A) IPE-copolyamides, (B) TPE-copolyamides. Measurements performed using a heating rate of 20 °C·min^{-1}, first heat. Curves are normalized to sample weight and are offset for clarity.

Table 4.3 DSC results of PA 10T-ref and copolyamides before and after post-condensation at 250 °C for 6 hours.

Sample	Before post-condensation			After post-condensation		
	T_{m1} (°C)[a]	T_{m2} (°C)[b]	ΔH_m (J·g^{-1})[c]	T_{m1} (°C)[a]	T_{m2} (°C)[b]	ΔH_m (J·g^{-1})[c]
PA 10T-ref	292	317	89	290	314	115
IPE-5	288	312	82	292	308	107
IPE-10	286	308	73	288	301	99
IPE-15	283	303	58	-	280	72
TPE-5	293	307	81	296	306	105
TPE-10	-	291	70	-	290	96
TPE-15	-	286	53	-	274	64

[a] T_{m1} is reported as the peak temperature of the peak at lower temperature.

[b] T_{m2} is reported as the peak temperature of the peak at higher temperature.

[c] ΔH_m is reported as the melting enthalpy of the combined double melting endotherms.

4.4.2 Thermal cure behavior

Rheology experiments were performed to study the cure behavior of the post-condensed copolyamides. The complex viscosity $|\eta^*|$ of all samples as function of temperature and time are shown in Figure 4.6. The $|\eta^*|$of the PA 10T-ref drops rapidly to 10^2-10^3 Pa·s when the sample melts, however, the copolyamides show much higher melt $|\eta^*|$ of 10^4-10^5 Pa·s, indicating that the copolyamides are to a certain extent cured during post-condensation.

The temperature program for the rheology test was set to mimic the film pressing conditions. A cure temperature of 350 °C was used to cure the

copolyamides. The $|\eta^*|$ values of IPE-5 and TPE-5 start to increase around 300 °C, and reach a plateau after a 15 minutes hold at 350 °C. Little change in $|\eta^*|$ was found when extending the cure time, indicating that the copolyamides are close to being fully cured in the first 15 minutes at 350 °C. The samples with higher PE concentrations require less time at cure to reach the $|\eta^*|$ plateau. Following the rheological results, melt pressing at 350 °C for 15 minutes was used as the cure conditions for preparing the thermoset films. We also noticed that the PA 10T-ref undergoes a slight increase in $|\eta^*|$at 350 °C over time, which may be due to the post-polymerization or crosslinking.

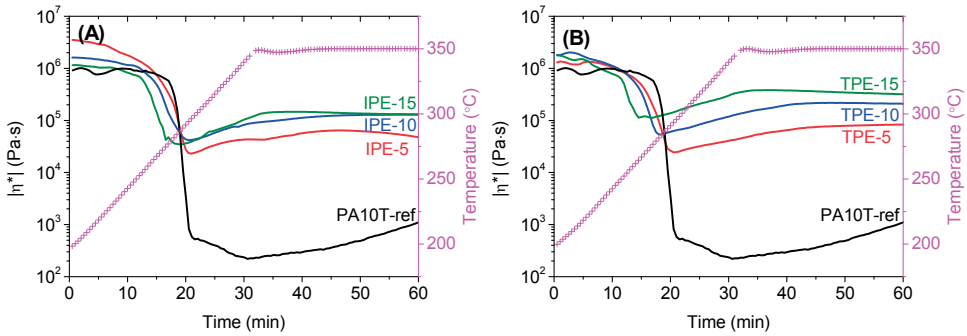

Figure 4.6 Rheological measurements of PA 10T-ref and copolyamides. (A) IPE copolyamides; (B) TPE copolyamides. $|\eta^*|$ as a function of temperature (200-350 °C) and 30 min. isothermal hold at 350 °C. Experiments were performed using a frequency of 1 Hz and heating rate of 5 °C·min^{-1} under N_2 atmosphere. The test specimens were prepared after a pre-cure at 250 °C under vacuum for 6 hours.

4.5 Morphology of the thermoset films

4.5.1 Melting and crystallization

Figure 4.7 and Table 4.4 summarize the DSC results of the after-cure film samples. The thermoplastic PA 10T-ref film with the same thermal history is included as a reference.

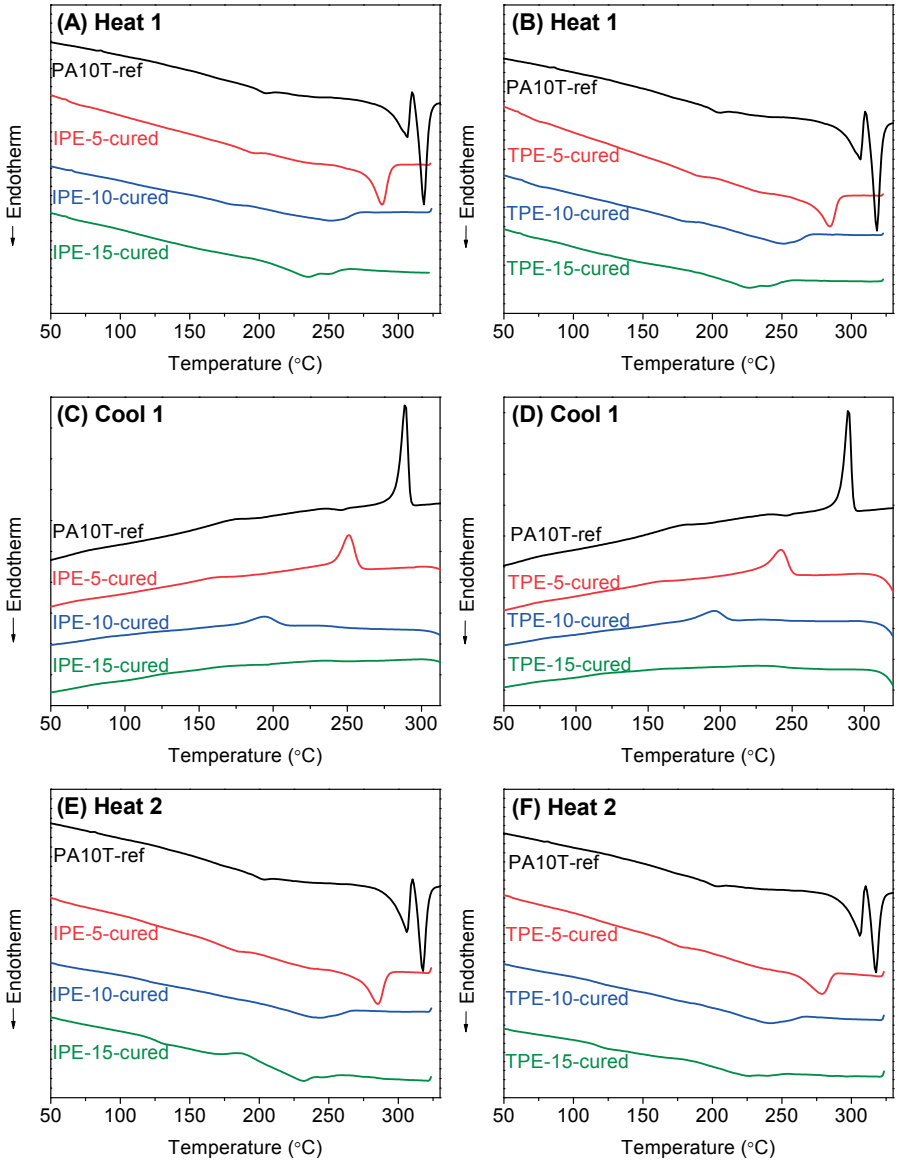

Figure 4.7 DSC traces of the PA 10T-ref film, IPE-cured films and TPE-cured films (A) and (B) 1st heating scan, (C) and (D) cooling scan, (E) and (F) 2nd heating scans. Results obtained using a heating/cooling rate of 20 °C·min^{-1} under N_2 atmosphere. Curves are normalized to sample weight and are offset for clarity.

Table 4.4 DSC results of the PA 10T-ref thermoplastic film, IPE-cured and TPE-cured thermoset films

Sample	Heat 1		Cool 1		Heat 2	
	T_m [a] (°C)	ΔH_m (J·g^{-1})	T_c [b] (°C)	ΔH_c (J·g^{-1})	T_m [a] (°C)	ΔH_m (J·g^{-1})
PA 10T-ref	318	82	289	73	318	74
IPE-5-cured	288	39	251	36	285	31
IPE-10-cured	251	30	194	21	244	25
IPE-15-cured	235	24	-	-	232	20
TPE-5-cured	285	33	242	31	279	25
TPE-10-cured	250	27	195	18	242	20
TPE-15-cured	227	20	-	-	226	15

[a] T_m is reported as the peak temperature of the second peak if there are double melting endotherms present.

[b] T_c is reported as the peak temperature of the crystallization exotherm during cooling.

The T_m and ΔH_m of the thermoset films are substantially reduced when compared to the PA 10T reference polymer, which shows reversible melting and crystallization behavior. For the copolyamides, crystallization of the polymer chains is to a large extent hindered by the cure of the PE reactive side-groups. The cured copolyamides containing 5 and 10 mol% PE side-groups are expected to have a lower crosslinking density and are still able to crystallize upon cooling. The ΔH_m is reduced to 33–39 J·g^{-1} for the IPE-5- and TPE-5-cured films, and 27-32 J·g^{-1} for the IPE-10- and TPE-10-cured films, compared to the PA 10T-ref (82 J·g^{-1}). Also, crosslinking has suppressed the melting temperatures by 22-57 °C depending on the amount of PE side-groups. For the IPE-15- and TPE-15-cured films we do not

observe a crystallization exotherm during cooling, however, upon the second heating a small but discernable cold crystallization exotherm can be detected at ~185 °C.

Moreover, the difference between the melting and crystallization temperature, which is the supercooling temperature ($\Delta T = T_m - T_c$), increases with increasing concentration of PE groups, suggesting that crystallization becomes more difficult at higher PE concentration.[30] Compared to the TPE-cured films, the IPE-cured films exhibit higher T_m and ΔH_m, which is consistent with the results of the copolyamide precursors.

4.5.2 WAXD analysis of thermoset films

Room temperature WAXD experiments were performed to study the crystalline structure of the after-cure thermoset films and the results are shown in Figure 4.8. The thermoplastic PA 10T-ref film was also included for reference purposes and has the same thermal history as the cured IPE and TPE thermoset films. The IPE-5-cured and TPE-5-cured thermosets show the same WAXD reflections as the PA 10T-ref film, which means that the crystal form of the thermosets and the thermoplastic PA 10T reference polymer are the same.

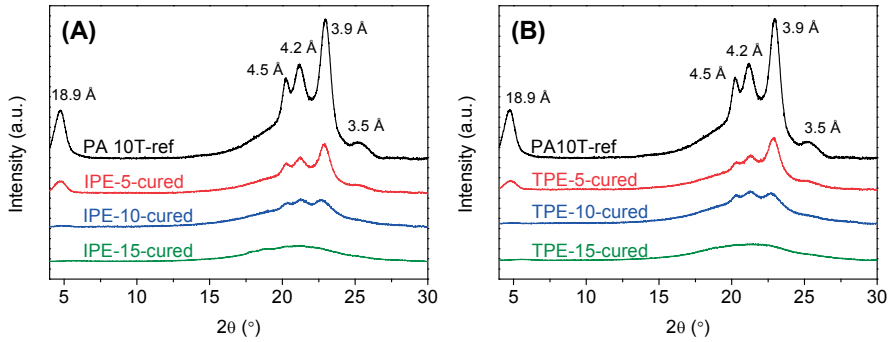

Figure 4.8 WAXD intensity as a function of the scattering angle 2θ (A) film samples of PA 10T-ref, IPE-5-cured, IPE-10-cured and IPE-15-cured; (B) film samples of PA 10T-ref, TPE-5-cured, TPE-10-cured and TPE-15-cured. The *d*-spacing values are shown above the corresponding peaks.

The reflections become less prominent for IPE-10-cured and TPE-10-cured thermosets, and are barely visible in the IPE-15-cured and TPE-15-cured thermoset spectra, indicating a strong reduction in crystallinity. As shown in Figure 4.2S, the WAXD patterns of PA 10T-ref and the thermosets with 5 and 10 mol% PE could be deconvoluted into an amorphous halo and five crystalline reflections using a Gaussian curve-fitting procedure. The crystallinity index (*CI*), which is indicative of the degree of crystallinity, was calculated according to Equation 4.4.

$$CI\ (\%) = \frac{Area_{crystalline}}{Area_{crystalline} + Area_{amorphous}} \quad (4.4)$$

These results are listed in Table 4.5, and show agreement with the trend observed in DSC measurements.

Table 4.5 Summary of *CI* values, DMTA results and gel fraction results after full cure.

Sample	*CI* (%)[a]	*E'* at 25 °C	T_g (°C)[b]	T_{break} (°C)[c]	Gel fraction (%)
PA 10T-ref	47	4.4	127	297	0
IPE-5-cured	36	4.6	127	401	74
IPE-10-cured	23	4.3	125	415	80
IPE-15-cured	-[d]	3.8	133	417	92
TPE-5-cured	35	3.8	123	413	72
TPE-10-cured	22	4.0	123	417	78
TPE-15-cured	-[d]	3.6	125	415	83

[a] *CI* values were calculated using Equation 4.4.

[b] T_g is reported at the maximum of E".

[c] T_{break} is reported at the temperature where the sample fails.

[d] cannot be quantified because the reflections are too weak to be deconvoluted.

4.6 Thermo-mechanical properties

DMTA measurements were performed to study the thermo-mechanical properties of PA 10T-ref thermoplastic film and cured thermoset films. The storage modulus (*E'*) and loss modulus (*E"*) as a function of temperature are shown in Figure 4.9.

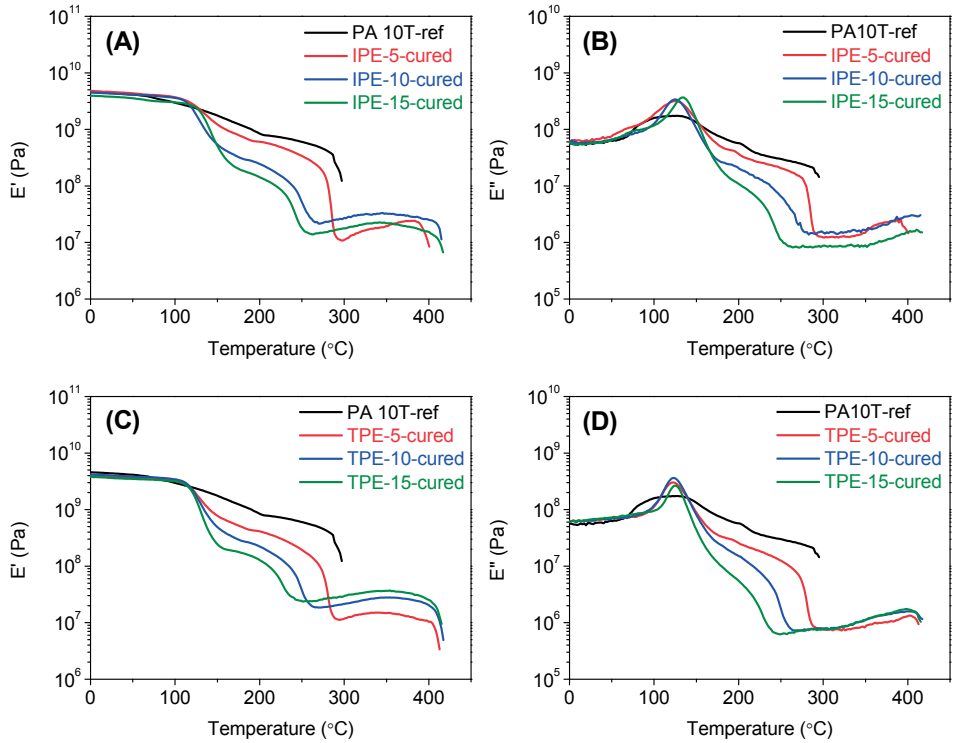

Figure 4.9 DMTA of PA 10T-ref thermoplastic film, IPE-cured thermoset films and TPE-cured thermoset films. (A) and (C) Storage modulus (*E'*) as a function of temperature; (B) and (D) loss modulus (*E"*) as a function of temperature. Heating rate 2 °C·min^{-1} under N_2 atmosphere and a frequency of 1 Hz.

Table 4.5 lists the DMTA results and the gel fraction of all samples. PA 10T-ref displays typical thermo-mechanical properties of a semi-crystalline thermoplastic with a temperature at break (T_{break}) of 297 °C because of melting. The thermoset analogs, on the other hand, are stable to temperatures well above 400 °C, which is

about 100 °C higher than the melting point of PA 10T. The cured films cannot be completely dissolved in TFA, and the gel fraction of the cured films are 72-92%. This means that most polymer chains are crosslinked and are part of a network structure, especially in the thermosets of higher PE concentration, which show a higher gel fraction value.

At temperatures below T_g, the polymer chain segments are rigid for all samples, as a result, a similar *E*' of ~4 GPa is obtained. However, in the temperature range between T_g and T_m, the thermoset films show a lower *E*' than PA 10T-ref due to lower degree of crystallinity. In this sense, crystallinity has a more significant effect on the *E*' within this temperature range than crosslinking. Above the melting temperature, the thermoset samples show an *E*' of 10-20 MPa. An increase of E' is observed until ~350 °C, which might be caused by the post-cure of leftover PE groups or alignment of the mobile chains within the network. Above 350 °C, the *E*' starts to decrease until the sample fails, which is probably due to the start of thermal scission of polymer chains. Copolyamides with as low as 5 mol% of IPE or TPE comonomer can be cured into thermal-stable thermosets, while further increasing the concentration of PE side-groups does not lead to additional improvement in *E*'. It should be noted that trapped entanglements of polymer chains may be formed during crosslinking and may also contribute to the modulus.

The *E*" peak of thermoset films, especially of the ones with high PE concentration, are much narrower than that of the PA 10T-ref film, which indicates a restricted mobility of the amorphous chain segments. The PA 10T-ref with the highest degree of crystallinity shows a broad *E*" peak, which confirms the fact that the mobility of the amorphous chains is significantly restricted by the rigid crystalline domains. The peak temperatures of *E*" are taken as the T_g of the samples. We have found that the thermoset films show a similar T_g compared to the PA 10T-ref film (127 °C). In this crosslinked semi-crystalline system, the introduced crosslinking restricts the mobility of amorphous chains, however, strongly hinders the crystallization which on the other hand increases their mobility. These conflicting effects, as a consequence, result in nearly unchanged T_g.

4.7 Mechanical properties

Stress-strain measurements were performed to investigate the mechanical properties of the thermosets. All samples except IPE-15-cured show brittle fracture

without yielding, as shown in Figure 4.10. Figure 4.11 shows the tensile strength, elastic modulus, elongation at break and toughness of the PA 10T-ref, cured IPE and cured TPE films.

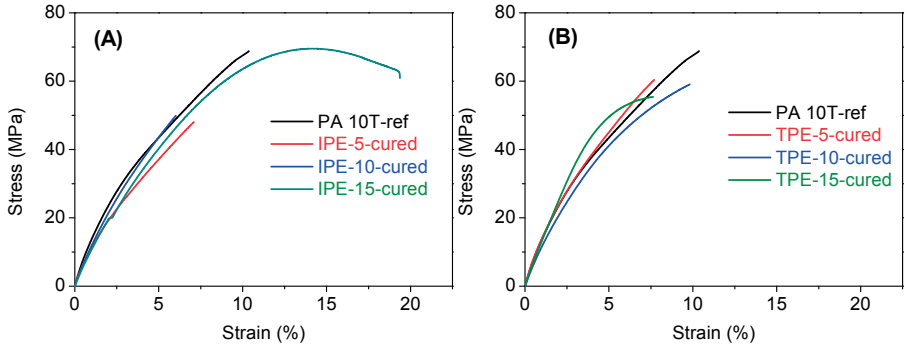

Figure 4.10 Stress-strain behavior of (A) PA 10T-ref and IPE-cured, (B) PA 10T-ref and TPE-cured film samples. Best results out of 3 stress-strain experiments are shown.

The thermoset samples exhibit tensile strengths of ~40-60 MPa, which are lower than the tensile strength of PA 10T-ref (63 MPa). The PA 10T-ref shows the highest elastic modulus (1.5 GPa) compared to the thermoset films (1.1-1.4 GPa) due to its high degree of crystallinity. Although the thermoset samples are crosslinked in the amorphous phase, they still display an elongation at break of 5-8%, which exceeds that of the other thermoset polymers (typically ε<5%).[31, 32] In this sense, we may conclude that the mechanical properties of the thermosets are not significantly deteriorated compared to the thermoplastic PA 10T reference polymer.

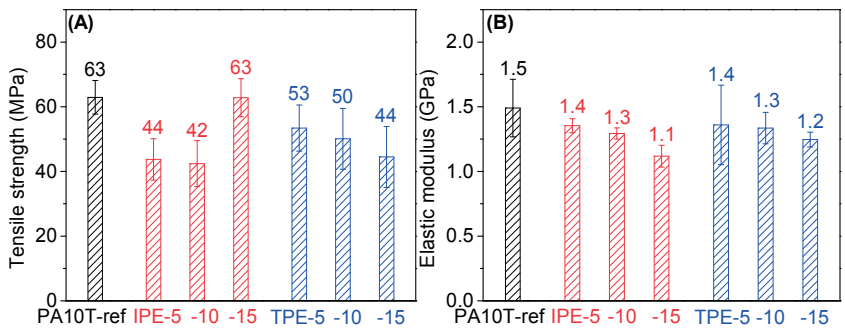

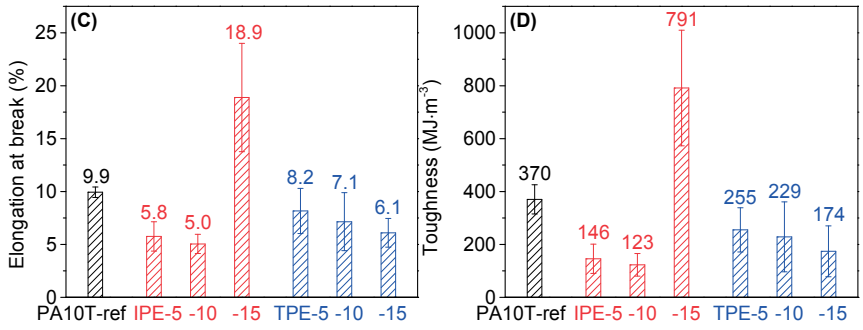

Figure 4.11 (A) Tensile strength, (B) elastic modulus (C) elongation at break and (D) toughness of PA 10T-ref film, cured IPE films (IPE-5, -10 and -15) and cured TPE films (TPE-5, -10 and -15). Data shown is the average of 3 experiments.

Among the thermoset samples, the IPE-15-cured film shows an outstanding elongation at break value (~19%), which in turn results in a high toughness of 791 $MJ \cdot m^{-3}$. The values of elongation at break for semi-aromatic polyamides, such as PA 6T, PA 9T and PA 10T based thermoplastics, are reported to range from 1.5–10%.[33-36] The IPE-15-cured sample shows a significant improvement over well-known commercial polyamides, potentially expanding the use of semi-aromatic PAs to engineering applications where toughness is important. The high elongation and toughness of the cured IPE-15 film may originate from the larger free volume induced by the kinked IPE comonomer (exocyclic bond angle = 120°) and low degree of crystallinity due to cure.

4.8 Approaches towards PA 10T thermosets

By changing the concentration of the PE side-groups in the reactive copolyamides, the crosslinking density of the thermosets can be controlled, consequently leading to an adjustable degree of crystallinity. This strongly affects the morphology and the thermo-mechanical properties of the obtained thermosets. DMTA experiments confirm that semi-crystalline thermosets with crosslinked amorphous phase can be prepared via a side-group functionalized copolymer approach. A molecular representation of the copolyamide precursor and the semi-crystalline network structure is shown in Figure 4.12.

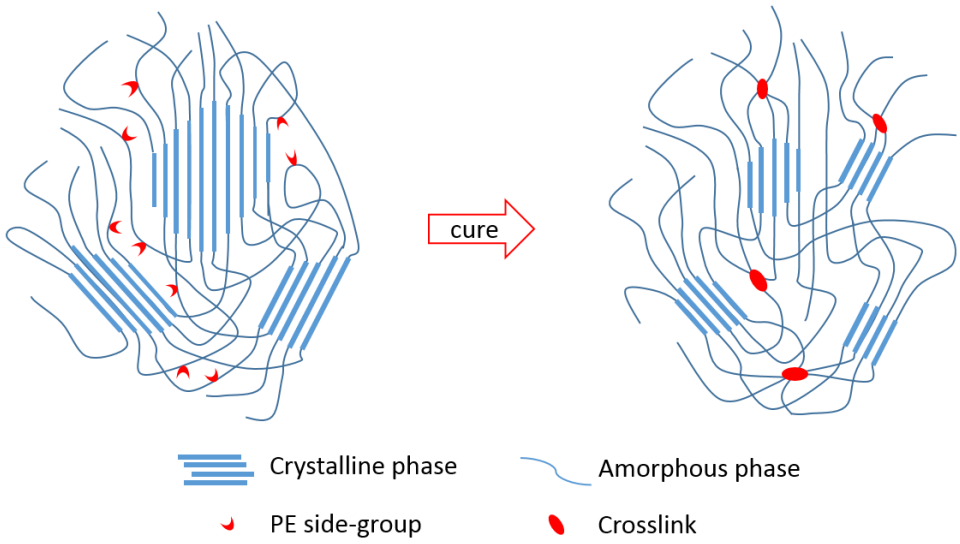

Figure 4.12 Schematic illustration of the molecular structure of the side-group functionalized copolyamide precursor and the semi-crystalline thermoset. Blue curvy lines represent the amorphous chain segments, the straight blue (bold) lines represent the crystalline chain segments and the red dots represent the crosslinks in the amorphous phase.

PA 10T thermosets prepared from reactive end-capped PA 10T oligomers (M_n = 1K and 3K g·mol^{-1}) have been reported in Chapter 3. Their low melt viscosity (<10^2 Pa·s) may be beneficial for preparing fiber-reinforced composites. However, compression molding and other melt processing techniques may be difficult as the low vicous precursor melt is difficult to contain. On the other hand, the copolymer approach described in Chapter 4 uses high M_n side-group functionalized copolyamides as precursors, which are easier to melt-press into thermoset films because of their high melt viscosity (>10^3 Pa·s). Also, the PE concentration in the copolyamide is not directly related to the M_n of the polymer, which allows controlling the final morphology of the thermoset only by changing the amount of the PE comonomer.

The semi-crystalline thermosets obtained from both approaches show the same WAXD pattern as the PA 10T-ref film sample, which means that the crystalline domains in the thermosets are dominated by the PA 10T backbone composition. The crosslinks resulting from PE end-caps or IPE/TPE comonomers cannot

participate in crystallization. The melt transition and degree of crystallinity of the thermosets are depressed by crosslinking and can be controlled by the crosslinking density, i.e. the M_n of the reactive oligomers in the oligomer approach and the IPE/TPE concentration in the copolymer approach. Overall, the two approaches show different processing characteristics but lead to PA 10T based thermosets with the same morphology.

4.9 Conclusions

In this chapter, we have demonstrated that phenylethynyl (PE) side-group functionalized copolyamides can be thermally cured into semi-crystalline thermosets. PA 10T-based reactive copolyamides with 5, 10 and 15 mol% of PE side-groups were successfully synthesized using a solution polymerization method. Two types of PE-containing comonomers (IPE- and TPE-monomer) with isophthalic and terephthalic structures have been synthesized and incorporated in the copolyamides. The comonomers disrupt the crystallization of the copolyamides, among which the IPE series exhibit higher T_m and ΔH_m than the corresponding TPE series. Melt rheology experiments show that the copolyamide precursors can be crosslinked in 15 min. at 350 °C, showing a complex melt viscosity of ~10^5 Pa·s. DMTA measurements showed that thermoset films exhibit an E' of 10-20 MPa at the plateau above T_m, and the films are stable up to ~400 °C as a result of network formation. The melt transition and degree of crystallinity in the final thermoset films are strongly depressed by the thermal cure process, especially in the thermosets with high crosslinking density. The thermoset films exhibit a T_g of 127 °C, which is similar to the PA 10T reference thermoplastic film. Stress-strain experiments show that the IPE-15-cured films show outstanding elongation at break (~19%) and toughness (791 MJ·m^{-3}), which is a significant improvement over the PA 10T homopolymer (9.9% and 370 MJ·m^{-3}). In conclusion, we have demonstrated that a semi-aromatic polyamide based thermoset can be prepared using PE side-group functionalized copolyamide precursors. This approach can be used to expand the thermal use window of semi-aromatic polyamides. The presence of two plateau regions ($T_g - T_m$ and > T_m) is of interest, as this will enable the design of polyamides with high-temperature shape-memory capabilities.

4.10 References

1. Liu, Y. L.; Chen, Y. W. *Macromolecular Chemistry and Physics* **2007,** 208 (2), 224-232.
2. Liu, Y.-L.; Hsieh, C.-Y.; Chen, Y.-W. *Polymer* **2006,** 47 (8), 2581-2586.
3. Connell, J. W.; Smith, J. G.; Hergenrother, P. M. *Journal of Macromolecular Science, Part C* **2000,** 40 (2-3), 207-230.
4. Kim, Y. J.; Chung, I. S.; In, I.; Kim, S. Y. *Polymer* **2005,** 46 (12), 3992-4004.
5. Iqbal, M.; Norder, B.; Mendes, E.; Dingemans, T. J. *Journal of Polymer Science Part A: Polymer Chemistry* **2009,** 47 (5), 1368-1380.
6. Dingemans, T., 5.26 - High-Temperature Thermosets. In *Polymer Science: A Comprehensive Reference*, Matyjaszewski, K., Möller, M., Eds. Elsevier: Amsterdam, 2012; pp 753-769.
7. Chen, P. Y.; Marvel, C. *Journal of Polymer Science: Polymer Chemistry Edition* **1981,** 19 (3), 619-627.
8. Sankaran, V.; Lin, S. C.; Marvel, C. *Journal of Polymer Science: Polymer Chemistry Edition* **1980,** 18 (2), 495-503.
9. Jensen, B. J.; Hergenrother, P. M.; Nwokogu, G. *Polymer* **1993,** 34 (3), 630-635.
10. Smith, J.; Connell, J.; Hergenrother, P. *Polymer* **1997,** 38 (18), 4657-4665.
11. Connell, J.; Smith, J.; Hergenrother, P. *High Performance Polymers* **1998,** 10 (3), 273-283.
12. Connell, J.; Smith, J.; Hergenrother, P. *High Performance Polymers* **1997,** 9 (3), 309-321.
13. Sasaki, T.; Yokota, R. *High Performance Polymers* **2006,** 18 (2), 199-211.
14. Jensen, B.; Hergenrother, P.; Nwokogu, G. *Journal of Macromolecular Science, Part A: Pure and Applied Chemistry* **1993,** 30 (6-7), 449-458.
15. Ma, X.; Lv, Z.; Wang, D.; Guan, S.; Chen, C.; Wang, G.; Zhang, D.; Jiang, Z. *Journal of Photochemistry and Photobiology A: Chemistry* **2007,** 188 (1), 43-50.
16. Li, W.; Tang, H.; Chen, X.; Fan, X.; Shen, Z.; Zhou, Q. *Polymer* **2008,** 49 (19), 4080-4086.
17. Lin, S. C.; Marvel, C. *Journal of Polymer Science: Polymer Chemistry Edition* **1979,** 17 (8), 2337-2350.

18. Zhao, H.-B.; Chen, L.; Yang, J.-C.; Ge, X.-G.; Wang, Y.-Z. *Journal of Materials Chemistry* **2012,** 22 (37), 19849-19857.
19. Zhao, H.-B.; Wang, X.-L.; Guan, Y.; Wang, X.-L.; Chen, L.; Wang, Y.-Z. *Polymer* **2015,** 70, 68-76.
20. Zhao, H.-B.; Liu, B.-W.; Wang, X.-L.; Chen, L.; Wang, X.-L.; Wang, Y.-Z. *Polymer* **2014,** 55 (10), 2394-2403.
21. Roberts, C. C.; Apple, T. M.; Wnek, G. E. *Journal of Polymer Science Part A: Polymer Chemistry* **2000,** 38 (19), 3486-3497.
22. Knijnenberg, A.; Bos, J.; Dingemans, T. J. *Polymer* **2010,** 51 (9), 1887-1897.
23. Wang, W. Z.; Zhang, Y. H. *Chinese Journal of Polymer Science* **2010,** 28 (4), 467-473.
24. Flory, P. J. *Transactions of the Faraday Society* **1955,** 51, 848-857.
25. Novitsky, T. F.; Lange, C. A.; Mathias, L. J.; Osborn, S.; Ayotte, R.; Manning, S. *Polymer* **2010,** 51 (11), 2417-2425.
26. Gaymans, R.; Van der Ham, A. *Polymer* **1984,** 25 (12), 1755-1758.
27. Kasai, P. H.; McBay, H. C. *The Journal of Physical Chemistry* **1984,** 88 (24), 5932-5934.
28. Gong, C.; Luo, Q.; Li, Y.; Giotto, M.; Cipollini, N. E.; Yang, Z.; Weiss, R.; Scola, D. A. *Journal of Polymer Science Part A: Polymer Chemistry* **2010,** 48 (18), 3950-3963.
29. Liu, M.; Li, K.; Yang, S.; Fu, P.; Wang, Y.; Zhao, Q. *Journal of Applied Polymer Science* **2011,** 122 (5), 3369-3376.
30. Papageorgiou, G. Z.; Tsanaktsis, V.; Bikiaris, D. N. *CrystEngComm* **2014,** 16 (34), 7963-7978.
31. Iqbal, M. All-aromatic Liquid Crystal Thermosets and Composites Thereof. TU Delft, Delft, **2010**.
32. Guan, Q. Design, Synthesis and Characterization of Novel (Multiblock) Copoly(esterimide)s and Their Shape-memory Properties. TU Delft, Delft, **2016**.
33. Kingfa Sci. & Tech. CO., L. *Heat Resistant Polyamide 10T Vicnyl*; **2008**; pp 1-24.
34. Evonik Resource Efficiency GmbH, E. R. E. *VESTAMID® HTplus: PA 6T/X and PA 10T/X product range and main properties*; **2016**; pp 1-24.
35. Kuraray Europe GmbH, K. E. *High Performance Polyamide Genestar^{TM} PA 9T-Application in Automotive*; pp 1-12.
36. EMS-Grivory; *Grivory HT: Enhanced Performance at High Temperatures*; **2016**; pp 1-40.

Chapter 5 High-temperature Shape Memory Behavior of PA 10T Thermosets

Abstract

In this chapter we will discuss the performance of semi-crystalline PA 10T-based thermosets as single-component high-temperature (>200 °C) shape memory polymers (SMPs). The shape fixation and recovery properties of the thermoset films were investigated using a rheometer in torsion mode. The crystalline domains act as the reversible switch for the fixation and recovery of the temporary shape in dual-shape memory measurements. The semi-crystalline thermoset films were prepared via a reactive oligomer approach or via a polymer approach with reactive side-group functionalities. By controlling the M_n of the reactive oligomers or the phenylethynyl (PE) concentration of the PE side-group functionalized polyamides, we were able to design PA 10T thermosets with a broad recovery temperature range of 227-294 °C. We found that the melt transition and the degree of crystallinity plays an important role on the shape memory behavior in terms of recovery temperature and recovery velocity. High temperature triple-shape memory behavior can be achieved as well when we use the melt transition ($T_m \geq$ 200 °C) and the glass transition (T_g = 125 °C) as the two switches.

5.1 Introduction

Interest in shape memory polymers (SMPs) has grown rapidly since 1980s.[1-4] SMPs are stimuli-responsive polymers which are able to adopt a temporary shape upon deformation and to revert back to the permanent shape upon exposure to an appropriate stimulus such as heat, light, solvent, electrical or magnetic field.[5] Typical applications are heat-shrink tubing, temperature sensors and actuators, biomedical and surgical materials, and aerospace devices.[6, 7]

So far, thermo-responsive SMPs are the most investigated systems.[7, 8] Their shape memory effect (SME) is an entropic phenomenon, where the molecular chains of the SMP are at the lowest energy (highest entropy) state in its permanent shape. Any deformation would change the conformation of the polymer chains from the thermodynamic equilibrium. The higher entropic state is locked in by cooling below the switching temperature, and subsequently released when the segmental mobility is reactivated upon heating, driving the molecular chains back to their lowest energy state, recovering the original shape of the macroscopic object.[8, 9]

Generally, thermo-responsive SMPs have at least two different "phases" as shown in Figure 5.1.[10] The first one is a polymer network which should be sufficiently stable in the shape memory process and is responsible to retain the original shape. The polymer network can be achieved by introducing molecular entanglements, chemical crosslinks, crystalline domains, or interpenetrating phases. The deformation of the network is the driving force for the shape recovery. The second one is a reversible switch which can be influenced by temperature. It is responsible to fix the temporary shape upon cooling and to trigger the shape recovery upon heating. This reversible switch may be crystallization/melting process, vitrification/glass transition, transition between different liquid crystalline phases, and reversible covalent or non-covalent bonds.[11]

The glass transition (T_g) and melting (T_m) are the two most important thermal transitions for thermo-responsive SMPs. Polymers with a T_g higher than room temperature can be used for T_g-based SMPs. They generally reveal a slower shape recovery compared to the T_m-based SMPs, because melting is usually a faster process. Polyurethanes, polyesters and (methyl)acrylate-based polymer networks have been investigated as SMPs based on the glass transition. Crosslinked semi-crystalline networks or (multi)block copolymer systems have been developed to design T_m-based SMPs, which opens a door to reversible two-way SME based on

crystallization induced elongation and melting induced contraction.[12-14] The most investigated "switch phase" of T_m-based SMPs are polyolefins, polyethers and polyesters, in particular, poly(ε-caprolactone) for biomedical applications.[6] One important milestone in the development of SMPs is the commercial application of heat shrinkable polyethylene (PE) films and tubings.[15] However, most SMPs reveal a switching temperature lower than 100 °C, which may not meet the requirements for aerospace, automotive or electronic applications.

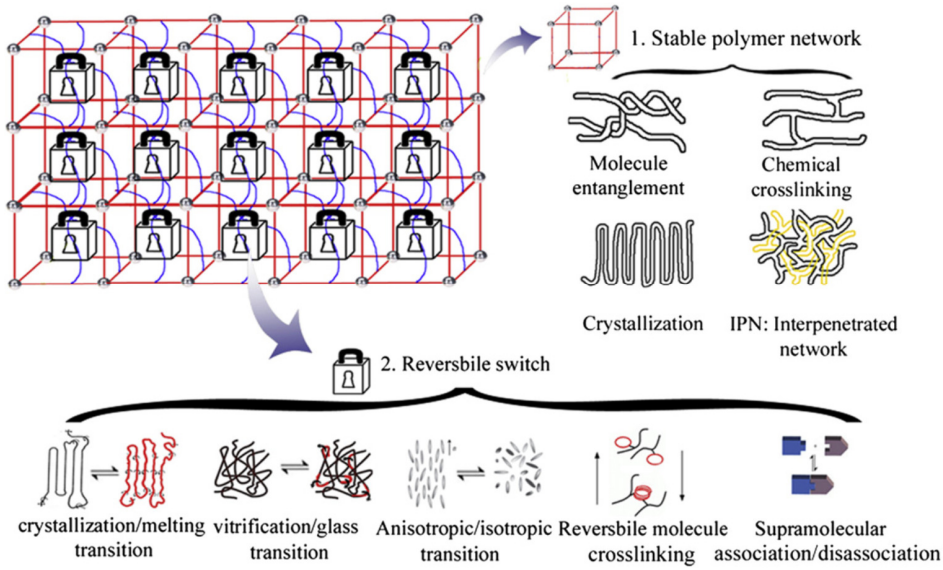

Figure 5.1 Various molecular structure of SMPs. A stable polymer network and reversible switch are the prerequisites for SMPs. Reprinted from Meng, H.; Li, G. *Polymer* **2013**, 54, (9), 2199-2221 with permission.[10]

Recently, several examples of high-temperature (>200 °C) SMPs have been reported.[16-25] Vaia and coworkers synthesized an amorphous fluorinated polyimide (Scheme 5.1 A) with a shape recovery temperature of 220 °C.[25] This was the first example of a single-component high-temperature SMP. However, this fluorinated polyimide can only be obtained as thin films, which excludes the possibility to produce complex shapes using melt processing methods. Weiss et. al. have introduced ionic moieties into polyetheretherketone (PEEK) (Scheme 5.1 B) leading to a T_g-based SMP with a switching temperature close to 200 °C, where the exact

switching temperature depends on the metal counter ions used.[18] In a later publication, this system was further developed into a T_m-based SMP by incorporation of sodium oleate, which displays a higher switching temperature of 230-240 °C due to the melting of sodium oleate.[19]

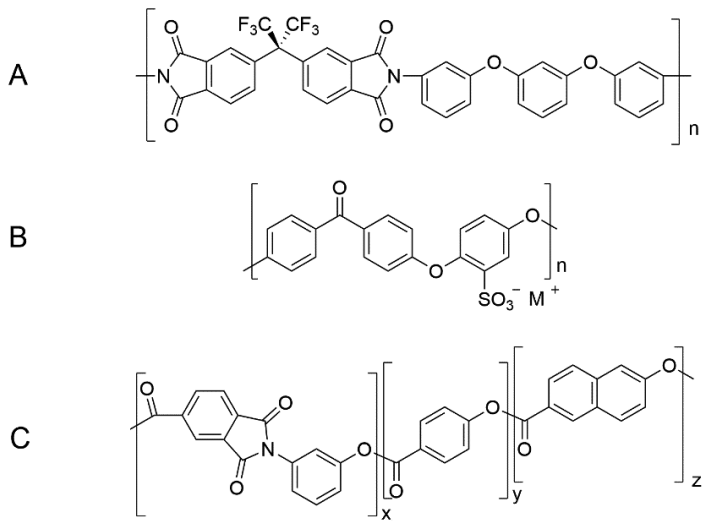

Scheme 5.1 Polymer structure of reported high-temperature SMP examples: (A) amorphous fluorinated polyimide;[25] (B) sulfonated PEEK;[18] (C) thermotropic liquid crystalline poly(esterimide).[21]

In contrast to the dual SMPs mentioned above, triple SMPs were first reported by Lendlein's group,[26] featuring two independent temporary shapes. They require two programming steps and show two recovery steps (Figure 5.2). Triple SME is not fundamentally different from dual SME, and this concept can be extended to multiple SME. Triple SME can be realized in a polymer material possessing two distinct thermal transitions[19, 26-28] or one single broad transition such as a broad glass transition.[20, 29] High temperature triple SMPs based on a single-component thermotropic liquid crystalline poly(esterimide) (Scheme 5.1 C) thermosets have recently been reported by Guan et. al. The polymer shows two glass transition temperatures at ~120 °C and ~ 220 °C, both of which can be used as switches for triple SME.[21]

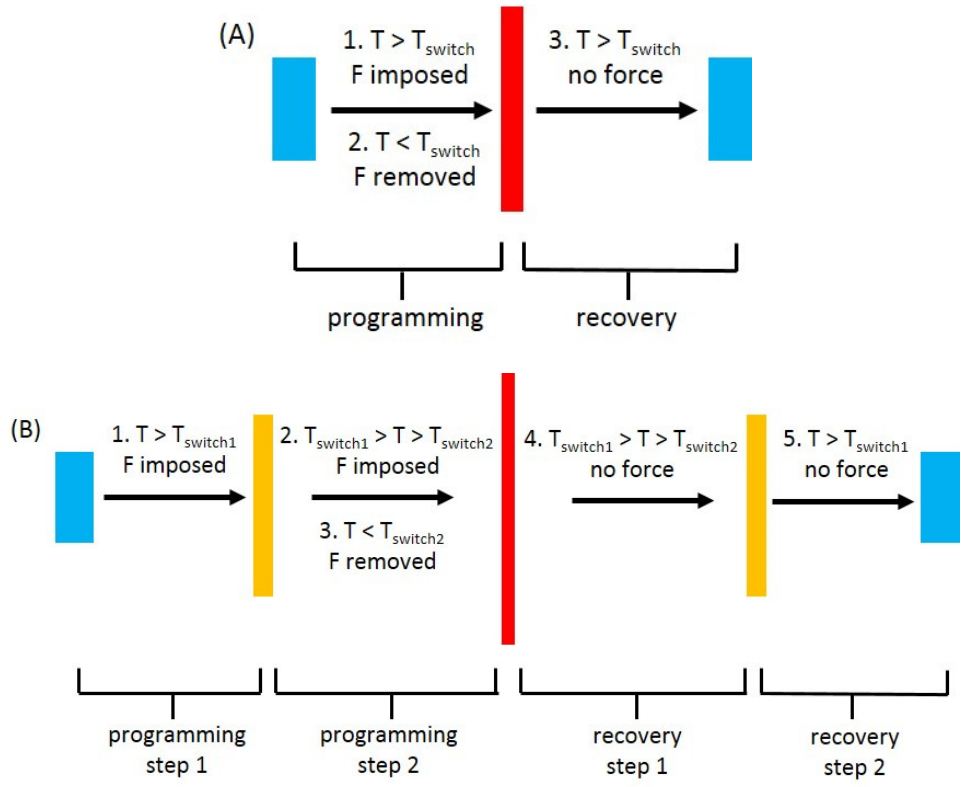

Figure 5.2 Schematic illustrations of (A) dual-SME; (B) triple-SME. T_{swicth} is the switching temperature of the SMP.

Semi-aromatic polyamide thermosets based on poly(decamethylene terephthalamide) (PA 10T) have been synthesized, characterized and discussed in Chapters 3 and 4. We showed that this class of polymers exhibits high melting temperatures and good thermo-mechanical properties. The polymers reported in Chapters 3 and 4 exhibit a semi-crystalline network, which is one of the morphological requirements for designing SMPs (see Figure 5.1). The melting and crystallization of the crystalline phase in the thermosets can be used as the high-temperature switch for a dual SME. More sophisticated triple and one-way reversible SME can be designed with the glass transition as the second switch. To the best of our knowledge, this is the first demonstration of a high-temperature SMP based on a single-component semi-crystalline PA thermoset.

5.2 Experimental

5.2.1 Materials

The synthesis of phenylethynyl (PE) end-capped PA 10T oligomers and side-group functionalized copolyamides has been described in Chapters 3 and 4, respectively. Their structures are shown in Scheme 5.2. The polymers were melt pressed into thermoset films using a standard melt-compression technique as described in Chapter 3 and 4. Both approaches lead to semi-crystalline PA 10T-based thermoset films (T_m = 227–288 °C), and they show two plateau regions in DMTA experiments (T_g – T_m and > T_m), which enables the design of polyamides with high-temperature SME.

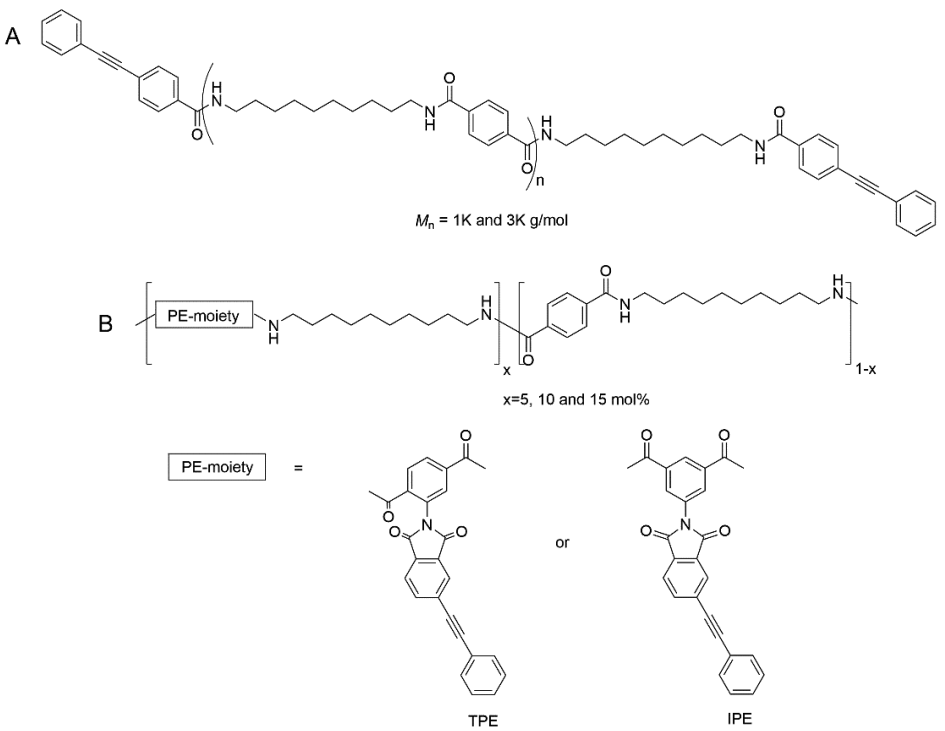

Scheme 5.2 Structures of (A) PE end-capped PA 10T oligomers; (B) TPE and IPE side-group functionalized copolyamides.

The film samples prepared from PA 10T reactive oligomers (M_n of 1K and 3K) are denoted as PA 10T-PE-1K and PA 10T-PE-3K. TPE-5, TPE-10 and TPE-15 represent the film samples prepared from reactive TPE-copolyamides with 5, 10 and 15 mol% of reactive TPE comonomer, respectively. IPE-5, IPE-10 and IPE-15 are the film samples based on the IPE-copolyamides. The solution-polymerized PA 10T-4 thermoplastic sample (Mn = 7500 g/mol) in Chapter 2 was used as the reference sample in this chapter, and denoted as PA 10T-ref.

5.2.2 Characterization

The thermal and thermo-mechanical characterization of the polyamide thermoset films using DSC and DMTA has been reported in Chapter 3 and 4.

The shape programming and recovery cycles were performed using a Thermofisher Haake MARS III rheometer equipped with a solid clamp geometry under N_2 atmosphere, as shown in Figure 5.3. Rectangular thin films with a width of ~2.5 mm and thickness of ~0.25 mm were loaded into the setup with a length of 15 mm between the clamps. The samples were deformed in a torsion mode at a constant strain rate of 0.1%·s^{-1} equivalent to a rotation speed of 3.4°·s^{-1}.

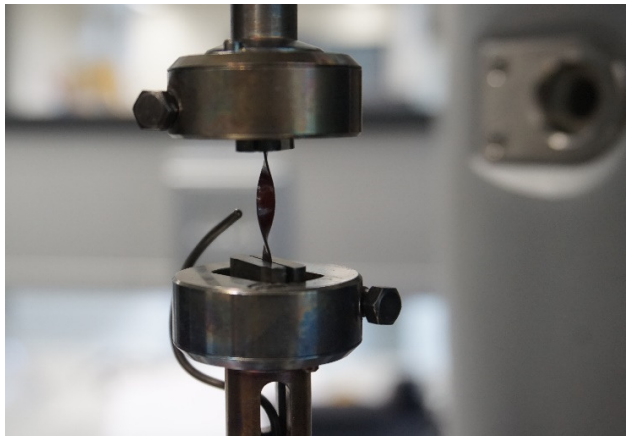

Figure 5.3 The test setup of torsion mode in a Thermofisher Haake MARS III rheometer equipped with a solid clamp geometry.

The procedure of one cycle for a dual SME test includes the following steps: (1) heat the sample to the programming temperature (T_{prog}); (2) rotate the sample to the predetermined angle (φ_d); (3) keep the angle constant, cool to the fixation temperature (T_f) at 10 °C·min^{-1} and stabilize for 10 minutes; (4) remove the stress; (5) heat the sample to T_{prog} at 10 °C·min^{-1} in a stress-free condition followed by an isothermal hold at T_{prog} for 10 minutes to stabilize. This cycle was repeated multiple times to characterize the reproducibility of the shape memory performance. The rotation angle of the sample was monitored and recorded during the whole test. For triple SME measurements, the sample was consecutively deformed in two steps in one programming cycle. Two different T_{prog}s were used, one being above T_m and the other between T_m and T_g.

5.3 Shape memory effect in torsion mode

Traditionally, the SME is quantified in cyclic thermo-mechanical extension or bending tests.[30] Characterization in a torsion mode has also been reported in a few examples.[31] Torsion tests involve non-homogeneous strains and stresses in the cross-section of a rectangular bar, and enable the SMPs to reach large deformations with moderate strains, which are believed to be more representative of practical applications of SMPs.[32-34] Therefore, a torsion mode setup was used to characterize the SME of our semi-crystalline thermoset PA films. The procedure for one torsion cycle of a dual SMP is illustrated in Figure 5.4. The deformation and fixation of the film samples are performed under strain control, and the recovery is in a stress-free condition under stress control.

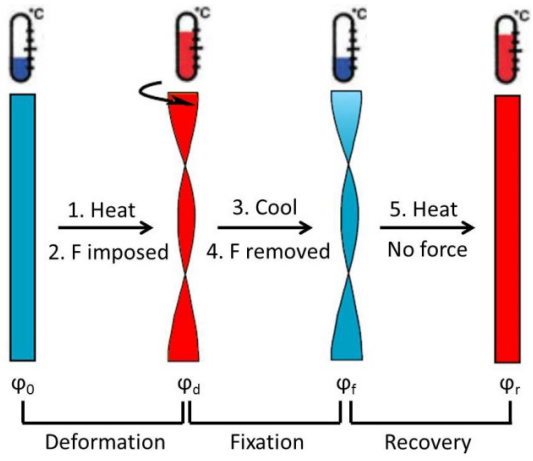

Figure 5.4 The illustration of a shape deformation, fixation and recovery cycle of the dual SME in a torsion mode.

The SME of a semi-crystalline thermoset is illustrated by combining DSC and DMTA results using TPE-10 as an example. Figure 5.5 (A) shows the shear stress, rotational angle and DSC trace of TPE-10 as a function of temperature. The sample was kept at an angle of ~180°, generating a shear stress of ~0.4 MPa at the start of cooling. This stress gradually decreased to a minimum of ~0.3 MPa at 205 °C due to stress relaxation. With further decrease in the temperature, the stress starts to increase rapidly, because the sample crystallizes resulting in a fast increase in modulus, which is demonstrated as an exotherm in DSC. This stress storing process reaches a maximum stress of ~3 MPa at 100 °C, which is the driving force for the shape recovery.

Figure 5.5 (B) shows the rotational angle as a function of temperature in the recovery step. The storage modulus (*E*') obtained from DMTA and the DSC trace from a DSC experiment are also included for illustration. Upon heating, the angle shows a slight decrease when the sample passes through the glass transition, which is associated with the release of the stress trapped in the mobile amorphous region. A subsequent slow increase in the angle is observed, which can be explained by thermal expansion.[35] When the sample starts melting, the angle recovers rapidly due to the fast release of the trapped stress. The sample shows a stable *E*' plateau (~20 MPa) above the melting temperature, indicating that the stable network is responsible for the permanent shape.

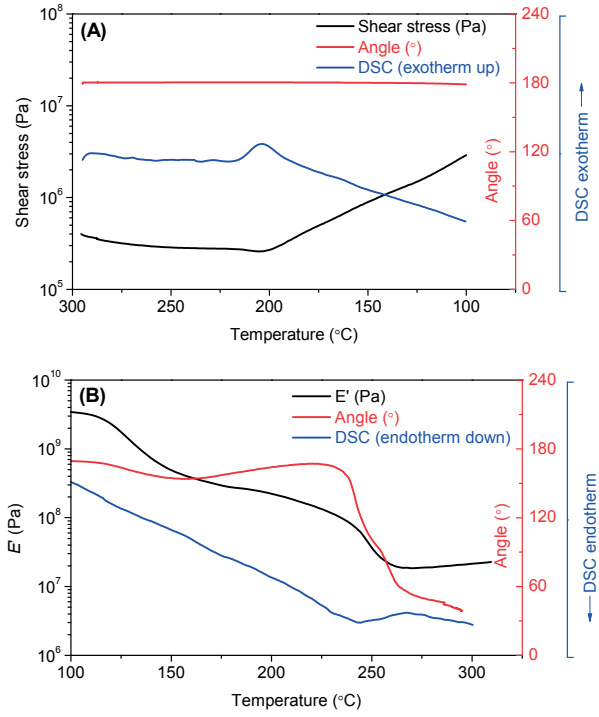

Figure 5.5 The shape fixation and recovery procedures for TPE-10; (A) shear stress, rotational angle and DSC trace as a function of temperature during cooling in the fixation step; (B) rotational angle, DSC trace and storage modulus (*E'*) as a function of temperature during heating in the recovery step.

5.4 Dual-shape memory behavior

Due to the semi-crystalline nature of the synthesized polyamide thermosets, their melting and crystallization processes can be used as the thermo-responsive switch for dual-shape memory behavior. Three consecutive deformation, fixation and recovery cycles in a torsion mode were conducted for each sample to test the shape memory performance over multiple cycles.

Shape fixation rate (R_f) and shape recovery rate (R_r) are the most important parameters to characterize the shape memory performance.[36] R_f describes how accurately the temporary shape can be fixed, and R_r quantifies the ability of the polymer to memorize its permanent shape. When performing the measurements in torsion mode, R_f and R_r can be calculated using Equation 5.1 and 5.2.

$$R_f = \frac{\varphi_f}{\varphi_d} \times 100\% \qquad (5.1)$$

$$R_r = \frac{\varphi_d - \varphi_r}{\varphi_d} \times 100\% \qquad (5.2)$$

where φ_d, φ_f and φ_r denote the rotational angle after deformation, at the fixed temporary shape at T_f and after recovery, respectively. The instantaneous recovery velocity V_r can be calculated as the time derivative of the angle as shown in Equation 5.3.

$$V_r = \frac{\partial \varphi}{\partial t} \qquad (5.3)$$

Plotting V_r against temperature reveals the temperature range corresponding to the shape recovery process.

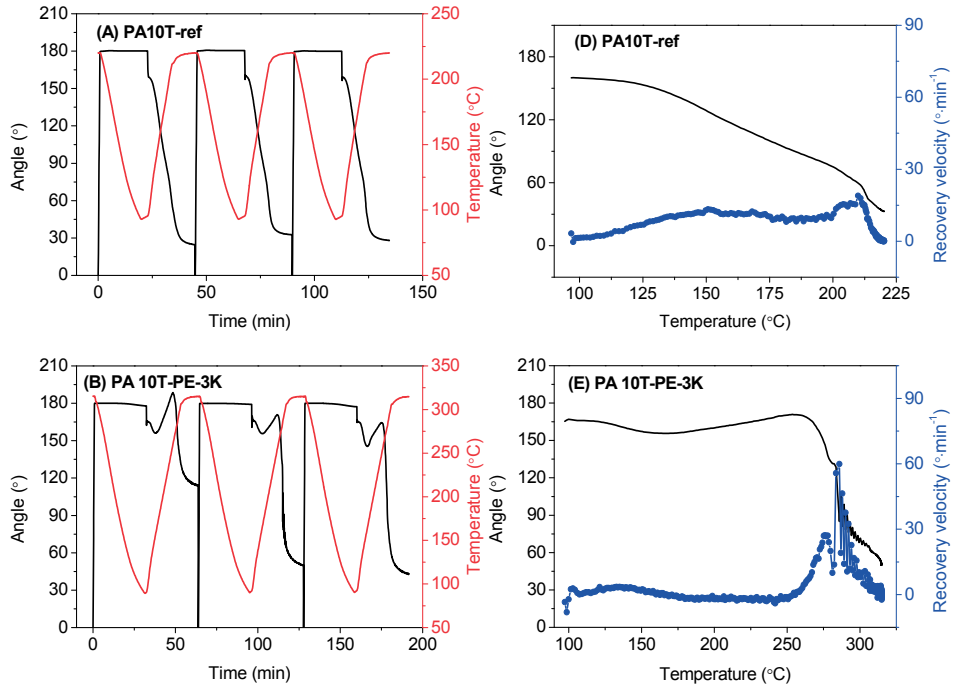

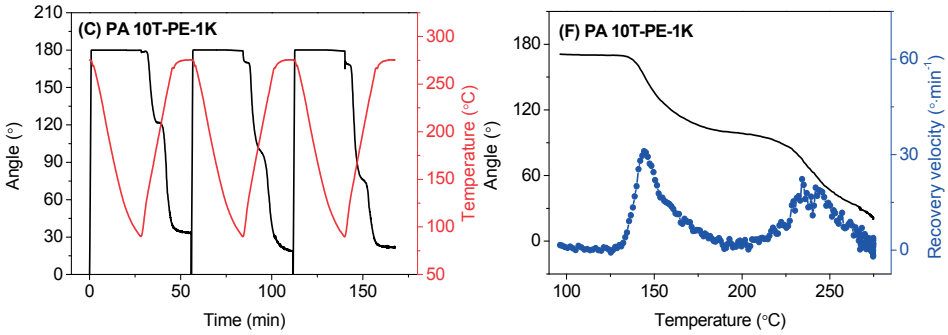

Figure 5.6 Three consecutive dual-shape memory cycles for (A) PA 10T-ref, (B) PA 10T-PE-3K; (C) PA 10T-PE-1K; Shape recovery velocity as a function of temperature in the 2nd cycle for (D) PA 10T-ref; (E) PA 10T-PE-3K; (F) PA 10T-PE-1K. Cooling/heating rate 10 °C·min^{-1} and N_2 atmosphere.

The thermoplastic PA 10T-ref film cannot be deformed to a recoverable shape above the melting temperature, thus the glass transition was used as the switch for the shape memory effect. As shown in Figure 5.6 (A), the sample was deformed at 220 °C, which lies between T_g (127 °C) and T_m (318 °C), and the shape was fixed at 100 °C where the sample is in a glassy state. Therefore, the deformation of the sample takes place in the amorphous state. The mobility of the amorphous chain segments is strongly restricted by the rigid crystalline domains, generating a shear stress as high as 11 MPa at 100 °C. This results in a relatively lower R_f of 89% than the R_f of the PA 10T-PE-3K and PA 10T-PE-1K thermoset samples (93-99 %) as shown in Table 5.1.

Table 5.1 Dual-shape fixation and recovery results of the PA 10T-ref thermoplastic and PA 10T-PE-3K and PA 10T-PE-1K thermoset films.

Sample	T_g (°C)	T_m[a] (°C)	ΔH_m (J·g^{-1})	T_{prog}[b] (°C)	T_r[c] (°C)	Gel fraction (%)	Cycle 1		Cycle 2		Cycle 3	
							R_f (%)	R_r (%)	R_f (%)	R_r (%)	R_f (%)	R_r (%)
PA 10T-ref	127	318	82	220	210	0	89	86	89	82	89	84
PA 10T-PE-3K	127	283	33	315	285	80	93	36	94	72	94	76
PA 10T-PE-1K	129	244	8	275	144 240	88	99	81	98	90	95	88

[a] T_m refers to the max of the melting peak as observed in DSC experiments.

[b] T_{prog} refers to the programming temperature.

[c] T_r refers to the temperature at the maximum recovery velocity.

In contrast to PA 10T-ref, PA 10T-PE-3K and PA 10T-PE-1K thermoset films are stable up to ~400 °C in DMTA, and present two plateau regions (T_g-T_m and >T_m), as shown in Figure 3.10. This allows deforming the film samples to a temporary shape in the second plateau region (>T_m). PA 10T-PE-3K and PA 10T-PE-1K were deformed at 315 °C and 275 °C, respectively, which is about 30 °C higher than their T_ms (283 °C and 244 °C). Unlike the scaffold of crystalline domains in the thermoplastic PA 10T-ref, the network formed by chemical crosslinks acts as the scaffold and provides the permanent shape in the thermoset analog.

The shape-memory performance of the first few cycles is usually not representative, as can be seen in Figure 5.6 (B) and (C). This is generally attributed to residual strain from the processing history of the sample.[17, 36] The PA 10T-PE-3K film shows a very low R_r of 36% in the first cycle compared to the following cycles (R_r = 72% and 76%), whereas the R_r of the PA 10T-PE-1K film shows a medium change over cycles (R_r = 81%, 90% and 88%). Such significant difference is likely to

originate from the different crosslinking densities of these two samples. PA 10T-PE-3K has a lower crosslinking density and therefore longer polymer chains between crosslinks, which is more likely to store residual strain. The recovery of all samples cannot reach 100% because the irreversible chain-segment orientation and the relaxation effect in the polymer network partly dissipate the stored stress.[24]

The shape recovery velocity of the second cycle is plotted as a function of temperature as shown in Figure 5.6 (D), (E) and (F). PA 10T-ref shows a low velocity (<20°·min^{-1}) through the recovery process, because the shape recovery is triggered by the activation of the amorphous chain segments, which are strongly restricted by the crystalline domains. Low recovery velocity is generally observed in T_g-based shape-memory polymers.[8] In contrast, PA 10T-PE-3K shows a quick recovery in the temperature range of 260-310 °C, and reaches a maximum V_r of ~60°·min^{-1} at 285 °C, which is close to its T_m (283 °C). The shape recovery is triggered by the melting of the crystalline domains, which is a relatively fast process.

The PA 10T-PE-1K film was deformed at 275 °C in one step, however, this polymer shows two distinct recovery steps with a maximum recovery velocity of 20-30°·min^{-1} at around 144 °C and 240 °C, respectively. The first recovery takes place when the sample passes through the glass transition, and reaches an R_r of ~42% at 200 °C. The second recovery is triggered by the melting of the crystalline domains. These two recovery steps indicate that the crystalline domains of the thermoset are not able to form a penetrating scaffold throughout the sample. The amorphous chains cannot be completely locked by the crystalline domains and this allows the sample to partially recover at the temperature between T_g and T_m. These results demonstrate that the degree of crystallinity, which is reflected in the ΔH_m values in Table 5.1, strongly affects the shape memory behavior of our semi-crystalline PA polymer.

The dual-shape memory behavior of the TPE and IPE polyamide thermosets were investigated using the same method. Table 5.2 shows the shape fixation and recovery results of these samples. All samples reveal good shape fixation with R_f values of 93-99%. The IPE-15 and TPE-15 samples with the highest crosslinking density, which is reflected by the gel fraction values in Table 5.2, exhibit very high R_r values (R_r > 90%), and the other samples show R_r values of 50-66% in the 1st cycle and 78-86% in the 2nd and 3rd cycles.

Table 5.2 Dual-shape fixation and recovery results of TPE and IPE thermoset films.

Sample	T_g (°C)	T_m (°C)	ΔH_m (J·g^{-1})	T_{prog}[b] (°C)	T_r[c] (°C)	Gel fraction (%)	Cycle 1		Cycle 2		Cycle 3	
							R_f (%)	R_r (%)	R_f (%)	R_r (%)	R_f (%)	R_r (%)
TPE-5	123	285	33	315	277	72	93	62	93	82	94	82
TPE-10	123	250	27	295	242	78	98	66	96	78	96	79
TPE-15	125	227	20	275	140 227	83	99	93	99	93	97	96
IPE-5	127	288	39	315	294	74	95	51	93	86	95	84
IPE-10	125	251	30	295	252	80	96	50	94	80	96	78
IPE-15	133	235	24	275	141 244	92	98	96	95	95	96	96

[a] T_m refers to the max of the melting peak as observed in DSC experiments.

[b] T_{prog} refers to the programming temperature.

[c] T_r refers to the temperature at the maximum recovery velocity.

Figure 5.7 shows the dual-shape memory cycles and the recovery velocity of the TPE thermoset films. Similar to the PA 10T-PE-3K sample, TPE-5 and TPE-10 exhibit one recovery step in the temperature range of 260-300 °C and 230-270 °C, respectively. The TPE-15 film displays two recovery steps, which is also observed for the PA 10T-PE-1K film. The two recovery steps are due to the low degree of crystallinity in TPE-15 and PA 10T-PE-1K, where the amorphous chain segments cannot be completely fixed when the temperature is above T_g. TPE-5, TPE-10 and PA 10T-PE-3K, on the other hand, show higher degrees of crystallinity and this prevents the T_g-induced shape recovery.

The difference between these samples clearly indicates that the shape memory behavior strongly depends on the degree of crystallinity of the semi-crystalline

thermosets. By changing the concentration of the PE side-groups in the reactive copolyamides, the crosslinking density of the thermosets can be controlled, consequently leading to adjustable crystallinity and shape memory properties. The IPE polyamide thermosets, shown in Figure 5.1S (Appendix), reveal similar shape memory behavior as the corresponding TPE analog.

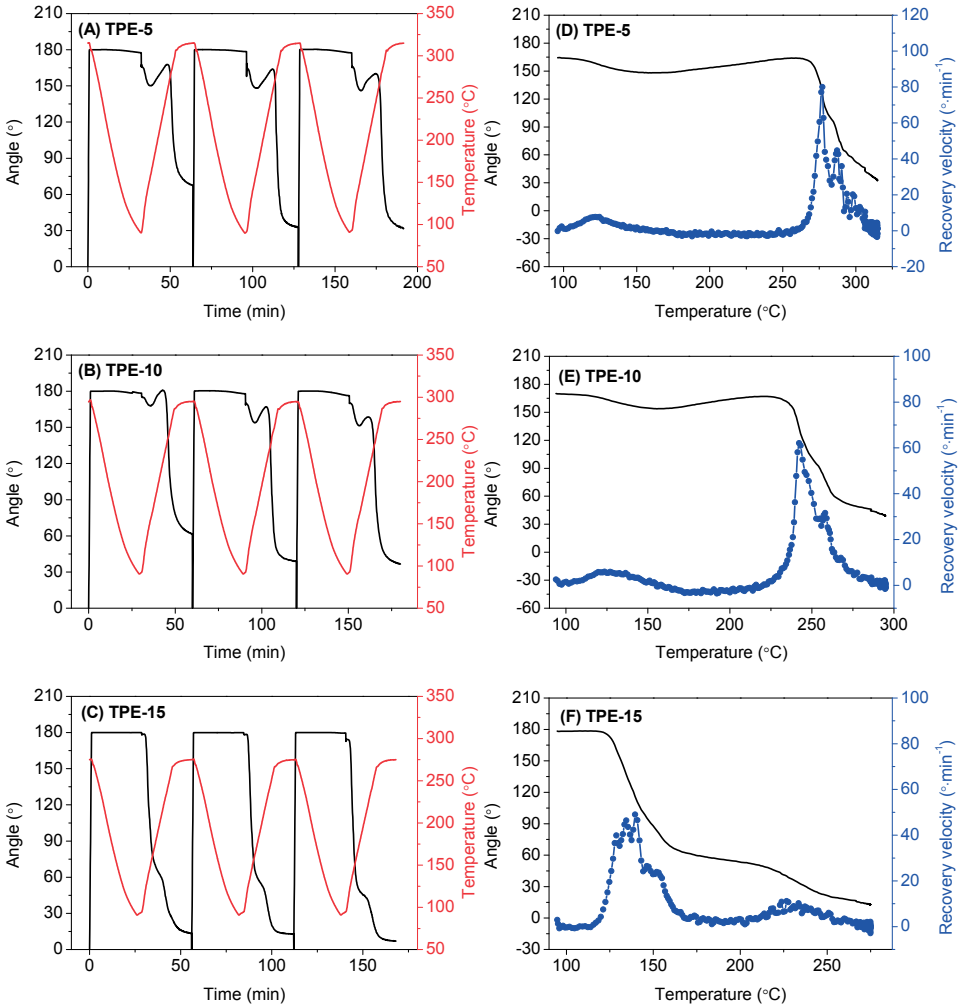

Figure 5.7 Three consecutive dual-shape memory cycles for (A) TPE-5, (B) TPE-10; (C) TPE-15; Shape recovery velocity as a function of temperature in the 2nd cycle for (D) TPE-5; (E) TPE-10; (F) TPE-15. Cooling and heating rate 10 °C·min^{-1} and N_2 atmosphere.

5.5 Triple-shape memory behavior

Based on our study above, two reversible processes, the glass transition and the melting process, can both act as the switch to trigger shape recovery. Unlike the traditional high-temperature triple-SMP composed of multiple components, we were able to design a single-component triple-SMP using both switches to achieve two distinct recovery processes.

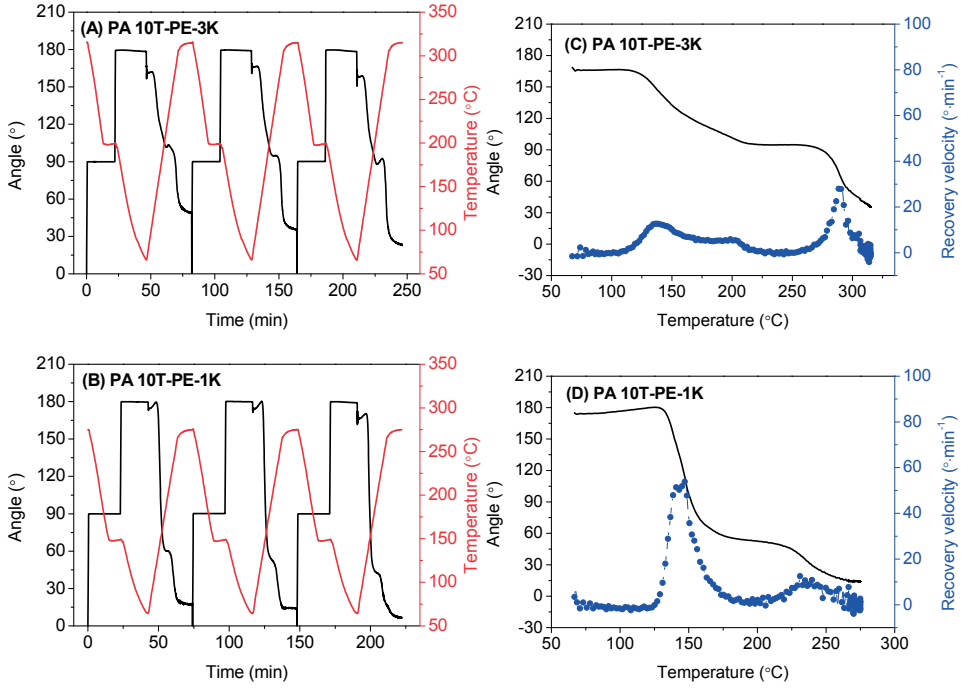

Figure 5.8 Three consecutive triple-shape memory cycles for (A) PA 10T-PE-3K; (B) PA 10T-PE-1K; Shape recovery velocity as a function of temperature in the 2nd cycle for (C) PA 10T-PE-3K; (D) PA 10T-PE-1K. Cooling and heating rate 10 °C·min^{-1} and N_2 atmosphere.

Figure 5.8 (A) shows the three consecutive triple-shape memory cycles for PA 10T-PE-3K. The film sample was first heated up to 315 °C, which is above the T_m (283 °C), and rotated by 90° from the original shape A (φ_A) to a temporary shape B (φ_B). The sample was cooled to 200 °C, a temperature between T_m and T_g, to fix the

shape B. A second rotation of 90° was then applied to reach the temporary shape C (φ_C). The sample was subsequently cooled to 60 °C, which is below T_g (127 °C), to fix the shape C. The external stress was then removed, leading to the final fixed temporary shape (φ_f). A shape fixation rate (R_f) of ~90% was calculated using Equation 5.4.

$$R_f = \frac{\varphi_f}{\varphi_C} \times 100\% \qquad (5.4)$$

In the subsequent recovery step, the sample was heated up to 315 °C in a stress-free state to monitor the recovery of the rotational angle. The shape recovery was accomplished in two distinct steps, as shown in Figure 5.8 (A). This means the thermoset can memorize two temporary shapes in one single shape memory cycle. The shape recovery rate $R_{r(C\rightarrow B)}$ and $R_{r(B\rightarrow A)}$ were calculated based on Equation 5.5 and 5.6, respectively.[21]

$$R_{r(C\rightarrow B)} = \frac{\varphi_f - \varphi_{B/rec}}{\varphi_C - \varphi_B} \times 100\% \qquad (5.5)$$

$$R_{r(B\rightarrow A)} = \frac{\varphi_{B/rec} - \varphi_{A/rec}}{\varphi_B - \varphi_A} \times 100\% \qquad (5.6)$$

where φ_A, φ_B and φ_C denote the rotational angle of shape A (φ_A = 0°), shape B (φ_B = 90°) and C (φ_C = 180°); $\varphi_{B/rec}$ and $\varphi_{A/rec}$ are the rotational angles of the first and second recovered shapes, respectively. Figure 5.8 (B) shows the triple-shape memory cycles of PA 10T-PE-1K. This polymer exhibits a lower T_m (244 °C) when compared to PA 10T-PE-3K (283 °C), therefore, lower programming temperatures (275 °C and 150 °C) were used.

PA 10T-PE-3K shows moderate $R_{r(C\rightarrow B)}$ values of 67-80% in the first recovery step and $R_{r(B\rightarrow A)}$ values of 60-73% in the second recovery step, as listed in Table 5.3. Compared to PA 10T-PE-3K, PA 10T-PE-1K shows much higher $R_{r(C\rightarrow B)}$ values of 128-138%, and lower $R_{r(B\rightarrow A)}$ values of 40-49%. The first recovery is triggered by the glass transition, and is due to the release of stress in the amorphous phase. The major recovery takes place in the first step indicating that the crystalline phase cannot completely lock the stress in the amorphous phase. The stress, which is supposed to release in the second recovery step, is actually partially released in the first recovery step. This, together with the stress induced by the second deformation, drives the sample to reach a high recovery rate (>100%) in the first step. This result is consistent with the result we obtained for the dual-shape memory experiments, and originates from the low degree of crystallinity of the PA 10T-PE-1K thermoset.

Figure 5.8 (C) and (D) show the shape recovery velocity of PA 10T-PE-3K and 1K samples as a function of temperature. The first recovery step of PA 10T-PE-3K shows a lower V_r (13°·min^{-1}) than the second step (28°·min^{-1}), because of the limited mobility of the amorphous chain segments restricted by the crystalline domains. In contrast, the PA 10T-PE-1K sample shows much higher V_r (54°·min^{-1}) in the first step, which is due to its low degree of crystallinity.

Table 5.3 Triple-shape fixation and recovery results of thermoset films

Sample	T_{prog1}[a] (°C)	T_{prog2}[a] (°C)	T_{r1}[b] (°C)	T_{r2}[b] (°C)	Cycle 1			Cycle 2			Cycle 3		
					R_f (%)	$R_{r(C-B)}$ (%)	$R_{r(B-A)}$ (%)	R_f (%)	$R_{r(C-B)}$ (%)	$R_{r(B-A)}$ (%)	R_f (%)	$R_{r(C-B)}$ (%)	$R_{r(B-A)}$ (%)
PA 10T-PE-3K	315	200	137	289	91	67	60	93	80	66	89	79	73
PA 10T-PE-1K	275	150	144	240	97	128	49	97	135	44	93	139	40
TPE-5	315	200	132	285	88	64	69	86	74	79	86	79	79
TPE-10	295	175	138	250	92	79	91	92	89	80	91	91	82
TPE-15	275	150	133	236	93	97	84	92	123	55	93	136	45
IPE-5	315	200	133	297	91	57	46	86	68	89	88	78	78
IPE-10	295	175	137	247	94	76	103	92	98	82	92	100	79
IPE-15	275	150	147	245	96	81	109	95	103	79	94	107	81

[a] T_{prog1} and T_{prog2} refer to the 1st and 2nd programming temperature, respectively.

[b] T_{r1} and T_{r2} refer to the temperature at the 1st and 2nd maximum recovery velocity, respectively.

The triple-shape memory cycles and recovery velocity of the TPE thermosets are shown in Figure 5.9. The TPE-5 and TPE-10 films show moderate $R_{r(C\rightarrow B)}$ and $R_{r(B\rightarrow A)}$ (64-91%), and higher V_r values in the second recovery step, which is similar to the behavior of PA 10T-PE-3K. Whereas the TPE-15 sample, similar to PA 10T-PE-1K, exhibits high $R_{r(C\rightarrow B)}$ (97-136%) and V_r values (38°·min^{-1}) in the first recovery step, because this polymer has the lowest degree of crystallinity. IPE polyamide thermosets exhibit similar shape memory behavior as the corresponding TPE analog, as shown in Figure 5.2S (Appendix).

The temperatures at the first maximum recovery velocity (T_{r1}) of all samples are within a narrow range of 132-147 °C, because the T_g of all samples is around 125 °C. However, the temperatures of the second maximum recovery velocity (T_{r2}), which depend on the T_m of the samples, display a broad variation between 236 °C and 297 °C. Therefore, the triple-shape memory behavior of the thermosets is highly tunable within a wide temperature regime.

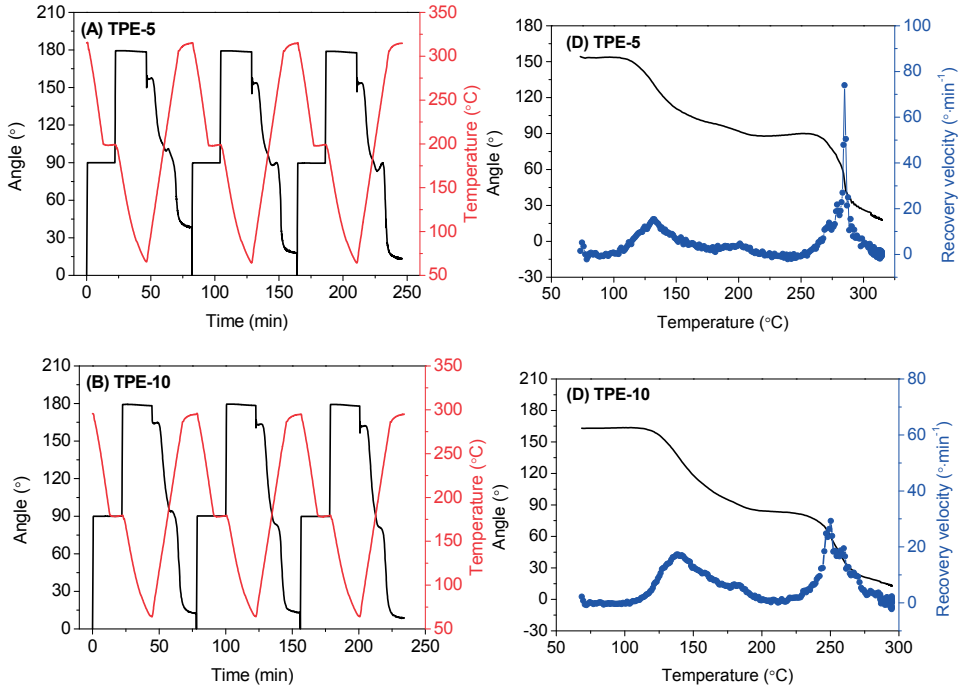

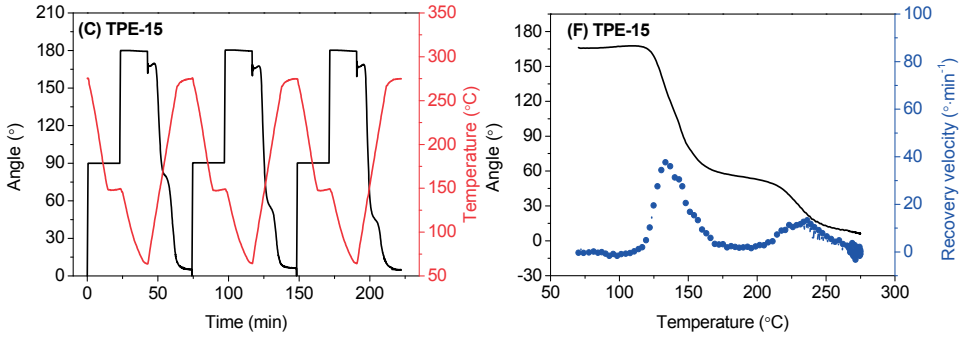

Figure 5.9 Three consecutive triple-shape memory cycles for (A) TPE-5; (B) TPE-10; (C) TPE-15; Angular velocity of shape recovery as a function of temperature in the 2nd cycle for (D) TPE-5; (E) TPE-10; (F) TPE-15. Cooling and heating rate 10 °C·min^{-1} and N_2 atmosphere.

Instead of deforming the sample in one direction only, we can involve both forward and backward deformations in a triple-shape memory cycle, therefore, the corresponding temporary shapes would recover in a reverse direction. To demonstrate this, the TPE-10 thermoset sample, which shows a high R_f (> 90%), $R_{r(C-B)}$ (~90%) and $R_{r(B-A)}$ (~80%), was selected as a representative example.

The results of Test I are shown in Figure 5.10 (A) and (B). The sample was programmed forward and backward by 180° in two steps, and reached a final temporary shape, which is identical to the original shape. The subsequent heating resulted in an increase in angle in the first recovery step achieving a maximum recovery velocity at 142 °C and an $R_{r(C-B)}$ of 79-91% at 213 °C. By increasing the temperature further, the sample recovered in the reverse direction reaching a maximum recovery velocity at 243 °C and an $R_{r(B-A)}$ of 81-87% (Table 5.4). These results demonstrate that our semi-crystalline PA thermosets show one-way reversible shape memory behavior. The reversible shape changes in this experiment occurred without application of any external force. The shape changes were driven by internal stress of the oppositely strained networks formed in the first and second programming steps.

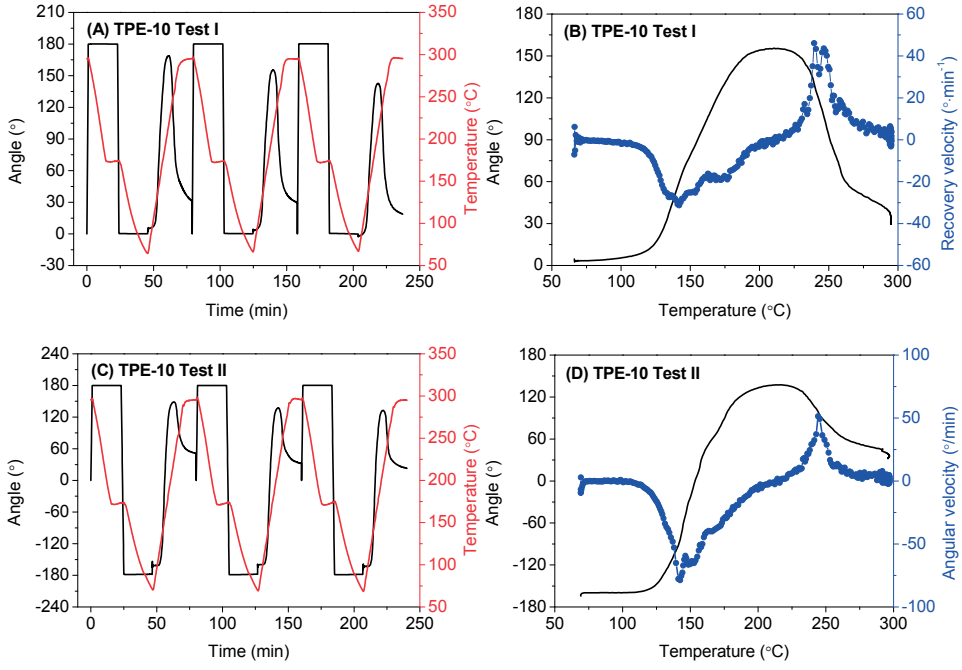

Figure 5.10 Three consecutive triple-shape memory cycles for TPE-10 and shape recovery velocity as a function of temperature in the 2nd cycle. (A) and (B) deformation of 180° and -180° in two steps, respectively; (C) and (D) deformation of 180° and -360° in two steps, respectively.

We can adjust the second programming step from $\Delta\varphi_{d2}$ = -180° to $\Delta\varphi_{d2}$ = -360° in Test II, which results in two opposite temporary shapes, as shown in Figure 5.10 (C) and (D). The sample shows a R_f of 89-91%, $R_{r(C\text{-}B)}$ of 82-86% and $R_{r(B\text{-}A)}$ of 54-61% (Table 5.4). The maximum recovery velocity occurs at 142 and 244 °C in the first and second recovery steps, respectively, which is consistent with the results of Test I. Our results clearly demonstrate that high-temperature SME with tunable recovery directions and amplitudes can be designed based on our semi-crystalline polyamide thermosets.

Table 5.4 Triple-shape fixation and recovery results of TPE-10 deformed in two opposite directions

Test	Cycle No.	$\Delta\varphi_{d1}$[a] (°)	$\Delta\varphi_{d2}$[a] (°)	R_f (%)	$R_{r(C-B)}$ (%)	$R_{r(B-A)}$ (%)	T_{max}[b] (°C)
I	**Cycle 1**	180	-180	97	91	81	213
	Cycle 2	180	-180	98	85	81	211
	Cycle 3	180	-180	99	79	87	209
II	**Cycle 1**	180	-360	90	86	54	218
	Cycle 2	180	-360	89	83	59	213
	Cycle 3	180	-360	91	82	61	212

[a] $\Delta\varphi_{d1}$ and $\Delta\varphi_{d2}$ refer to the deformation angles in the 1st and 2nd deformation steps.

[b] T_{max} refers to the temperature at the maximum angle.

5.6 Conclusions

In summary, we have demonstrated that our semi-crystalline PA thermosets can be used as single-component SMPs. The dual- and triple-shape fixation and recovery performances were investigated in a torsion mode. Two approaches have been explored: crosslinked semi-crystalline PA films were prepared by curing reactive PA 10T oligomers (approach 1) and films were prepared by curing reactive side-group functionalized copolyamides (approach 2). Compared to the thermoplastic PA 10T reference polymer, the PA 10T-PE-3K, TPE-5 and TPE-10 thermoset films show high-temperature dual-shape memory behavior behavior (>200 °C) when T_m is used as the switching temperature. The densely crosslinked PA 10T-PE-1K and TPE-15 show two distinct recovery steps because the degree of crystallinity is too low and cannot provide a scaffold that locks the shape at the temperature between T_g and T_m. There is no difference in SME between the two approaches, because the resultant thermoset films show a similar degree of

crystallinity. Triple-shape memory and one-way reversible shape memory behavior can be demonstrated when the T_g (~125 °C) is used as the second switching temperature. The use of phenylacetylene (PE) reactive functionalities allows us to control the degree of crystallinity in the final polyamide thermosets and in turn tune their shape-memory behavior in terms of recovery temperature, velocity and efficiency.

5.7 References

1. Xie, T. *Polymer* **2011,** 52, (22), 4985-5000.
2. Hu, J.; Zhu, Y.; Huang, H.; Lu, J. *Progress in Polymer Science* **2012,** 37, (12), 1720-1763.
3. Rousseau, I. A. *Polymer Engineering & Science* **2008,** 48, (11), 2075-2089.
4. Behl, M.; Razzaq, M. Y.; Lendlein, A. *Advanced Materials* **2010,** 22, (31), 3388-3410.
5. Pilate, F.; Toncheva, A.; Dubois, P.; Raquez, J.-M. *European Polymer Journal* **2016,** 80, 268-294.
6. Hager, M. D.; Bode, S.; Weber, C.; Schubert, U. S. *Progress in Polymer Science* **2015,** 49, 3-33.
7. Leng, J.; Lan, X.; Liu, Y.; Du, S. *Progress in Materials Science* **2011,** 56, (7), 1077-1135.
8. Zhao, Q.; Qi, H. J.; Xie, T. *Progress in Polymer Science* **2015,** 49, 79-120.
9. Wu, X.; Huang, W. M.; Zhao, Y.; Ding, Z.; Tang, C.; Zhang, J. *Polymers* **2013,** 5, (4), 1169-1202.
10. Meng, H.; Li, G. *Polymer* **2013,** 54, (9), 2199-2221.
11. Lewis, C. L.; Dell, E. M. *Journal of Polymer Science Part B: Polymer Physics* **2016**.
12. Chung, T.; Romo-Uribe, A.; Mather, P. T. *Macromolecules* **2008,** 41, (1), 184-192.
13. Behl, M.; Kratz, K.; Zotzmann, J.; Nöchel, U.; Lendlein, A. *Advanced Materials* **2013,** 25, (32), 4466-4469.
14. Zhou, J.; Turner, S. A.; Brosnan, S. M.; Li, Q.; Carrillo, J.-M. Y.; Nykypanchuk, D.; Gang, O.; Ashby, V. S.; Dobrynin, A. V.; Sheiko, S. S. *Macromolecules* **2014,** 47, (5), 1768-1776.
15. Rainer WC, R. E., Hitov JJ, Sloan AW, Stewart WD. Heat-shrinkable polyethylene. US 3144398, 1964.

16. Xiao, X.; Kong, D.; Qiu, X.; Zhang, W.; Liu, Y.; Zhang, S.; Zhang, F.; Hu, Y.; Leng, J. *Scientific reports* **2015,** 5.
17. Xiao, X.; Kong, D.; Qiu, X.; Zhang, W.; Zhang, F.; Liu, L.; Liu, Y.; Zhang, S.; Hu, Y.; Leng, J. *Macromolecules* **2015,** 48, (11), 3582-3589.
18. Shi, Y.; Weiss, R. *Macromolecules* **2014,** 47, (5), 1732-1740.
19. Shi, Y.; Yoonessi, M.; Weiss, R. *Macromolecules* **2013,** 46, (10), 4160-4167.
20. Yang, Z.; Chen, Y.; Wang, Q.; Wang, T. *Polymer* **2016,** 88, 19-28.
21. Guan, Q. Design, Synthesis and Characterization of Novel (Multiblock) Copoly(esterimide)s and Their Shape-memory Properties. TU Delft, Delft, 2016.
22. Xiao, X.; Qiu, X.; Kong, D.; Zhang, W.; Liu, Y.; Leng, J. *Soft Matter* **2016,** 12, (11), 2894-2900.
23. Bai, Y.; Mao, L.; Liu, Y. *Journal of Applied Polymer Science* **2016,** 133, (30).
24. Wang, Q.; Bai, Y.; Chen, Y.; Ju, J.; Zheng, F.; Wang, T. *Journal of Materials Chemistry A* **2015,** 3, (1), 352-359.
25. Koerner, H.; Strong, R. J.; Smith, M. L.; Wang, D. H.; Tan, L.-S.; Lee, K. M.; White, T. J.; Vaia, R. A. *Polymer* **2013,** 54, (1), 391-402.
26. Bellin, I.; Kelch, S.; Langer, R.; Lendlein, A. *Proceedings of the National Academy of Sciences* **2006,** 103, (48), 18043-18047.
27. Behl, M.; Lendlein, A. *Journal of Materials Chemistry* **2010,** 20, (17), 3335-3345.
28. Xie, T.; Xiao, X.; Cheng, Y. T. *Macromolecular Rapid Communications* **2009,** 30, (21), 1823-1827.
29. Xie, T. *Nature* **2010,** 464, (7286), 267-270.
30. Wagermaier, W.; Kratz, K.; Heuchel, M.; Lendlein, A., Characterization methods for shape-memory polymers. In *Shape-memory polymers*, Springer: 2009; pp 97-145.
31. Diani, J.; Fredy, C.; Gilormini, P.; Merckel, Y.; Régnier, G.; Rousseau, I. *Polymer testing* **2011,** 30, (3), 335-341.
32. Baghani, M. *International Journal of Engineering Science* **2014,** 76, 1-11.
33. Baghani, M.; Naghdabadi, R.; Arghavani, J.; Sohrabpour, S. *Journal of Intelligent Material Systems and Structures* **2012,** 23, (2), 107-116.
34. Diani, J.; Gilormini, P.; Frédy, C.; Rousseau, I. *International Journal of Solids and Structures* **2012,** 49, (5), 793-799.
35. Véchambre, C.; Buléon, A.; Chaunier, L.; Gauthier, C.; Lourdin, D. *Macromolecules* **2011,** 44, (23), 9384-9389.
36. Lendlein, A.; Kelch, S. *Angewandte Chemie International Edition* **2002,** 41, (12), 2034-2057.

Summary

The work presented in this thesis describes a route towards semi-crystalline polyamide (PA 10T) thermosets. A mild temperature solution polymerization method was developed to synthesize melt-processable PA 10T precursors with crosslinkable functionalities. These functionalities can be placed at the polymer chain-ends or as pedent groups on the polymer backbone. The reactive precursors were thermally cured into polyamide thermosets and their morphology and thermo-mechanical properties of the final thermosets. Finally, semi-crystalline PA 10T thermoset films were evaluated as single-component high-temperature shape memory materials.

In *Chapter 2*, we will describe how to prepare PA 10T using a solution polymerization method and we will report on the thermo-mechanical properties and morphology of the as-prepared polymers and melt-pressed films thereof. PA 10T with a maximum M_n of 7.5 kg·mol^{-1} could be prepared in NMP with 8 wt% $CaCl_2$ and triethylamine as acid scavenger. The as-prepared PA 10T shows a T_g of 127 °C and two melting endotherms at 292 and 317 °C, respectively. This behaviour is associated with a crystal-to-crystal transition as confirmed by DSC and WAXD.

In *Chapter 3* we will demonstrate that phenylethynyl (PE) reactive end-groups can be used to prepare oligomeric semi-aromatic polyamides (M_n = 1K and 3K g·mol^{-1}) with excellent melt processability characteristics ($|\eta^*|$ in the range of 10-100 Pa·s). Based on rheology experiments on crosslinked PA 10T films we concluded that 35-41% of the PE end-groups contribute to crosslinking and the remainder of the PE functionalities undergoes chain extension reactions. DMTA measurements showed that 3K and 1K thermoset films are stable up to ~400 °C as a result of network formation. The melt transition and degree of crystallinity in the final thermoset films are strongly depressed by the thermal cure process.

In *Chapter 4*, we will discuss a different route towards PA 10T-based thermosets. Two PE-containing comonomers based on isophthalic acid (IPE) and terephthalic acid (TPE) were synthesized and incorporated in the backbone of the copolyamides using the same solution polymerization method as discussed in *Chapter 3*. As anticipated, the comonomers disrupt crystallization of the final polymer. The thermoset films exhibit a stable plateau with an E' of 10-20 MPa above T_m, as determined by DMTA, and the thermoset films are stable up to ~400 °C as a result of network formation. The melt transition and degree of crystallinity of the final

thermoset films are strongly depressed by the thermal cure process, especially in thermosets with a high crosslinking density. Stress-strain experiments show that the IPE-15-cured films exhibit outstanding elongation at break (~19%) and toughness (791 $MJ \cdot m^{-3}$), which is a significant improvement over the PA 10T reference polymer (~10% and 370 $MJ \cdot m^{-3}$).

The semi-crystalline thermoset films obtained in Chapter 3 and 4 show two E' plateau regions (between T_g and T_m and > T_m). This makes it possible to design polyamides with high-temperature shape-memory capabilities. In *Chapter 5,* we will show that our thermoset films can be used as single-component shape memory polymers. The dual- and triple-shape fixation and recovery performance was investigated using a rheometer with torsion mode set-up. Compared to the thermoplastic PA 10T reference polymer, slightly crosslinked films show high-temperature dual-shape memory behavior behavior (>200 °C) when their respective T_m was used as the switching temperature. Triple-shape memory and one-way reversible shape memory behavior could be demonstrated when the T_g (~125 °C) was used as the second switching temperature. There is no difference in SME between the reactive oligomer or reactive side-group precursor approach, because the resultant thermoset films show a similar degree of crystallinity.

Samenvatting

In dit proefschrift presenteren we een nieuwe route voor de synthese van semi-kristallijne polyamide (PA 10T) thermoharders. We hebben een lage temperatuur polycondensatiemethode ontwikkeld die het mogelijk maakt om PA 10T reactieve (vernetbare) precursors te synthetiseren die vervolgens via de smelt verwerkt kunnen worden. De reactieve phenyletynyl groepen kunnen aan de uiteinden van de polymeerketens geplaatst worden, dan wel als zijgroepen aan de polymeerketen. De reactieve precursors zijn vervolgens thermisch vernet tot polyamide thermoharders, en de morfologie en thermo-mechanische eigenschappen zijn onderzocht. Tenslotte zijn de hoge temperatuur geheugeneigenschappen van deze nieuwe semi-kristallijne PA 10T thermoharders gekarakteriseerd.

In *Hoofdstuk 2* beschrijven we de synthese van PA 10T via een oplossing-gebaseerde polymerisatiemethode en rapporteren we de thermo-mechanische eigenschappen en morfologie van de PA 10T polymeren en polymeerfilms. Het is mogelijk gebleken om PA 10T te synthetiseren met een M_n van 7.5 kg·mol^{-1} in NMP met 8 gew% $CaCl_2$ en *triethylamine* als *acid scavenger*. PA 10T gesynthetiseerd via deze methode heeft een T_g van 127 ^oC en laat twee smelt-endothermen (T_{m1} = 292 en T_{m2} = 317 ^oC) zien. Dit smeltgedrag is geassocieerd met een kristal-naar-kristal overgang wat kon worden bevestigd met DSC en WAXD.

In *Hoofdstuk 3* laten we zien dat *phenylethynyl* (PE) reactieve eindgroepen gebruikt kunnen worden om oligomere semi-aromatische polyamides (M_n = 1K en 3K g·mol^{-1}) te synthetiseren met excellente verwerkingseigenschappen (|□*|tussen 10 en 100 Pa·s). Middels rheologie experimenten hebben we kunnen aantonen dat 35-41% van de PE eindgroepen bijdraagt aan het vormen van vernettingspunten. De rest van de PE eindgroepen ondergaan ketenverlenging. DMTA-experimenten laten zien dat de 3K en 1K thermoharders stabiel zijn tot 400 ^oC wat een direct gevolg is van de vernettingsreacties. De smeltovergang en kristallisatiegraad van de thermharders zijn ten gevolge van de uithardingschemie sterk onderdrukt.

In *Hoofdstuk 4* introduceren we een alternatieve route om PA 10T thermoharders te synthetiseren. Twee phenylethynyl co-monomeren, gebaseerd op *isophthalic acid* (IPE) en *terephthalic acid* (TPE), zijn gesynthetiseerd en ingebouwd in de PA 10T keten middels de polymerisatiemethode beschreven in

Hoofdstuk 3. Zoals verwacht verstoren beide co-monomeren de kristallisatie van de polymeerketens. DMTA-analyse laat zien dat de thermoharders een stabiel rubberplateau hebben (*E*' = 10-20 MPa) boven het smeltpunt (T_m) en dat de thermoharders stabiel zijn tot 400 °C ten gevolge van de vernettingsreacties. Ook hier zijn de smeltovergang en kristallisatiegraad van de thermoharders sterk onderdrukt als een direct gevolg van de vernettingsreacties. Dit effect is groter naarmate de vernettingsdichtheid toeneemt. Kracht-rek experimenten laten zien dat de IPE-15 thermoharder een ongebruikelijk hoge breukrek (~19%) en taaiheid (791 $MJ \cdot m^{-3}$) hebben. Dit is een significante verbetering als men dit vergelijkt met de referentie PA 10T thermoplast (~10% and 370 $MJ \cdot m^{-3}$).

De semi-kristallijne thermoharders, zoals beschreven in *Hoofdstuk 3* en *4*, laten twee rubber plateau gebieden zien en wel tussen de T_g en T_m en $>T_m$. Deze eigenschap maakt het mogelijk om polyamides te ontwerpen met hoge temperatuur vormgeheugen eigenschappen. In *Hoofdstuk 5* laten we zien dat onze thermoharders gebruikt kunnen worden als geheugenpolymeren. Het *dual*- en *triple-shape* fixatie- en herstel-gedrag is onderzocht met een torsie-rheometer. Vergeleken met het thermoplastische PA 10T referentiepolymeer laten de licht vernette PA 10T filmpjes *dual-shape* geheugengedrag zien (> 200 °C), waarbij de T_m als schakeltemperatuur kan worden gebruikt. Het is ook mogelijk gebleken om *triple-shape* en *one-way* reversibel geheugengedrag te demonstreren door de T_g (~125 °C) als tweede schakeltemperatuur te gebruiken. Het geheugengedrag van beide reactieve precursors, *i.e.* oligomeer met reactieve eindgroepen of polymeer met reactieve zijgroepen, is hetzelfde omdat de uiteindelijke thermoharders dezelfde kristalliniteitsgraad vertonen.

Appendix

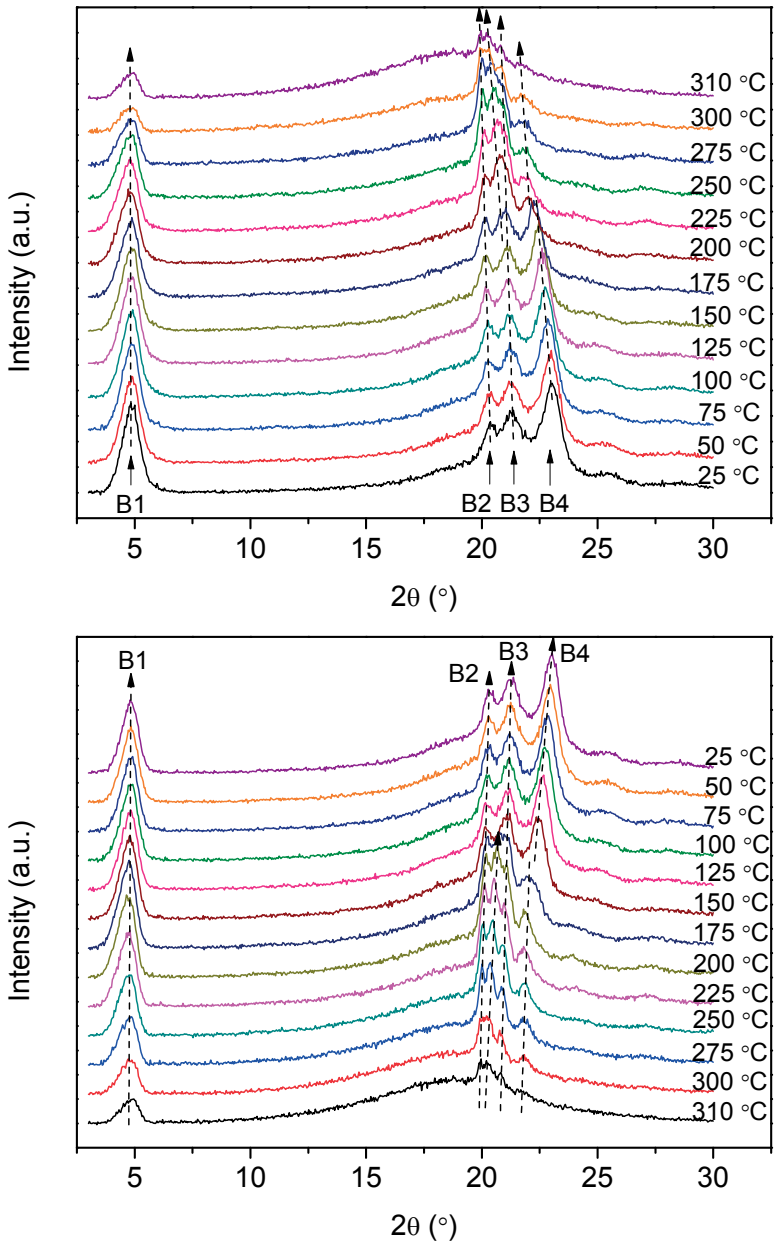

Figure 2.1S The temperature dependence of WAXD patterns of the melt-pressed PA 10T-3 film (A) heating process; (B) cooling process. The arrows point out the development of the reflections.

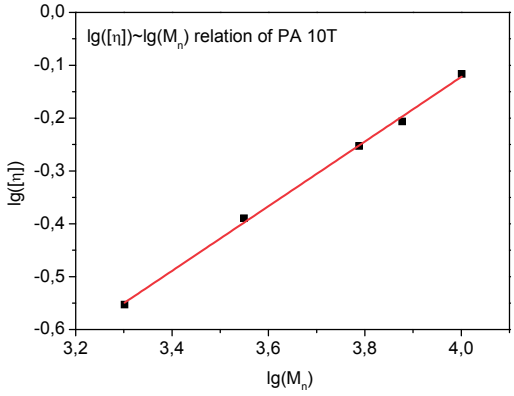

Figure 4.1S $\lg([\eta])$~ $\lg(M_n)$ relation of PA 10T homopolymers in TFA at 25 °C.

$$[\eta] = K * {M_n}^{\alpha}$$

$$\lg([\eta]) = \lg K + \alpha * \lg(M_n)$$

K=2.70*10^{-3} dL·g^{-1}, α=0.61.

The Mark-Houwink constants (K and α) for PA 10T in TFA were determined using a series of PA 10T homopolymers with different M_n. The intrinsic viscosity ([η]) of these PA 10T samples were measured in TFA (99%) at 25 °C. The lg[η] data is plotted as the function of lgM_n as shown in Figure 4.1S. The data points are linearly fitted, and the obtained slope and intercept are α and lgK values, respectively.

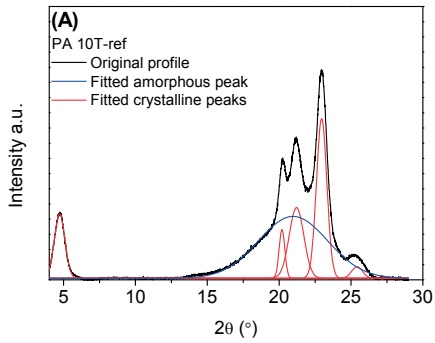

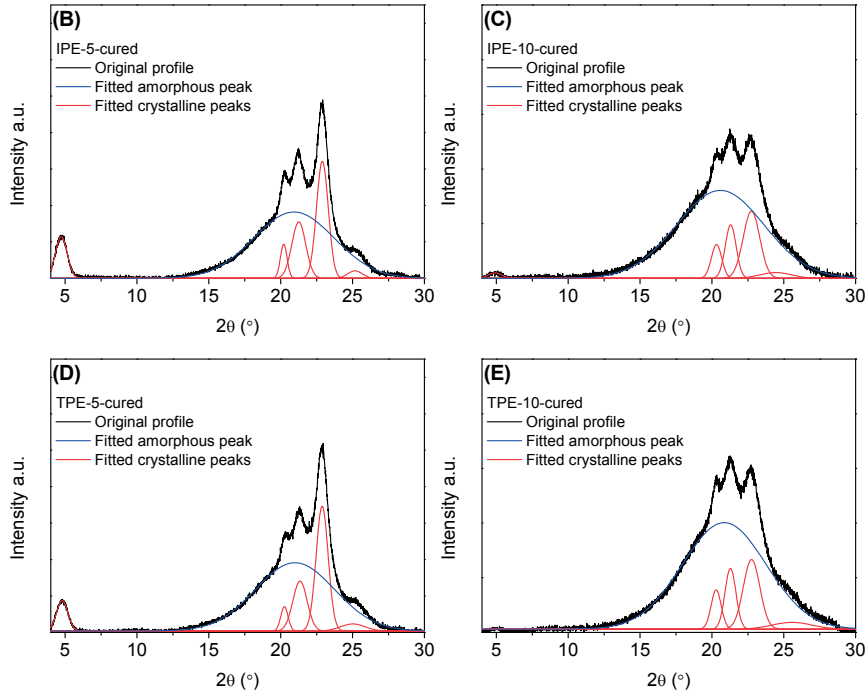

Figure 4.2S Peak fitting of XRD patterns (A) PA 10T-ref film; (B), (C), (D) and (E) IPE-5, IPE-10, TPE-5 and TPE-10 thermoset films. The patterns were fitted using Gaussian functions in OriginPro 8. Blue line shows the amorphous halo; red line shows the crystalline peak.

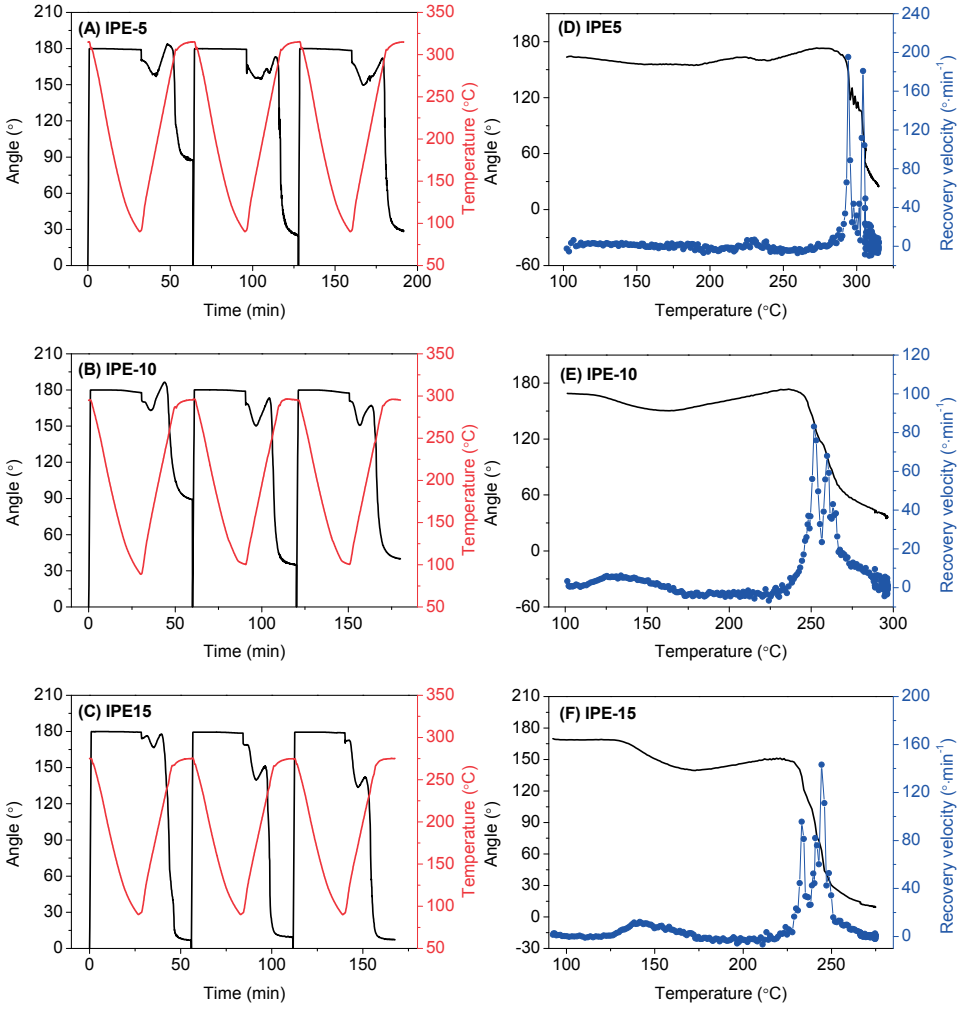

Figure 5.1S Three consecutive dual-shape memory cycles for (A) IPE-5, (B) IPE-10; (C) IPE-15; Shape recovery velocity as a function of temperature in the 2nd cycle for (D) IPE-5; (E) IPE-10; (F) IPE-15. Cooling and heating rate 10 °C/min under N_2 atmosphere.

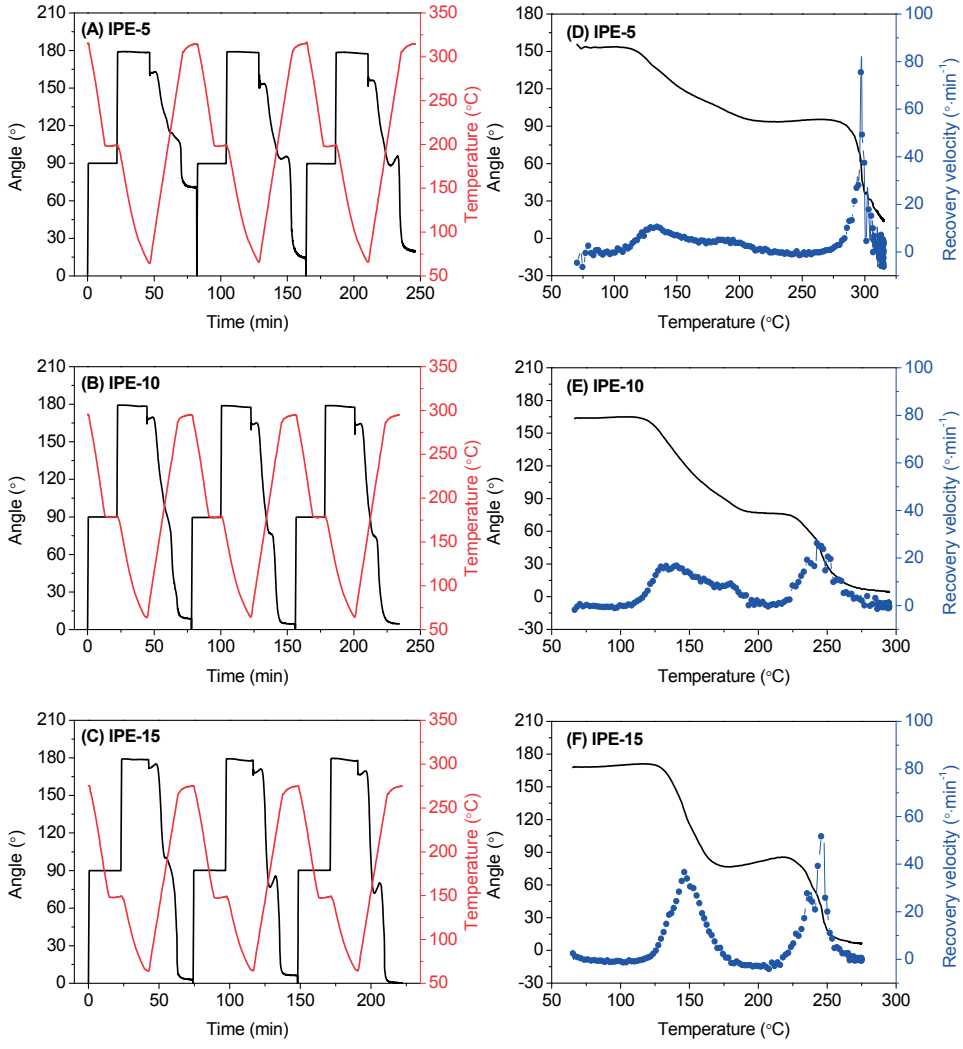

Figure 5.2S Three consecutive triple-shape memory cycles for (A) IPE-5; (B) IPE-10; (C) IPE-15; Shape recovery velocity as a function of temperature in the 2nd cycle for (D) IPE-5; (E) IPE-10; (F) IPE-15. Cooling and heating rate 10 °C·min^{-1} under N_2 atmosphere.

Acknowledgements

The completion of this thesis and the work done in the last four and a half years would not have been possible without the supervision, help and support of many individuals involved directly or indirectly. I would like to take this opportunity to thank all who have contributed to this work.

First of all, I would like to sincerely thank my promoter and supervisor Prof. Theo Dingemans, for accepting me as a PhD candidate in his group, and giving me the chance to work on this novel and interesting research project. Your wisdom, excellent research guidance and commitment to the highest standards greatly support me in my work and improve my research ability. Your patience and enthusiasm strongly encourage me walking out of struggles that I came across on the way. You can always look at my research from different distance and angles, draw me back from being trapped, and show me the overview picture and the right path. In addition, I have learnt a lot from you about scientific writing, presenting and collaborating with other people.

I owe gratitude to Prof. Sybrand van der Zwaag for his warm guidance and support to my PhD research. Your special view point and insight into the research is always very inspiring. I am heartily thankful to Dr. Johan Bijleveld for your valuable and efficient support in both lab work and paper work. Thank you very much for your selfless help and great effort spent on my thesis.

I owe special thanks to Dr. Ruud Rulkens (DSM) for his guidance and enlightening comments. Thank you for inviting me to visit DSM to have a glance at the real industry which greatly inspired me about my future plan. I owe thanks to Prof. Stephen Picken for sharing his extensive knowledge on data interpretation, and his great assistance in understanding complex ideas about polymer physics. I have learnt a lot from the discussions with both of you. I also thank Prof. Sergei Sheiko (University of North Carolina) for inspiring the study on shape memory polymers.

I would like to thank Lijing Xue and Frans Oostrum for their day-to-day maintenance work in the chemistry and physics labs. You are always willing to help in case of any problem during experiments. I thank Kees Goubitz, Ruud Hendrikx and Ben Norder for performing the XRD experiments. I also thank Petra Oude Lohuis (Teijin) for the SEC analysis in Teijin Aramid.

My sincere gratitude goes to all the committee members to spend your time on reviewing my thesis, giving comments and attending my PhD defence.

I would like to acknowledge the Dutch Polymer Institute (DPI) for financial support and the industrial coordinators, Dr. Ruud Rulkens (DSM), Dr. Hanneke Boerstoel (Teijin), Dr. Warrick Allen (SKF), Dr. Gerard Werumeus Buning (DSM), Mr. Ronald Korstanje (DPI), Dr. Jacques Joosten (DPI) and other colleagues in the DPI community. Thank you for the interactive meetings and discussions.

I warmly acknowledge all colleagues within the NovAM family. It would not be such a wonderful experience without any of you. In particular, I would like to thank Maruti, Qingbao and Jianwei for your help on the use of lab equipment and plenty of fruitful discussions, which made me get hands-on skills quickly. Daniella, Martino and Srikanth, thank you for being my great officemates, making our office the most popular along the corridor. Thank you, Shanta, for all the administrative work. Ranjita, Wouter V. and Hongli, thank you for your warm help and support. I would further like to thank: Jie, Michiel, Željka, Ricardo, Wei, Xiaomin, Hao Chen, Qi, Xiaojun, Hao Yu, Haixing, Santiago, Mladen, Antonio, Nan, Wouter P., Arijana, Marianella, Mina, Jesus, Pim, Jibran, Nijesh, Hamideh, Paul, Hussein, Casper, Michael, Shuo, Vincenzo, Marlies, Sung-Hwan, Roserio, Amber, Zenan, Erik, Nora, Renee, Bart and the rest of the Novam colleagues for leaving me a memorable experience.

I would like to give my sincere thanks to Dr. Chaoying Wan (University of Warwick), Dr. Wentan Ren and Prof. Yong Zhang (Shanghai Jiao Tong University). I clearly remember the days that I was doing experiments together with Dr. Wan when I was a bachelor student. You opened the door of doing research on polymer materials for me, and encouraged me to go abroad for further education. Dr. Ren, I owe gratitude for your supervision on my master project and I really appreciate the maximum support that I received from you in every aspect of my life. Prof. Zhang, thank you for accepting me as a student working in your groups, where I built a solid base for the future career.

I would like to spread my thanks to all the friends that I meet in the Netherlands. Jinhu, Yang Zhen, Feifei, Xiaowei, Xueming, Xiaochen, Xiao Lin, Yuling, Cui, Tao Lv, Jingyu and Tian Xin, thank you all for being my intimate friends. We are in a warm (wolf) family sharing information, consoling each other, serving delicious food, organising games, sports and outings… My life in the Netherlands could not be so colourful without you. Thank you, Changgong, Huarong and Shijie for being my nice housemates. Yujing, Jiang Yi, Liu Ping, Qiu Jun, Yongliang, Huajie, Wandong, Zhao Tian, Kaihuan and Jicheng, thank you for your help and friendship with me. I wish all the friends mentioned above and not mentioned a beautiful future.

My beloved wife, Xin, the gratitude I owe you is beyond words. You are so brave to come all the way from China to join me in the Netherlands. We have experienced sweets and bitters of life, and we will walk hand-in-hand towards the enduring future.

In the end, I would love to thank my family and parents (父母), 谁言寸草心，报得三春晖？你们给了我生命和家，你们大爱无疆的牵挂和支持陪伴我一路前行！谢谢你们！

Ming Li (Jimmy)

Curriculum Vitae

Ming Li

Born on February 12, 1988

in Hebei, China

Sept. 2005 – June 2009

Bachelor of Science in Applied Chemistry (Macromolecules), School of Chemistry and Chemical Engineering, Shanghai Jiao Tong University, Shanghai, China

Sept. 2009 – March 2012

Master of Science in Materials Science, School of Chemistry and Chemical Engineering, Shanghai Jiao Tong University, Shanghai, China

Aug. 2012 – present

PhD candidate in Novel Aerospace Materials group, Faculty of Aerospace Engineering, Delft University of Technology, Delft, The Netherlands

List of publications and presentations

M. Li, T. J. Dingemans, Synthesis and characterization of semi-crystalline poly(decamethylene terephthalamide) thermosets, *Polymer*, 2017, 108: 372-382.

M. Li, T. J. Dingemans, Semi-crystalline poly(decamethylene terephthalamide) thermosets based on side-group functionalized copolyamides: synthesis and characterization, to be submitted.

M. Li, T. J. Dingemans, High-temperature shape memory behavior of semi-crystalline polyamide thermosets, to be sumbitted.

M. Li, T. J. Dingemans. Semi-crystalline polyamide thermosets with high temperature shape memory properties. Accepted oral presentation, 46th IUPAC World Polymer Congress, 2016, Istanbul, Turkey.

M. Li, T. J. Dingemans. Semi-crystalline polyamide thermosets and their shape memory properties. Plenary presentation, Dutch Polymer Days 2016, Lunteren, The Netherlands.

M. Li, T. J. Dingemans. Phenylethynyl terminated polyamide 10T oligomers and their cured thermosets: synthesis and characterization. Oral presentation, European Polymer Congress 2015, Dresden, Germany.

M. Li, T. J. Dingemans. Curable semi-aromatic semi-crystalline thermoplastics. Poster presentation, Dutch Polymer Days 2015, Lunteren, The Netherlands.

M. Li, T. J. Dingemans. Curable semi-aromatic and aliphatic semi-crystalline thermoplastics. Poster presentation, Dutch Polymer Days 2014, Lunteren, The Netherlands.

M. Li, W. Ren, Y. Zhang, Study on preparation and properties of gel polymer electrolytes based on comb-like copolymer matrix of poly(ethylene glycol) monomethylether grafted carboxylated butadiene-acrylonitrile rubber, *J. Polym. Res.*, 2012, 19: 9853.

M. Li, W. Ren, Y. Zhang, Study on properties of gel polymer electrolytes based on ionic liquid and amine-terminated butadiene-acrylonitrile copolymer chemically crosslinked by polyhedral oligomeric silsesquioxane, *J. Appl. Polym. Sci.*, 2012, 126 (1), 273-279.

Q. Zhang, M. Li, W. Ren, Y. Zhang, Improved ionic conductivity of NBR/epoxy resin/$LiClO_4$ composites by adding ionic liquid, *J. Macromol. Sci.* B, 2012, 51, 1041-1048.

C. Wan, M. Li, X. Bai, Y. Zhang, Synthesis and characterization of photoluminescent Eu(III) coordination halloysite nanotube-based nanohybrids, *J. Phys. Chem. C*, 2009, 113 (36), 16238–16246.